Numerical Modeling of Geocell Reinforced Beds

- Anu M George-

A Dissertation Submitted to
Indian Institute of Technology Hyderabad
In Partial Fulfillment of the Requirements for
The Degree of Master of Technology

भारतीय प्रौद्योगिकी संस्थान हैदराबाद
Indian Institute of Technology Hyderabad

Department of Civil Engineering

Declaration

I declare that this written submission represents my ideas in my own words, and where others' ideas or words have been included, I have adequately cited and referenced the original sources. I also declare that I have adhered to all principles of academic honesty and integrity and have not misrepresented or fabricated or falsified any idea/data/fact/source in my submission. I understand that any violation of the above will be a cause for disciplinary action by the Institute and can also evoke penal action from the sources that have thus not been properly cited, or from whom proper permission has not been taken when needed.
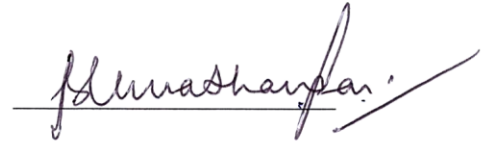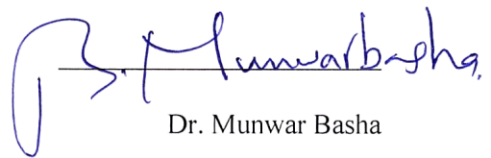
Anu M George

CE13M1011

Approval Sheet

This thesis entitled "Numerical Modeling of Geocell Reinforced Beds" by Anu M George is approved for the degree of Master of Technology from IIT Hyderabad.

Dr. Umashankar Balunaini

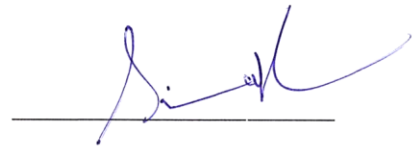Asst. Professor, Dept. of Civil Engg. , IIT Hyd

Examiner

Dr. Munwar Basha

Asst. Professor, Dept. of Civil Engg. , IIT Hyd

Examiner

Dr. Sireesh Saride

Assoc. Professor, Dept. of Civil Engg. , IIT Hyd

Adviser

Dr. Prasanth Kumar

Asst. Professor, Dept. of Mechanical Engg. , IIT Hyd

Chairman

Acknowledgements

This dissertation would not have been possible without the guidance and the help of several individuals who in one way or another contributed and extended their valuable assistance in the preparation and completion of this study.

First and foremost, my utmost gratitude to my thesis advisor, Dr. Sireesh Saride for the continuous support throughout my M-Tech research. Dr. Sireesh Saride has been my inspiration as I hurdle all the obstacles in the completion this research work. His interest and confidence in me has helped in the successful completion of my work.

I am also extremely grateful to Dr. B. Umashankar and Dr. B. Munwar Basha for their kind concern, constant support and steadfast encouragement throughout my M-Tech study.

I am obliged to Vijay Kumar, Sasanka Mouli, Vinay Kumar, Deepthi and Troy for unfailingly helping me with my Masters Project. A special note of thanks to my classmates and friends for the inexplicable love and affection that were showered on me. I am also grateful to my family for instilling confidence in me and giving me strength to plod on under difficult circumstances. Their stimulation, support and faith in me has helped in bringing out the best in me.

Anu M. George

To my family who stood by me through thick and thin

Abstract

Geocell is one of the geosynthetic products used primarily for reinforcing pavements. The numerical modeling of geocell was always a challenge because of its complex honeycombed geometry. This unique three dimensional structure of geocell provide an additional lateral confinement to the encapsulated soil thereby distributing the stresses developed under loading to a wider area. This mechanism of geocell increases the performance of the sand bed to a greater extent.

In this study, a realistic approach of modeling the three dimensional honeycomb shape of geocell is adopted by maintaining the actual curvature using Fast Lagrangian Analysis of Continua in 3D (FLAC3D) a finite difference software. An attempt has been made to simulate numerically the laboratory large scale geocell reinforced pavement systems under monotonic loading for studying the reinforcement mechanism of geocell reinforcement. The model consists of a test tank of 1m width 1m breadth and 1 m depth which is modeled using the primitive mesh radial cylinder. Monotonic loading is applied through a circular plate of diameter 0.15 m. The behavior of steel circular plate is assumed as elastic. The elastic-perfectly plastic Mohr-Coulomb model is used for modeling the soil behavior. The geocell is modeled using the Geogrid structural element with linear elastic behavior, which considers the interface properties of the soil and the geogrid. The simulations are performed for both homogeneous and layered cases. In homogeneous case, 75% relative density sand is used for the complete layer and in layered case 75% relative density sand is used for the base layer and weak subgrade (30% relative density sand and clay) is used for modeling the subgrade. A good agreement between the experimental and numerical results has been obtained in case of unreinforced and geocell reinforced soil beds.

Contents

Chapter 1

Introduction

1.1 Preamble

Geosynthetics have been increasingly used as one of the advanced construction materials in various geotechnical projects like retaining walls, landfills, slope protection and pavements. There are different types of geosynthetics viz. geotextiles, geogrids, geonet, geomembrane, geosynthetic clay liners, geopipe, geofoam and geocomposites available for various applications described.

Recently, the use of geosynthetics in the form of three dimensional confinement known as *geocells* have been widely used in the construction of pavements and foundations because of their advantages over two dimensional planar reinforcement. Geocells offer faster, cheaper, sustainable, environmental friendly solutions for the complex geotechnical problems. Figure 1.1 shows a photograph of typical geocell used in the field.

Figure 1.1: Typical geocell used in field *(Pic courtesy: MIAKOM)*

1.2 Modeling of Geocell mattress

The numerical modeling of geocell reinforcement has been a big challenge because of its complex three dimensional honeycombed structure. Earlier, the researchers like Madhavi Latha and Rajagopal, 2007 have used equivalent composite approach to model the geocell reinforced soil layers. Even though the approach was simple, it was unrealistic to model the geocell as an equivalent soil layer. Subsequently, Han et al, 2008 and Sireesh et al, 2009 have adopted and modelled diamond and square shape of geocells respectively for pavement and foundation applications. These models were realistic, but the stress concentration at the corners resulted in underestimating the performance of the geocell reinforced soil beds. Later, Yang et al, 2010 and Hegde and Sitharam, 2014 modeled the actual honeycombed shape of geocell by digitizing the coordinates from the photograph of a single geocell.

In the present study, geocell is modelled by placing geogrid elements on semicircular soil zones modeled using cylindrical mesh. The details of geocell modeling are discussed in Chapter 3 of this thesis.

1.3 Mechanism of Geocell Reinforcement

Planar reinforcements improve the performance of the reinforced sand bed by three mechanisms, namely by providing lateral restraint, by increasing the bearing capacity and by developing an additional membrane tension support under loading. In the case of geocell which possess a three dimensional honeycombed structure, there exists an additional lateral confinement on the infill material, thereby improving the performance of the reinforced sand bed to a greater extend. This mechanism is shown in the Figure 1.2.

There have been some exceptional research in the area of geocell reinforcement in the recent past (Bathrust and Jarrett, 1989; Bush et al, 1990; Mandal and Gupta, 1994; Krishnaswamy et al, 2000; Dash et al, 2001; Dash et al, 2003; Sireesh et al, 2009; Yang et al, 2010; Hegde and Sitharam, 2014) and the use of geocells as a reinforcement material has gained momentum over the years. Even though the numerical modeling of geocell reinforcement has been done by researchers like Yang et al, 2010 and Hegde and Sitharam, 2014, there are no studies available which are focusing on the actual confining mechanism of the geocell reinforcement. The current study focused on modeling the actual three dimensional structure of the geocell reinforcement and performing numerical analysis on the geocell reinforced homogeneous and layered sand beds. This study also focuses on the

confining mechanism of the geocell reinforced soil, which results in the improvement in the performance of the sand bed.
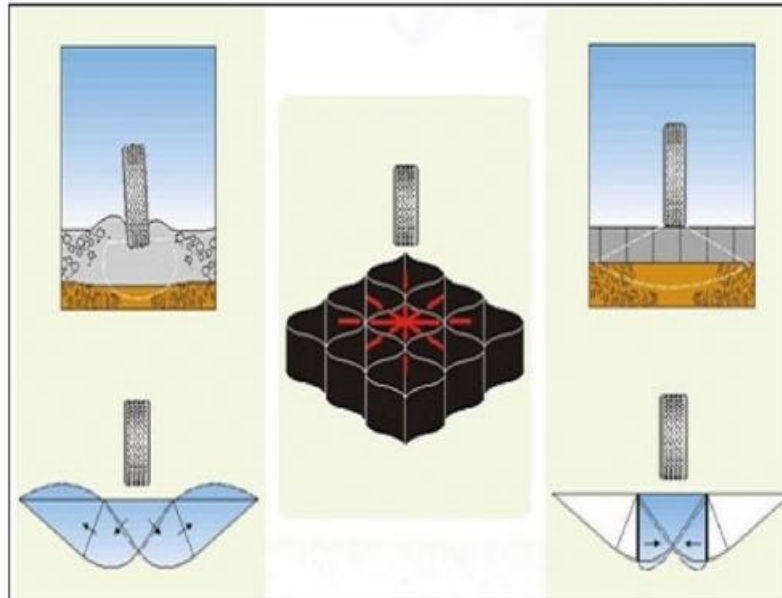
Figure 1.2: The concept of geocell reinforcement

1.4 Objective and Scope of the Study

The major objective of the present study is to model the natural honeycomb shape of the geocell and to develop an understanding of the confining behavior of geocell reinforced beds subjected to static loading using FLAC 3D finite difference programme.

The scope of the present research is as follows:

I.   Formulation of natural three dimensional shape of honeycomb structure of geocell mattress.
II.   Numerical simulation of the geocell reinforced homogenous and layered sand bed under monotonic loading.
III. To bring out the confinement mechanism of the geocell reinforcement.

1.5 Organization of the Thesis

In *Chapter 2* the literature survey about the experimental and numerical studies on geocell reinforcement under static loading has been discussed. Discussion has been carried on geocell reinforcement, foundation models and numerical and analytical modelling of geocell reinforcement. *Chapter 3* deals with modeling the natural honeycombed structure of geocell reinforcement by maintaining the actual curvature. The validation of geocell model using large triaxial test is also discussed in this chapter. *Chapter 4* discusses the behavior of geocell reinforcement when placed in homogeneous sand bed of 75% relative density using finite difference software FLAC 3D. The confining mechanism developed inside the geocell reinforcement is studied by evaluating the stresses and displacement developed under static loading. In *Chapter 5* the numerical modeling of geocell reinforced sand bed over weak subgrade is studied using FLAC model. Two subgrades were adopted for modeling- 30% relative density sand and clay. This chapter also studies the variation of confining stresses across the geocell wall as well as across the infill soil material. Parametric studies were also performed by varying the elastic modulus of geocell and interface shear modulus of geocell. Studies were also done on geocell with aperture and by placing a Geogrid layer at the bottom of the geocell. *Chapter 6* covers the modeling of stacked geocell and the behavior of stacked geocell under monotonic loading. Two models were adopted for the study- namely Type 1 with weld of first geocell over the weld of second geocell and Type 2 with weld of first geocell over the cell of second geocell. These two cases were again analyzed by placing a geogrid layer in between the two geocell layers. *Chapter 7* summarizes the results obtained from the study and the major conclusions drawn from the study.

Chapter 2

Literature Review

2.1 Introduction

Geosynthetic materials have been increasingly used for unpaved and paved road construction in recent years. One of the earliest uses of geosynthetics for roadway construction occurred in 1920s (Becham et al. 1935). The inclusion of geosynthetics at the subgrade-base interface, or even within the base course, can improve the service life and performance of paved as well as unpaved roads and reduce the required thickness of the base course (Giroud and Han 2004). Common geosynthetics used in roadway construction are geotextile, geomembrane, geogrid, geocell, geonet, geofoam, geocomposite, etc. This chapter presents a literature review of geocell reinforcement under monotonic loading.

2.2 Geocell and its Application in Pavements

Geocells are three-dimensional honeycombed cellular structures that provide confinement to compacted infill soil. Their confinement reduces the lateral movement of soil particles and forms a stiffened mattress or slab to distribute applied loads over a wider area. Geocells have been used in construction of slopes, retaining walls, channels, roads, and railways. In the late 1970s, the U.S. Army Corps of Engineers first developed the concept of a cellular confinement system over a grid confinement system to construct roads in soft terrain and wet weather conditions. Webster and Bach developed a method to weld polyethylene strips to form a cellular structure co-called "Sandgrid" (Presto Products Co. 2009). This cellular confinement system with high density polyethylene (HDPE) strips was used first for load support applications such as road constructions in the United States in the early 1980s. It was then used for slope erosion control and channel lining in the United States in 1984, and for earth retention in Canada in 1986. The new type of geocell is made of novel polymeric alloy that is characterized by flexibility at low temperatures similar to HDPE and an elastic behavior similar to engineering thermoplastic (Pokharel 2010; Yang 2010). Geocell has been increasingly used to confine base course materials in roadway construction. The main

5

mechanisms of confinement include active earth pressure within loaded cells, soil resistance in the adjacent cells, and hoop stresses in the cell walls. Under vertical loading, hoop stresses in the cell walls and soil resistance in the adjacent cells are mobilized so that the soil inside the cells is confined and the strength and stiffness of the soil is increased. The geocell-reinforced base layer acts as a stiff mattress or slab to distribute the vertical traffic load over a wider area of the subgrade. As a result, the vertical stresses applied on the subgrade are reduced and the bearing capacity is increased. Field trafficking tests and falling weight deflectometer measurements found that geocell reduced vertical stresses beneath the geocell layer by approximately 30%, reduced the deflections on the flexible pavement surface by approximately 15%, and increased the back calculated layer modulus by approximately 10% in comparison to an unreinforced section (Emersleben and Meyer 2008 2010). Al Qadi and Hughes (2000) reported that geocell confinement increased the resilient modulus of the aggregate layer in a flexible pavement by approximately two times.

2.3 Experimental Studies on Geocell reinforcement under Static Loading

In the earlier days interconnected paper cells filled with sand was used as reinforced layer for construction of low cost highways. Webster and Watkins (1977) built seven unpaved test road sections (one unreinforced section and six sections with different types of reinforced base courses) on soft clay to compare different reinforcement techniques. They found that one of the sections with a 30 cm thick sand base course reinforced by cellular-confinement (made up of isolated plastic tubes of 15 cm diameter and 30 cm long) performed better than the section with a 36 cm thick crushed stone base course by measuring the rut depth developed on the road after traffic loading. After this study, a cellular confinement system, named "grid cell", was soon developed, which is made up of square shaped grids and filled with sand. Later on full scale model test were performed by them (Webster and Watkins 1979a, 1979b) to investigate the factors affecting the performance of these cellular confinements.

Rea and Mitchell (1978) conducted laboratory tests to investigate the factors that influence the behavior of geocell reinforced sand. His studies include grid size, grid shape, grid material, thickness of the sand-grid layer, subgrade stiffness, types of sand, compaction and load type. They found that the optimum cell height to cell width ratio was around 2.25, beyond which the improvement in using geocell reinforcement is insignificant. They also suggested that the optimum ratio of footing diameter to the cell width must be about 1.5 to 2. They also studied about the effect of subgrade stiffness on the ultimate bearing capacity

of the geocell-reinforced sand. They observed that a higher subgrade stiffness resulted in greater ultimate bearing capacity of reinforced sand. The effect of subgrade stiffness on the ultimate bearing capacity of grid-reinforced sand is shown in the Figure 2.1.
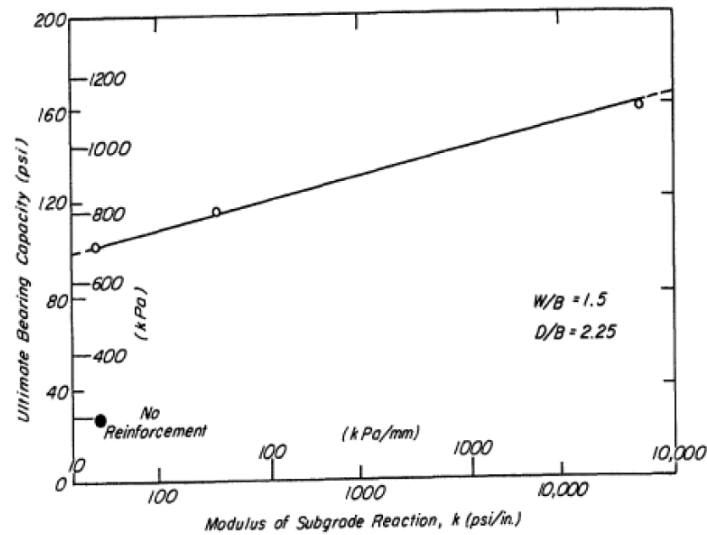

Figure 2.1: Effect of subgrade stiffness on the ultimate bearing capacity of grid reinforced sand (Rea and Mitchell, 1978)

Rajagopal (1999) also conducted triaxial test on sand samples reinforced with single and multiple geocells. His test results showed that the geocell reinforced soil sample has a friction angle almost same as that of the reinforced soil, but with an increased cohesion. He also suggested that the reinforced samples with at least three interconnected cells should be used in the triaxial test in order to accurately estimate the apparent cohesion. The configuration for single-cell and multi-cell reinforced soil sample for triaxial tests are shown in Figure 2.2.

Krishnaswamy et al. (2000) used diamond and chevron pattern geocells and performed laboratory model tests of embankments on a geocell reinforced layer over soft clay foundation. Four different types of geogrids were used for the formation of geocell layer. The geocells were filled with clayey sand and clay and the embankment was subjected to uniform surcharge pressure on the crest until failure. The influence of various parameters like tensile stiffness of the Geogrid material to fabricate the geocell material, height and the pocket size of the geocell layer, length of the geocell layer, and type of fill material inside the geocell on the behavior of the embankments were investigated in his study. His study

concluded that the provision of a layer of geocells at the base of the embankment improves the load capacity and deformation response of the embankment.
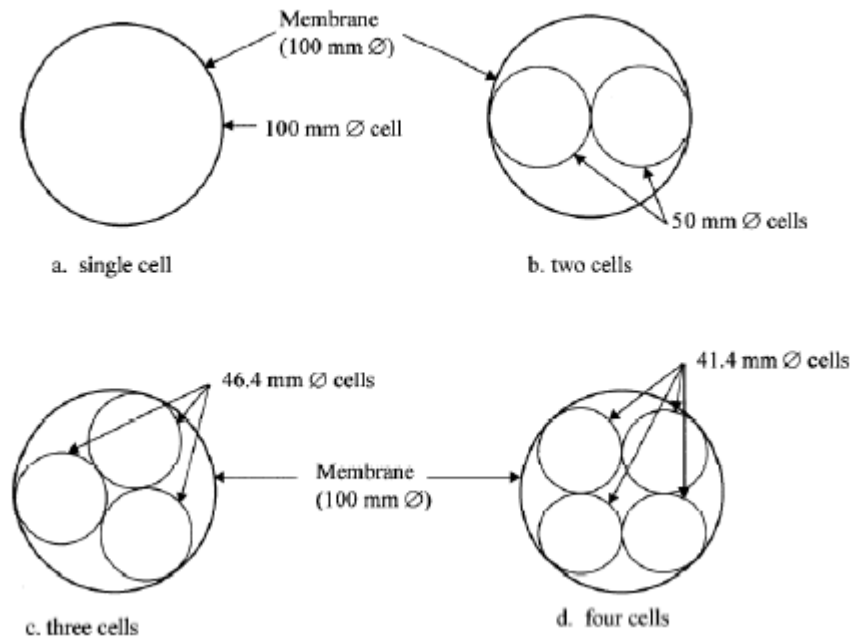

Figure 2.2: Configuration of single-cell and multi-cell reinforced soil sample for triaxial tests (Rajagopal et al, 1999)

Dash et al. (2001) conducted model studies on strip footing supported by geocell reinforced sand and have observed significant increase in the performance. In subsequent study, Dash et al. (2003) conducted model studies on a circular footing supported on geocell reinforced sand underlain by a soft clay bed. The test section was subjected to monotonic loading by a rigid circular footing. Footing load, footing settlement, and surface deformation on the fill were measured during the test. The test results showed that geocell confinement of the sand layer substantially increased the bearing capacity and reduced surface heaving of the foundation bed. An additional layer of geogrid placed at the base of the geocell mattress further enhanced the bearing capacity and stiffness of the foundation bed. He also investigated the effect of an additional planar reinforcement placed along with the geocell reinforcement in the sand beds. He observed that an additional layer of Geogrid reinforcement placed at the base of geocell mattress enhances the performance of the footing in terms of load carrying capacity and stability against rotation.

Weseloo (2004) carried out unconfined compression tests on single-cell and multi-cell reinforced soil. He developed an elastoplastic constitutive model for the infill soil and rate-dependent non-linearly elastic membrane models for the geocell. He analyzed the stress strain behavior of single-cell reinforced sand and multi-cell reinforced sand, and concluded that the stress-strain behavior measured from single cell reinforced soil could not represent that of multi cell reinforced soil. He proposed introducing an efficiency factor f_{eff} ($<=1$) to account for the multi cell effect.

$$f_{eff} = \frac{(\sigma_a)_{single-cell}}{(\sigma_a)_{multi-cell}}$$

where σ_a single-cell is the axial stress in a single cell structure at a specified diameter and axial strain rate, and σa multi-cell is the axial stress in a multi-cell structure at the same specified cell diameter and axial strain rate. The efficiency factor should be determined from unconfined compression tests.

The beneficial effects of geocell reinforcement have been studied by many researchers in the past. Sitharam et al. (2005) performed a series of laboratory-scale static load tests on a rigid circular footing placed on a fill surface and did parametric study on depth of placement of the geocell layer, width and height of the geocell layer, and influence of an additional layer of planar geogrid at the base of the geocell mattress.

Latha et al. (2006) conducted laboratory model tests to investigate the benefit of geocell confinement on the performance of earth embankments constructed over weak foundation soil. They evaluated the influence of several factors on the behavior of the embankment, such as tensile stiffness of geocell material, height and length of geocell layer, pocket size of the cell, pattern of formation of geocells, and type of fill material inside the cells. Geocell confinement was found to be beneficial in increasing the bearing capacity and reducing the deformation of the embankment.

The optimum location of geocell reinforcement was studied by Thallak et al. (2007). He placed geocell at different depth in his test and studied the improvement in the behavior of the test bed. He observed that the bearing capacity increased sharply when the geocell is placed at a shallower depth (less than 0.5 times circular footing width).

9

Singh et al. (2007) found that the ultimate bearing capacity of a square footing was appreciably increased by geocell confinement under the axial load as well as under the eccentric inclined load. It was observed that the confinement of soil under the footing resisted the lateral displacement of the in filled material, leading to a significant decrease in the settlement and an increase of the ultimate bearing capacity.

Field studies were performed by Keif and Rajagopal (2008) to examine the benefit of geocell reinforcement of the base layer in a flexible pavement. The results obtained from the field tests demonstrated that the vertical stress underneath the geocell-reinforced granular layer due to traffic loading was reduced by more than 50% in comparison to the unreinforced case. They also carried out finite element analysis of the test sections to study the improvement in the bearing capacity of the pavement. The results revealed that the bearing capacity of the subgrade layer was increased by approximately 2.5 times.

Ta-teh et al. (2009) conducted static and dynamic loading tests to determine the bearing capacity and dynamic properties of sandy soil confined with geocell. They concluded that desert subgrade can be improved in terms of bearing capacity and settlement compared to unreinforced sandy subgrade.

To investigate the behavior of geocell-reinforced bases under static and repeated loading Pokharel et al. (2009a) conducted experimental studies on two base course materials, Kansas River sand and quarry waste. The experimental results showed that geocell confinement increased the bearing capacity and stiffness of the Kansas River sand by improvement factors of 1.75 and 1.5 respectively, under static loading. However, geocell confinement had a minor effect on the stiffness of the quarry waste under static loading due to the existence of apparent cohesion. The unreinforced and geocell reinforced soil behavior is showed in Figure 2.3. The single geocell reduced the permanent deformation of the quarry waste base by a factor of approximately 1.5 in comparison to the unreinforced base under dynamic loading. The Kansas River sand had a lower percentage of elastic deformation compared to the unreinforced and reinforced quarry waste due to poor gradation, sub-rounded particles, and no apparent cohesion of the sand. The reinforced quarry waste had a higher percentage of elastic deformation than the unreinforced quarry waste due to the contribution of the geocell.
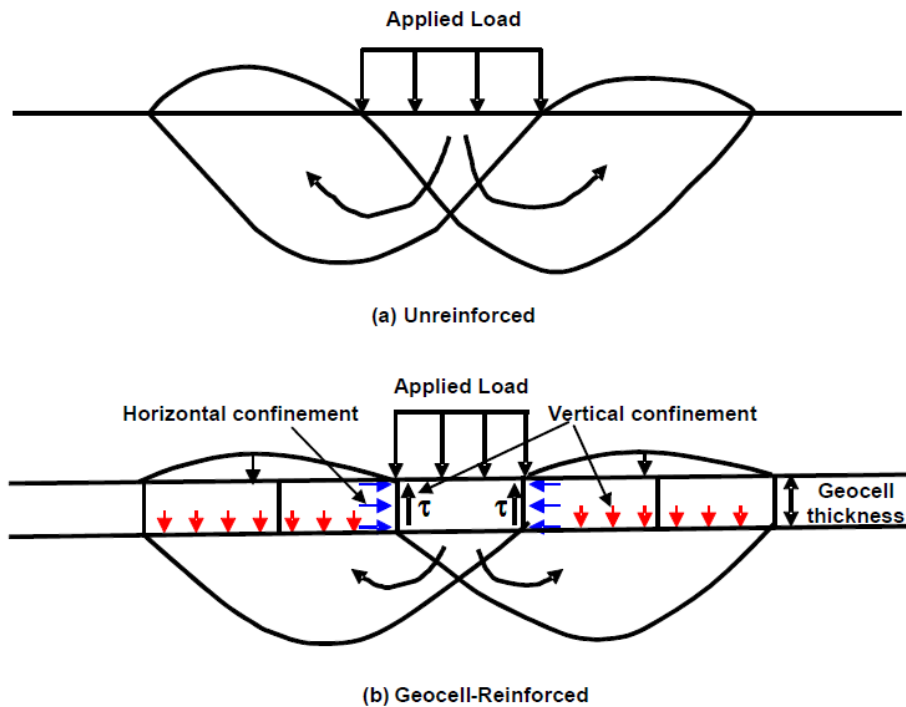
Figure 2.3: Unreinforced and geocell reinforced soil behavior (Pokharel et al, 2010)

Pokharel et al. (2009b) conducted another experimental study to evaluate the influence factors for single geocell-reinforced sand. This study found that the geocell placed in a circular shape had a higher bearing capacity and stiffness of the reinforced base than geocell placed in an elliptical shape. The performance of the geocell with a higher elastic modulus had a higher bearing capacity and stiffness of the reinforced section. The improvement factor for a geocell-reinforced base over its corresponding unreinforced base ranged from 1.5 to 2.5 in terms of bearing capacity and 1.3 to 2.0 in terms of stiffness. The geocell with a higher elastic modulus had a higher improvement factor. Due to poor subgrade conditions in a desert area, it is difficult to construct roads of good quality.

Moghaddas Tafreshi and Dawson (2010) worked on the comparison of bearing capacity of a strip footing on sand with geocell and with planar forms of geotextile reinforcement and concluded that for the same quantity of geotextile material, the geocell reinforcement system behaves much stiffer and carries greater loading and settles less than does the equivalent planar reinforcement system.

Tanyu et al. (2013) performed Laboratory evaluation of geocell-reinforced gravel subbase over poor subgrades and found that the presence of geocells reduced the plastic deflection of the working platforms by 30–50%, improved the resilient modulus of the subbase by 40–50%, and the modulus of subgrade reaction by more than two times.

Hegde and Sitharam (2013) performed laboratory model tests on square footing resting on geocell reinforced sand and clay beds. Three tests conducted namely unreinforced, geocell reinforced and geocell reinforced with additional planar grids. The results demonstrated that the ultimate bearing capacity of the sand bed was increased by 2.4 times and clay bed by 3.2 times. Effect of infill materials on the performance of geocell reinforced soft clay beds was studied by Hegde and Sitharam (2014a). They conducted plate load test on geocell reinforced soft clay beds to evaluate the effect of infill materials on the performance of geocell. Tests were performed for three types of infill materials namely aggregate, sand and local red soil. The results showed that the load carrying capacity of the geocell reinforced bed was increased by 13 times for aggregate infill, 11 times for sand infill and 10 times for red soil infill. Hegde and Sitharam (2014b) also studied about the joint strength and wall deformation characteristics of a single-cell geocell subjected to uniaxial compression.

2.4 Numerical Studies on Geocell reinforcement under Static Loading

Mitchell et al. (1979) carried out first analytical study on geocell reinforced soil and identified the seven possible mechanisms of failure of geocell reinforced sand overlying soft subgrade. The seven failure modes include cell penetration of subgrade, cell bursting, cell wall buckling, bearing capacity, bending, durability failure and excessive rutting. He also proposed some useful analytical formulas to predict the capacity of grid cell reinforced sand base course against different modes.

Large-scale triaxial tests were carried out by Bathurst and Karpurapu (1993) on 200 mm high isolated geocell-soil composite specimens and unreinforced soil specimens. Two different types of aggregate soils were used for the test. The height-to-diameter ratio of unity was maintained for reinforced specimens which matches with the dimensions of the system in a typical base reinforcement application. They proposed the use of apparent cohesion cr by analyzing the Mohr circles and the Mohr-Coulomb failure envelopes of the unreinforced and reinforced samples on account of the strength increase of geocell. The increase in strength was due to the increased confining stress provided by geocell on the infill material.

12

$$c_r = \frac{\Delta\sigma_3}{2}\tan(\frac{\pi}{4}+\frac{\phi}{2})$$

Where ϕ is the friction angle of the soil; $\sigma3$ is the increased stress which can be calculated from

$$\Delta\sigma_3 = \frac{2M}{d}\left[\frac{1-\sqrt{1-\varepsilon_a}}{1-\varepsilon_a}\right]$$

Where M is the tensile stiffness of the geocell material; d is the initial diameter of the geocell pocket; and σa is the axial strain for the soil.
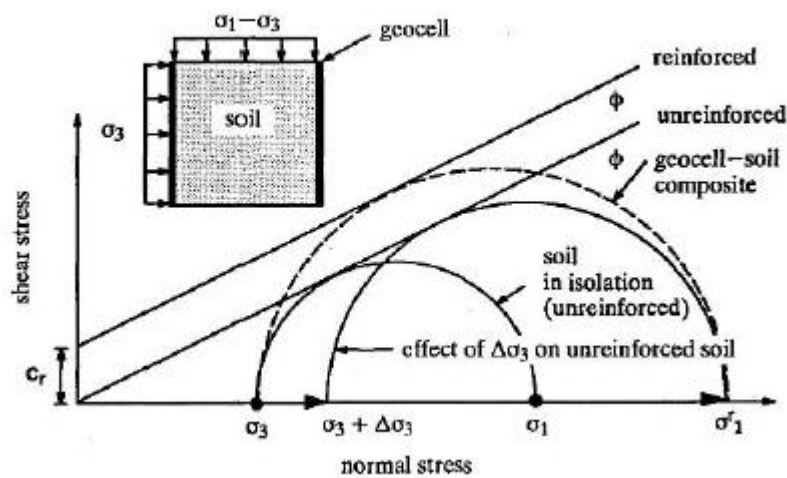

Figure 2.4: Mohr circle construction for calculating the apparent cohesion of the geocell-soil composite (Bathurust and Karpurapu, 1993)

The increase in stiffness of the soil reinforced with geocell was studied by Latha (2000) and proposed empirical equation to estimate the modulus number Kr of the geocell soil composite from the modulus number Ke of the unreinforced soil.

$$K_r = K_e + 200M^{0.16}$$

Where Kr and Ke corresponds to the modulus number K in the Duncan-Chang model.

Sitharam et al. (2006) conducted a numerical study using FLAC3D to evaluate the influence of geocell confinement on the bearing capacity of a circular footing supported on a sand bed subjected to vertical loading. The numerical analysis demonstrated that the footing 12 pressure was well distributed within the geocell mattress and was transferred to a wider area of the subsoil compared to the unreinforced sand bed.

Latha and Rajagopal (2007) performed parametric finite element analysis of geocell reinforced sand on top of clay subgrade supporting an embankment load using a two dimensional finite element software GEOFEM. They modeled the geocell reinforced soil as a composite material using Mohr- Coulomb model to simulate the improvement in the geocell reinforced soil due to confinement. Parametric finite element analyses of the geocell-supported embankments were carried out by varying the dimensions of the geocell layer, the tensile strength of the material used for fabricating the geocell layer, the properties of the infill soil, and the depth of the foundation layer. They also proposed some guidelines for selecting the geocell reinforcement to support embankments on weak foundation soils.

Han et al. (2008) modeled single cell-reinforced sand supporting rectangular footing show in Figure 2.5 using FLAC 3D finite difference software to investigate the mechanism of geocell-sand interaction. The numerical model used for the study is shown in the Figure. He used Mohr- Coulomb model and linear elastic membrane model to simulate sand and geocell respectively. He studied about the distribution of displacements in the sand and geocell walls and also the distribution of tensile and shear stresses acting on the walls of geocell under vertical loads.
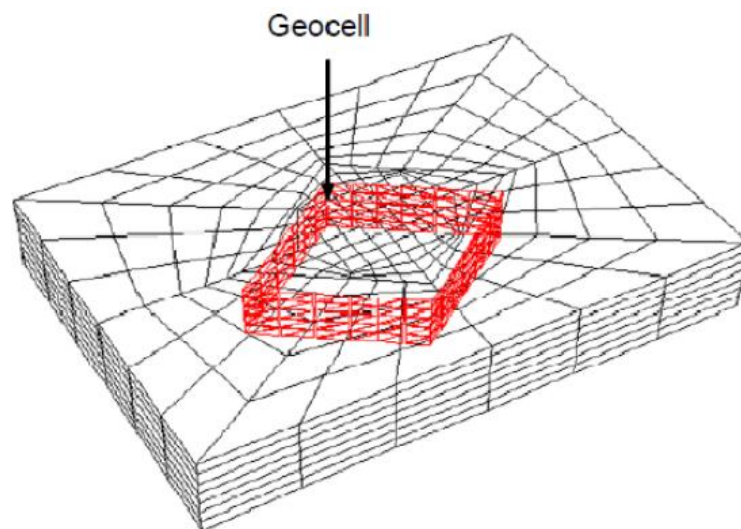

Figure 2.5: Three dimensional model of single geocell-reinforced soil (Han et al, 2008)

Latha et al. (2009a, 2009b) studied the behavior of geocell reinforced sand supporting a strip and square footing using GEOFEM and FLAC 3D respectively. In both the cases she modeled the geocell reinforced soil as a composite material using Duncan-Chang model. The relative performance of various geosynthetic reinforcements like planar geogrids, geocells, randomly distributed mesh elements were studied as shown in Figure 2.6. Her

14

study also showed that the mobilized shear stress contours becomes horizontal and shifts downwards with the provision of geocell layer indicating that the geocell mattress transmits the footing load to a deeper depth, thereby bringing about a higher load carrying capacity.

Fig. 4. Geosynthetics in different forms used for reinforcement: (a) planar layers, (b) randomly distributed mesh elements and (c) geocell layer.

Figure 2.6: Geosynthetic in different forms used for reinforcement: (a) planar layers, (b) randomly distributed mesh elements and (c) geocell layer (Madhavi Latha et al, 2009)

Sireesh et al. (2009) performed numerical simulation of laboratory model tests to study the behavior of geocell-reinforced sand and soft clay foundation beds under circular footing. He adopted square shaped geocell to perform simulation on multiple geocells using FLAC 3D software. He also studied the influence of geometric parameters of the geocell on the overall performance of the footing. The results showed that the geocell mattress redistributed the footing pressure over a wider area thereby improving the performance of the footing.

The actual honeycomb shape of geocell was modeled by Yang et al. (2010) for a single geocell as shown in the Figure 2.7. Three dimensional mechanistic response model was used to model geocell reinforced base because of the complex geometry of geocell. He performed parametric studies on calibrated model to investigate the effect of various factors like thickness of geocell reinforced layer, geocell modulus, subgrade stiffness and strength, interface shear modulus and infill material modulus.
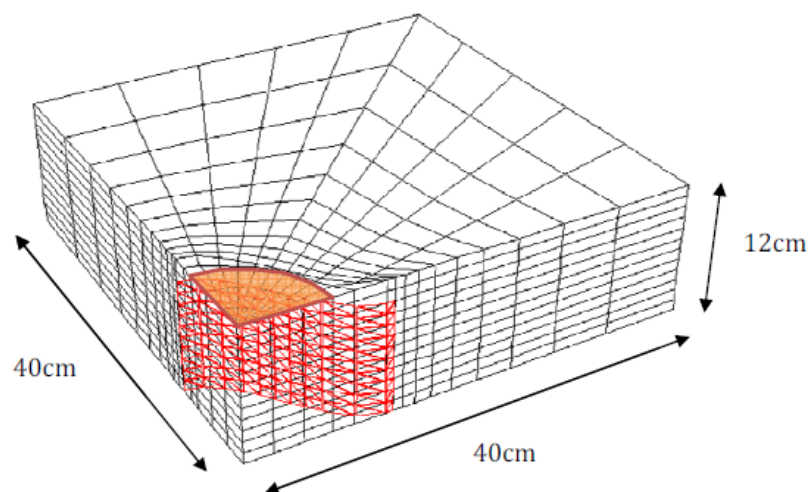
Figure 2.7: Three dimensional honeycomb shape of geocell (Yang et al, 2010)

Hegde and Sitharam (2014) adopted the honeycomb shape of geocell and performed modeling of geocell reinforced sand beds using FLAC 3D finite difference software. The model developed is shown in the Figure 2.8. Geocell were modeled using geogrid structural element and sand was modeled using Mohr-Coulomb model. Two cases were analyzed- only geogrid and geocell with additional basal geogrid. They observed that performance of foundation bed was directly influenced by the modulus and height of geocell. They also concluded that the pocket size of geocell inversely affect the performance of the reinforced beds.
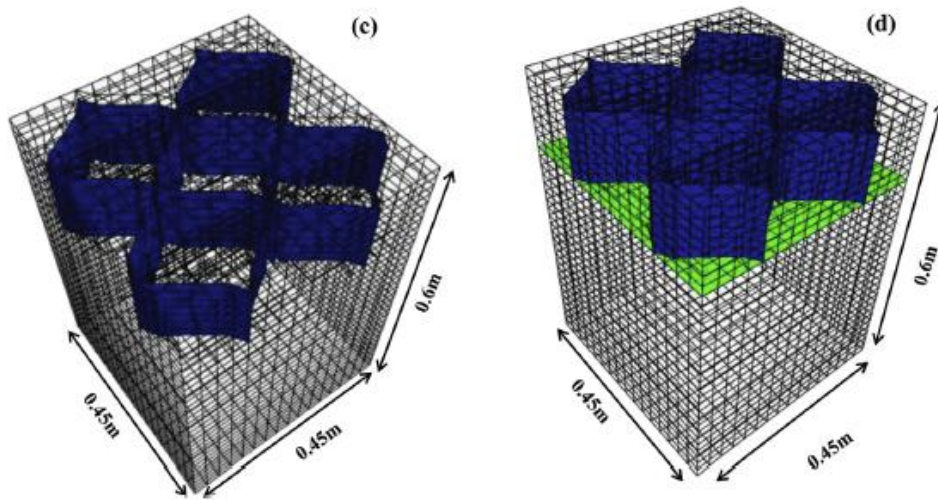

Figure 2.8: Three dimensional honeycomb shaped geocell reinforced sand bed (Hegde and Sitharam, 2014)

2.5 Summary

The literature survey clearly shows that there has been a wide spread research on the geocell reinforcement in various geotechnical applications like footings and pavements. The following findings have been observed from the past studies.

    i.   Geocell reinforced soil bed is both stiffer and stronger than unreinforced bed under static loading.

   ii.   Geocell performs better than other planar reinforcements.

 iii.   Geocell provide confinement, tension membrane effect, and wider distribution of applied stress, which result in increased bearing capacity and stiffness of the reinforced bed.

iv.   Properties of geocell and infill material play significant role in improving the performance of reinforced bed.

v.   The effectiveness of geocell reinforcement is influenced by the factors such as aspect ratio of geocell, type of location and loading and strength of subgrade.

vi.   Numerical models can be successfully used in the study of improvement in the performance of the soil bed under static loading.

The literature survey clearly shows that there has been a wide spread research on the geocell reinforcement in various geotechnical applications like footings and pavements. The following findings have been observed from the past studies. Another observation that can be figured out from this literature study is that most of the numerical studies on geocell discuss only about the vertical stress and displacement variation. Very little or no attention has been paid on the reinforcing mechanism of geocell. In the following chapters the reinforcing mechanism of geocell in homogeneous and layered cases are studied using FLAC 3D numerical model.

Chapter 3

Geocell Model Development and Validation

3.1 Introduction

A number of programs like PLAXIS, ANSIS, ABAQUS, and FLAC are available for mechanical analysis of geosystems. The first three are finite elements-based programs, while FLAC, Fast Lagrangian Analysis of Continua, developed by Itasca Consulting Group, relies on the finite difference solution of the differential equations. The difficulties involved in simulating the complexities such as boundary effects, scale effects, material non-homogeneity, non-linear behavior of materials, stress levels that are applicable to the field conditions and limitations of 1-g model tests are resolved with numerical methods.

Many researchers including Yetimoglu et al., 1994, Raghavendra, 1996, Peng et al., 2000, Boushehrian and Hataf, 2003 have simulated geogrid reinforced foundation systems using finite element methods. The ultimate soil capacity for circular smooth and rough footings subjected to axial static load with account of soil dilatancy have studied by Erickson and Drescher (2002) using FLAC. Numerical simulation has been done to model a layer of sand blanket overlying super soft clay with a geogrid layer at its interface using FLAC by Fakher and Jones (2001). They have discussed the influence of the bending stiffness of the reinforcement on the bearing capacity of the super soft clay and also studied the factors affecting the reinforcement mechanisms of geogrid reinforcement.

Researchers like Bathurst and Knight (1998), Madhavi Latha and Rajagopal (2007) and Madhavi Latha and Somwanshi (2009) worked with modeling of geocell reinforcement using equivalent composite approach in which the geocell-soil composite is treated as a soil layer with improved strength and stiffness. Han et al. (2008) modeled single geocell as box

18

shaped and carried out numerical simulation. Sireesh et al. (2009) also adopted square shaped geocell to perform simulation on multiple geocells.

Because of the complexity in modeling the actual honeycomb shape of geocell, limited literatures are available on numerical simulations of the geocell by maintaining the actual geocell shape. Yang et al. (2010) modeled the honeycomb shape of geocell for a single geocell using FLAC 3D software and simulated static and cyclic tests. Hegde et al. (2014, 2015) also adopted the same method for modeling the honeycomb shape of geocell and simulated static tests by considering sand and clay as the subgrade respectively.

3.2 Finite Difference Approach

The finite difference method is the oldest numerical method used for solving differential equations with initial and boundary value problems. In this method, every derivative in the set of governing equations are replaced by an algebraic expression in terms of stresses and displacements at discrete points in space. FLAC uses explicit, time marching method to solve these algebraic expressions.

3.3 FLAC 3D Software

3.3.1   Introduction to FLAC 3D Software

The Fast Lagrangian Analysis of Continua in 3 Dimensions (FLAC 3D) developed by Itasca Consulting Group, Inc. is a widely used finite difference commercial code in the geotechnical engineering field. It has been successfully used to numerically simulate a number of geotechnical problems. Besides many built-in soil constitutive models, it provides a user interface to implement new constitutive models. FLAC3D is therefore selected to implement the state dependent soil and geocell model.

The explicit finite different solution scheme used in FLAC has several advantages over finite elements, including the possibility of analyzing unstable systems. Additional features within the program include the possibility to add extra grid variables which store information at the grid points during intermediate steps. This allows to store stress paths at specific grid points, and to retrieve such information later.

3.3.2   Explicit Dynamic Solution Scheme

Implementing geomaterial models can result in several difficulties in numerical solution schemes. Three characteristics of geomaterials that cause specific problems in implementing constitutive models are:

1. Physical instability: Physical instability occurs in materials with softening behavior, such as rock, concrete and over-consolidated soils. The softening behavior occurs when the material fails and parts of it accelerate and the stored energy is released in the form of kinetic energy. Numerical solution schemes often have difficulties at this stage because the solution may fail to converge when a physical instability arises.

2. Path dependence of nonlinear materials: In most geo-mechanical systems, there are infinite number of solutions that satisfy the equilibrium, compatibility and constitutive relations that describe the system. These solutions are corresponding to different stress paths, respectively. A correct solution needs to be identified for the actual stress path. The numerical solution scheme should be able to accommodate different loading paths in order to apply the constitutive model properly.

3. Nonlinearity of the stress-strain relation. This is referred to as the dependence of the elasto-plastic stiffness matrix on the stress state. The numerical scheme needs to be able to accommodate the various forms of nonlinearity.

In the Itasca series of software, an approach called explicit dynamic solution (EDS) scheme is used. The above three characteristics of geo-materials, which cause difficulties in implementing the constitutive model, can all be addressed. The scheme allows the numerical analysis to follow the evolution of a geologic system in a realistic manner, without concerns about numerical instability problems. In the explicit, dynamic solution scheme, the full dynamic equations of motion are included in the formulation, and the static equilibrium state is reached by absorbing the energy in the system through inertial terms added in the formulation.

The EDS scheme allows the implementation of strongly nonlinear constitutive models because the general calculation sequence allows the field quantities (velocities/displacements and forces/stresses) at each element in the model to be physically isolated from one another during one calculation step. The general calculation sequence for

the EDS scheme is illustrated in Figure 3.1. The figure presents the calculation sequence of one loop calculation for one time step and for each tetrahedron element. In each sequence loop of the time step, the calculation solves two sets of equations: equilibrium of motion and constitutive relationships. The former is invoked to derive the new velocities and displacements from stresses and forces at each mass point. By application of the Gauss divergence theorem to the tetrahedron element, the derived velocities at each mass point are used to express the strain rates of the tetrahedron element. Then, the constitutive equations are used to calculate new stress from strain rates. The key feature here is that each box in Figure 3.1 updates all model variables from known values that remain fixed while control is within that box. For example, the lower box takes the set of velocities already calculated and, for each tetrahedron element, computes new stresses. The velocities and other variables are assumed to be frozen for the operation of the box, i.e., the newly calculated stresses do not affect the existing velocities. The assumption is valid provided the time step is so small that the calculated variables cannot propagate from one element to another during this time step. This EDS approach makes the implementation of the non-linear constitutive model possible. All inputs of strain rates and other variables in one tetrahedron element, during the time step, they are fixed and not affected by the calculations in other elements. The stress increment calculation from strain rate is straightforward and there is no need to use any iteration process even if the constitutive law is highly nonlinear.
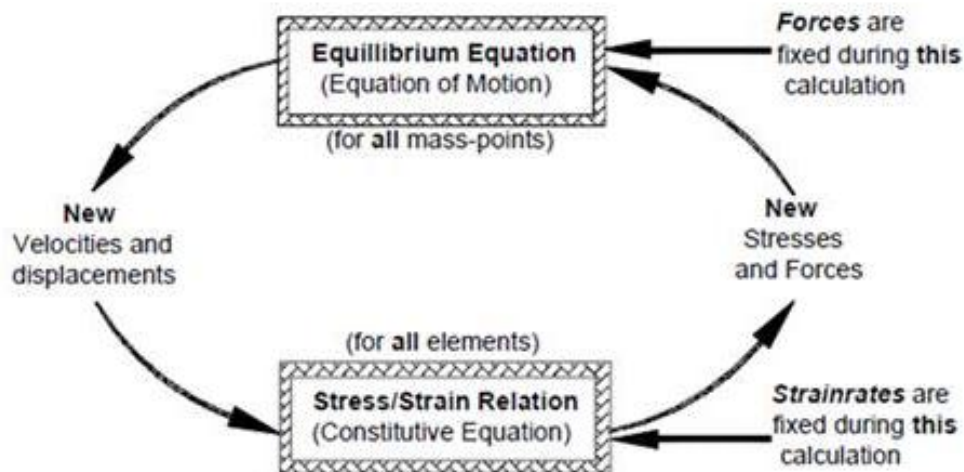
Figure 3.1: Calculation loop of EDS scheme in FLAC 3D

3.3.3 Mechanical Time Step for Numerical Stability

In FLAC 3D software, the idealized medium in the system is viewed as an assembly of point masses (located as the nodes) connected by linear springs. It was found from studying the oscillating mass-spring system with a finite difference scheme that a time step must be used that does not exceed a critical time step related to the minimum eigen period of the total system. Similarly, The EDS scheme in implementing non-linear constitutive models requires that the time step is so small that the calculated variables cannot propagate from one element to another during the time step. Hence, the stability criterion for the numerical scheme must provide an upper bound for the values of the time steps used in the finite difference scheme.

In FLAC 3D, a characteristic of the numerical scheme is that a uniform unit time step is adopted for the whole system. And, the nodal masses in the motion equations are taken as variables and adjusted to fulfill the local stability conditions.

The one-dimensional, one series mass-spring system governed by the differential equation

$$-kx = m\frac{d^2x}{d^2t}$$

(3.1)

where k is the stiffness of the spring, and m is the point mass. The critical time step corresponding to a second-order finite difference scheme for the equation is given by

$$\Delta t = \sqrt{\frac{4m}{k}}$$

(3.2)

For an infinite series spring-mass case, the limit-stability criterion has the form

$$m = k(\Delta t)^2$$

(3.3)

By selecting $\Delta t = 1$, the system will be stable if the magnitude of the point mass is greater than or equal to the spring stiffness. In FLAC 3D, the validity of Equation 3.2 is extended to one tetrahedron by interpreting m as the nodal mass contribution ml at local node l and k as the corresponding nodal stiffness contribution kl. The nodal mass contribution as derived from the infinite series criterion provides an upper-bound value for the system under consideration. In order to obtain a stable numerical scheme, the nodal mass contribution should be given a value that is equal to or larger than the nodal stiffness contribution. By a simple diagonalization technique of the local stiffness matrix, the nodal stiffness contribution at local node l is given by

$$k_{qq} = \frac{\alpha_1}{9V} \left[n_q^1 S^1 \right]^2$$

(3.4)

where, K is the bulk modulus, and G is the shear modulus. No summation is implied on repeated index q of k_{qq}, which runs from 1 to 3. Then the upper-bound value for the nodal stiffness contribution can be expressed as:

$$k^1 = \max(k_{11}, k_{22}, k_{33})$$

(3.5)

which yields the expression for the tetrahedron mass contribution at node l:

$$m^1 = \frac{\alpha_1}{9V} \max \left(\left[n_i^l S^l \right]^2, i = 1, 3 \right)$$

(3.6)

to provide a numerically stable solution.

3.4 Material Models

3.4.1   Soil Model

The primitive radial cylinder mesh, which is basically radially graded mesh around a cylindrical plate or footing, was used to simulate the soil model of 1m width, 1m breadth and 0.9m depth as shown in the Figure 3.2. It has twelve reference points with four size entries and four dimension entries.
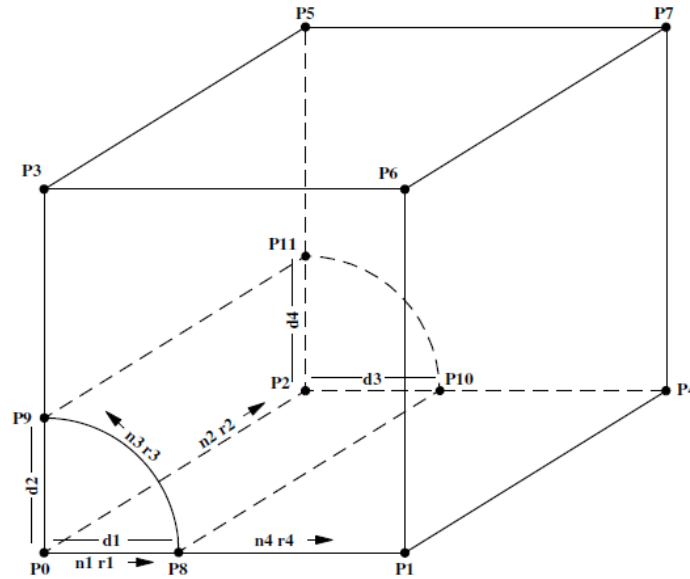
Figure 3.2: Radial cylinder mesh used in FLAC 3D

The elastic-perfectly plastic Mohr-Coulomb model was used to model sand layers in the numerical simulation. Mohr-Coulomb criterion with tension cutoff is used as the failure

criterion in FLAC 3D. The position of a stress point on this envelope is controlled by a non-associated flow rule for shear failure, and an associated rule for tension failure. The Mohr-Coulomb criterion in FLAC 3D is expressed in terms of the principal stresses σ_1, σ_2 and σ_3 which are the three components of the generalized stress vector for this model (n = 3). The components of the corresponding generalized strain vector are the principal strains ε_1, ε_2 and ε_3.

3.4.2 Geocell Model

To model geocell, geogrid structural elements are used as shown in the Figure 3.3 which are three-noded, flat, finite elements that are assigned a finite element type that resists membrane but does not resist bending loading. These elements will behave as an isotropic, linearly elastic material without failure limit. Wide width tension test was performed on the geocell material and the elastic modulus of the geocell material was determined from tensile stress-strain response. The secant modulus was determined corresponding to 2% axial strain. The interface properties of the geocell and the soil is incorporated in this model by providing interface shear modulus and interface friction angle as two third of the cohesion and friction angle of the infill material.
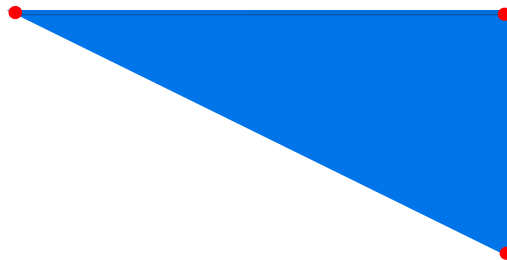
Figure 3.3: Three nodded geogrid element used to model the geocell in FLAC 3D

3.4.2.1 Diamond Shape

Initially, diamond shaped geocell was modeled by creating soil zones using degenerated-wedge shaped mesh. The quarter zone was modeled first and then using the symmetry, the complete diamond shape was created. The geocell dimensions were taken as 0.2m for smaller diagonal, 0.3m for larger diagonal 0.2m and the height of the geocell was maintained as 0.2m. Geogrid element was placed at the surface of this diamond shaped zone and then the zone was removed there by obtaining the geometry of diamond shaped geocell

24

as shown in the Figure. Only eight geogrid elements were used to create one diamond shaped geocell and a total of 48 elements were used to model the geocell mat of eight diamond shaped geocell as shown in the Figure 3.4.
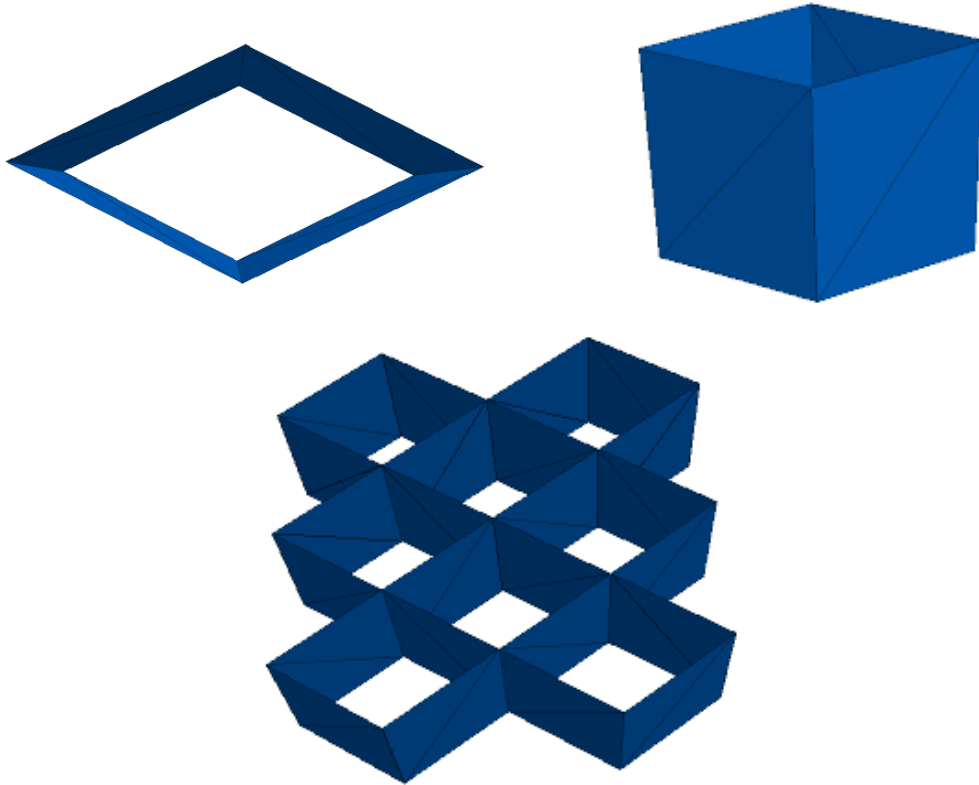
Figure 3.4: Diamond shaped geocell model in FLAC 3D

3.4.2.2 Primitive Honeycomb Shape

In order to simulate the actual shape of geocell, a primitive honeycomb shape was modeled by combining two different mesh zones- namely cylindrical mesh and degenerated wedge mesh. The curved portion of the geocell was modeled using the cylindrical mesh and the two angular ends of the geocell were modeled using degenerated wedge mesh. The width of the geocell is maintained as 0.3m in x-direction and 0.2m in y-direction as 0.2m respectively as shown in the Figure 3.5. 32 geogrid elements were used to model one geocell and a total of 192 elements were used to model the mat of geocell with eight geocells.
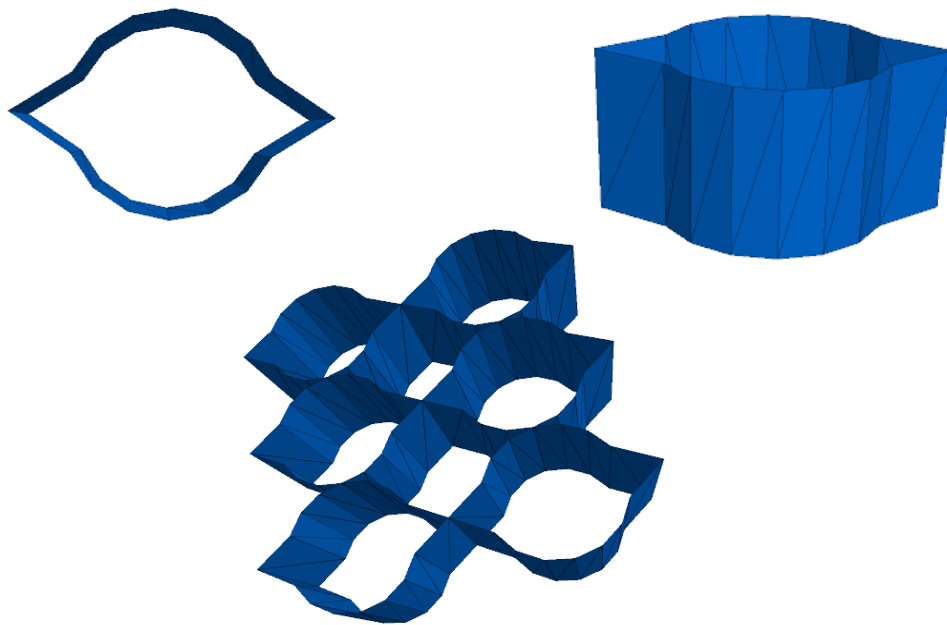
Figure 3.5: Primitive honeycomb shaped geocell model in FLAC 3D

3.4.2.3 Honeycomb Shape

Two cylindrical mesh zones are used to simulate the actual honeycomb shape of the geocell. The curved shape of the geocell was modeled using the cylindrical mesh zone of radius 0.075m and the corners are modeled using cylindrical mesh zone of radius 0.075m in x-direction and 0.15m in y-direction respectively as shown in Figure 3.6.
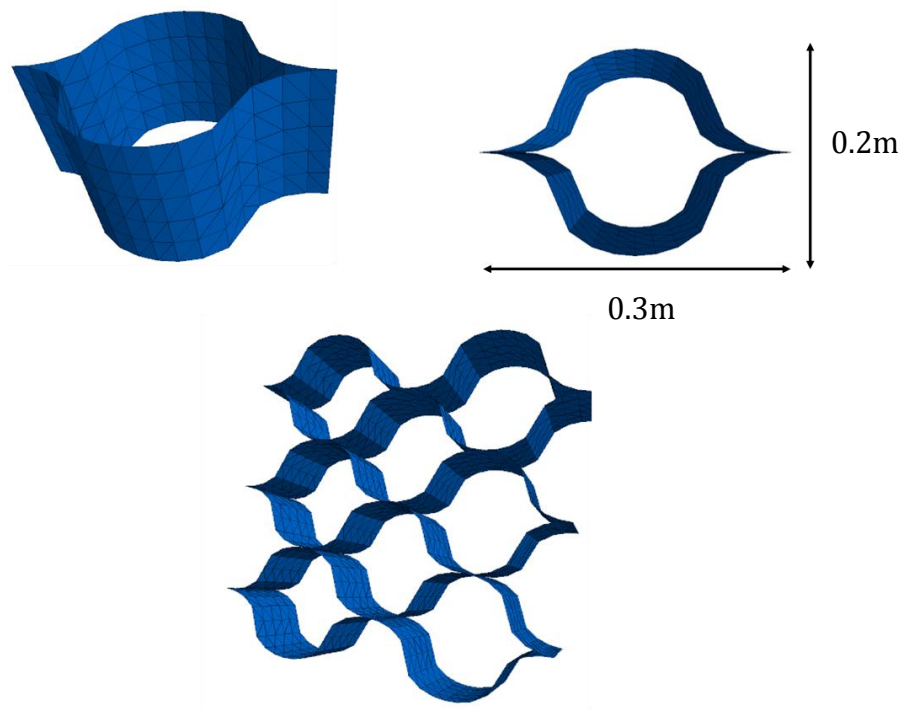
Figure 3.6: Honeycomb shaped geocell model in FLAC 3D

The number of geogrid elements required for modeling a single geocell was kept as 192 in order to ensure proper transfer of stresses between soil and geocell. The honeycomb shaped geocell model is showed in the Figure 3.6.

3.4.2.4 Comparison of Performance of different geocell

The effect of geocell in the ultimate bearing capacity of the geocell reinforced sand bed was also studied numerically. Three different shapes were used for the analysis- diamond, primitive honeycomb and actual honeycomb. The comparison of performance of different geocells are shown in Figure 3.7. It can be observed that the diamond shaped geocell performs less as compared to the actual honey comb shape. It is because of the stress concentration occurring at the corners of the diamond shaped geocell which will be considerably less in the case of actual honeycomb shape because of its curved shape.
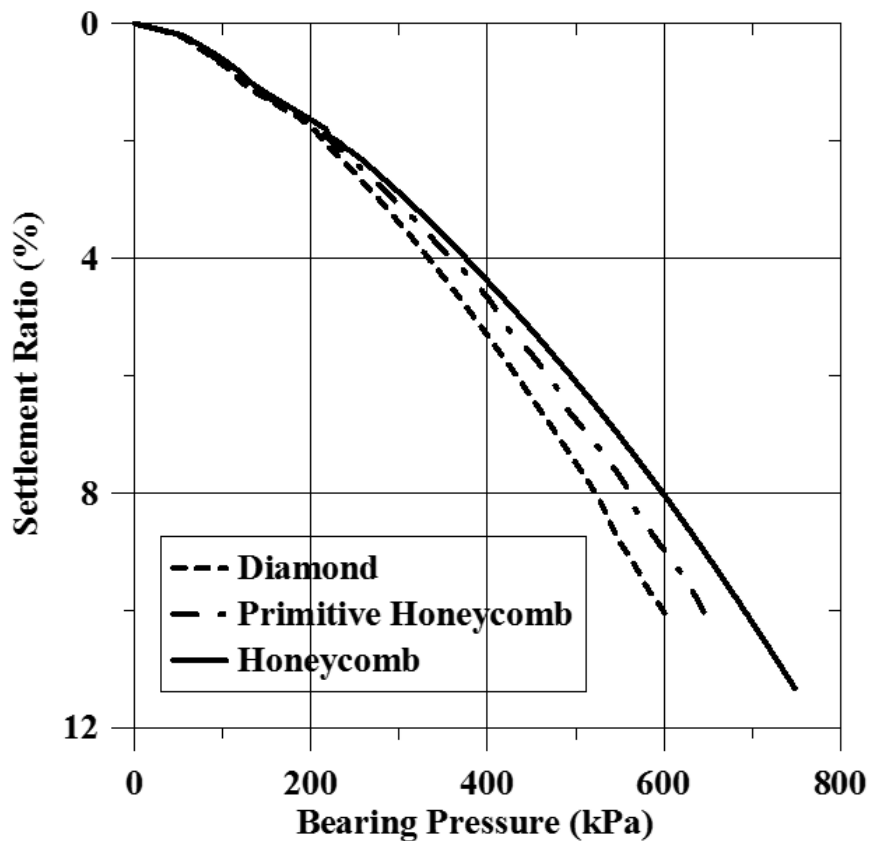
Figure 3.7: Comparison of performance of different geocell

3.5 Validation of Geocell Model using Large Triaxial Test

3.5.1 Overview

To validate the geocell reinforcement modeled using FLAC 3D software, numerical modeling of the large triaxial test shown in Figure 3.8 was simulated using FLAC 3D software. The model dimensions and the properties of the materials were adopted from the large diameter triaxial tests performed by Asha M. Nair and G. Madhavi Latha (2014). The stress-strain plots obtained from the numerical analysis were compared with the experimental results of large diameter triaxial test.
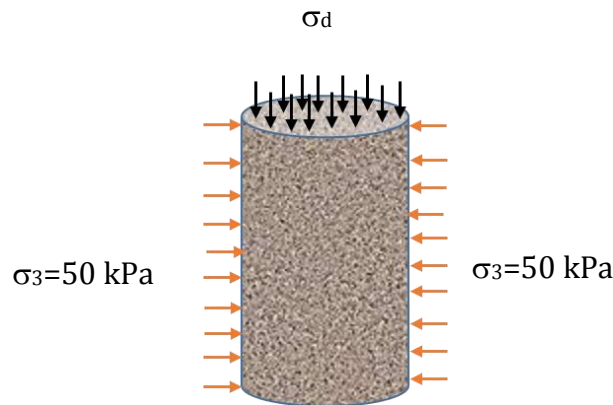
Figure 3.8: Large triaxial test model

3.5.2 Material Models and Parameters

3.5.2.1 Aggregate

A mixture of granular materials of various size ranges which conforms to Grade III of granular sub-base design as given by MORD specification was used for the experiment. To simulate the same, the elastic-perfectly plastic Mohr-Coulomb model was used with the material properties listed in the Table 3.1.

Table 3.1: Aggregate material properties (Asha M Nair and Madhavi Latha, 2014)

Properties	Aggregate
Model	Mohr-Coulomb
Bulk modulus (Pa)	18e6
Shear modulus (Pa)	11.2e6
Friction angle (degree)	43.57
Cohesion (kPa)	28.5
Dilation (degree)	8
Density (kg/m^3)	2060

3.5.2.2 Geotextile Geocell

Geogrid structural element is used to model geocell which are three-noded, flat, finite elements that are assigned a finite element type that resists membrane but does not resist bending loading. These elements will behave as an isotropic, linearly elastic material without failure limit.

The parameters used for modeling geocell reinforcement and the dimensions of the geocell used is given in the Table 3.2 and Table 3.3 respectively. Only single geocell is modeled in order to simulate the experimental setup. The geocell was placed on the cylindrical surface of the large triaxial test model and the test was simulated.

Table 3.2: Geocell properties (Asha M Nair and Madhavi Latha, 2014)

Properties	Geocell
Model	Linear Elastic
Young's modulus (Pa)	18e6
Poisson's Ratio	11.2e6
Interface Friction angle (degree)	43.57
Interface Cohesion (kPa)	28.5
Interface Shear Modulus	8

Table 3.3: Geocell dimensions (Asha M Nair and Madhavi Latha, 2014)

Dimensions of Geocell	
Width (mm)	300
Length (mm)	300
Height (mm)	600

3.5.3   Modeling of Triaxial test using FLAC 3D

Numerical models of large diameter triaxial tests were modeled in FLAC 3D and the model is validated by comparing the simulation results with the experimental results given in the study of Asha M. Nair and G. Madhavi Latha (2014). The constitutive models and the parameters used in modeling have been discussed in the previous sections.

3.5.3.1 Numerical Mesh and Boundary Conditions

Large diameter triaxial test were simulated in FLAC 3D by modeling a cylindrical sample of diameter 0.3 m and height 0.6 m. Cylindrical mesh is adopted to model the soil specimen. The vertical and lateral movements were fixed at the bottom boundary of the cylindrical model and the cylindrical surface of the model was kept free by allowing horizontal and vertical deformations on the sample under loading. Two simulations were performed- one without reinforcement and one with geocell reinforcement. Both the simulations were carried out at a confining stress of 50 kPa. An axial load was applied as velocity boundary at the top surface at a rate of 2.5*106 m/step. The model was solved for 75000 iteration steps until the vertical displacement on the top of the soil reached 10 percentage of the model diameter (= 30 mm). The triaxial model used for the simulation is shown in Figure 3.9.
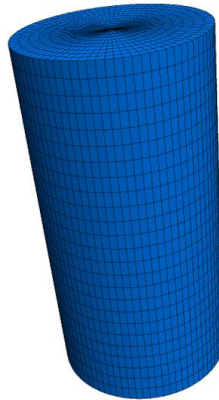
Figure 3.9: Large triaxial test model in FLAC 3D

3.5.3.2 Validation using Experimental Results

The stress-strain graphs were plotted and compared with the experimental results given in the study of Asha M. Nair and G. Madhavi Latha (2014) for validation of the geocell model. Overall, the numerical model well simulated the stress-strain plots of the unreinforced and geocell reinforced sand. The comparison of the experimental and numerical results of unreinforced and geocell reinforced models are plotted in Figure 3.10 and Figure 3.11 respectively. Even though Mohr-Coulomb model is used as the aggregate model instead of actual parabolic nature of aggregates, the model well simulated the initial modulus of the model and the final ultimate bearing pressure. Figure 3.12 shows the comparison of numerical results obtained for unreinforced and geocell reinforced cases.
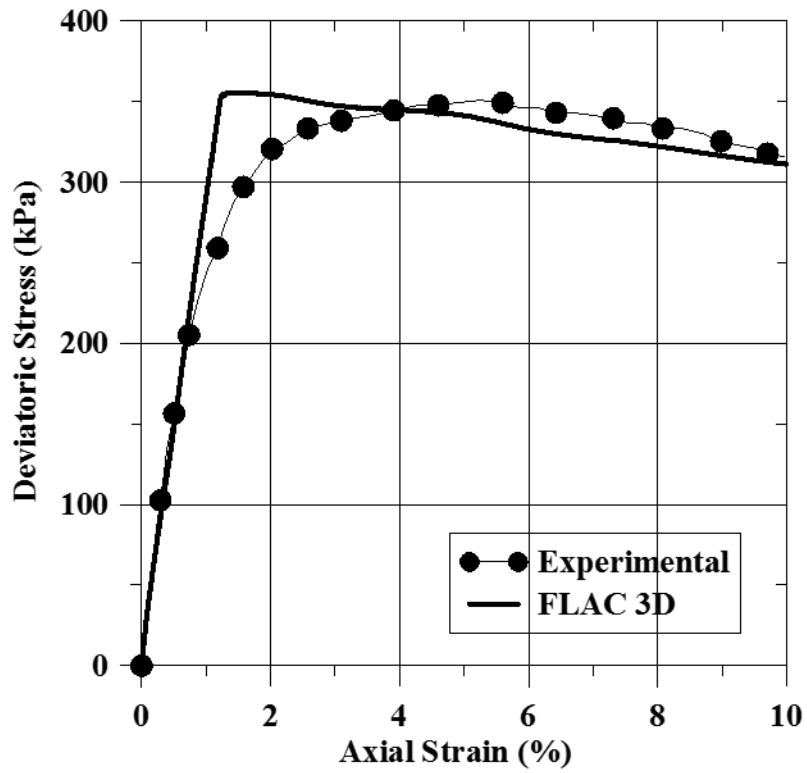
Figure 3.10: Deviatoric stress vs. axial strain - validation of unreinforced sand model
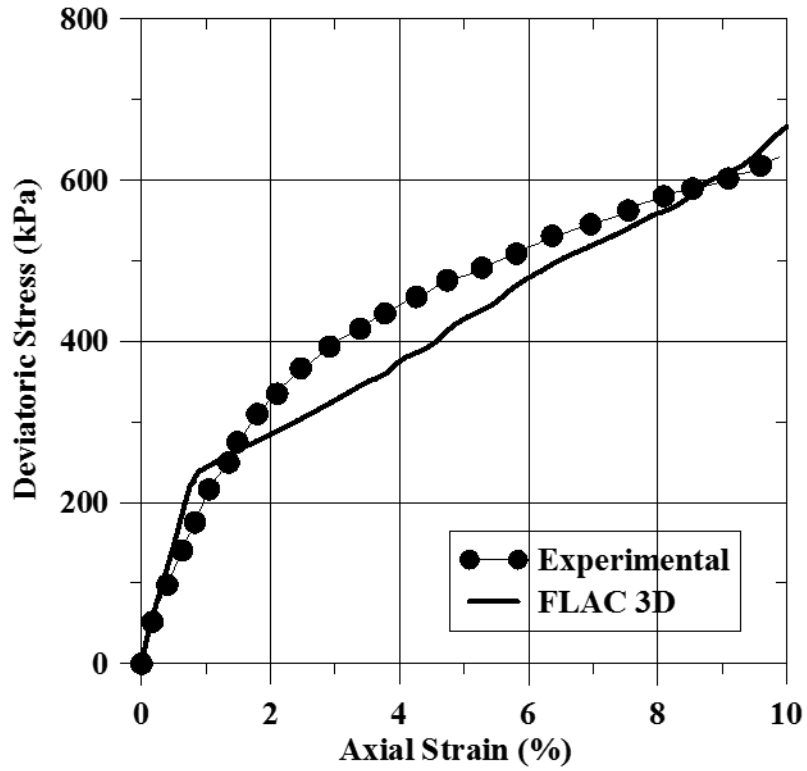
Figure 3.11: Deviatoric stress vs. axial strain - validation of geocell reinforced sand model

31
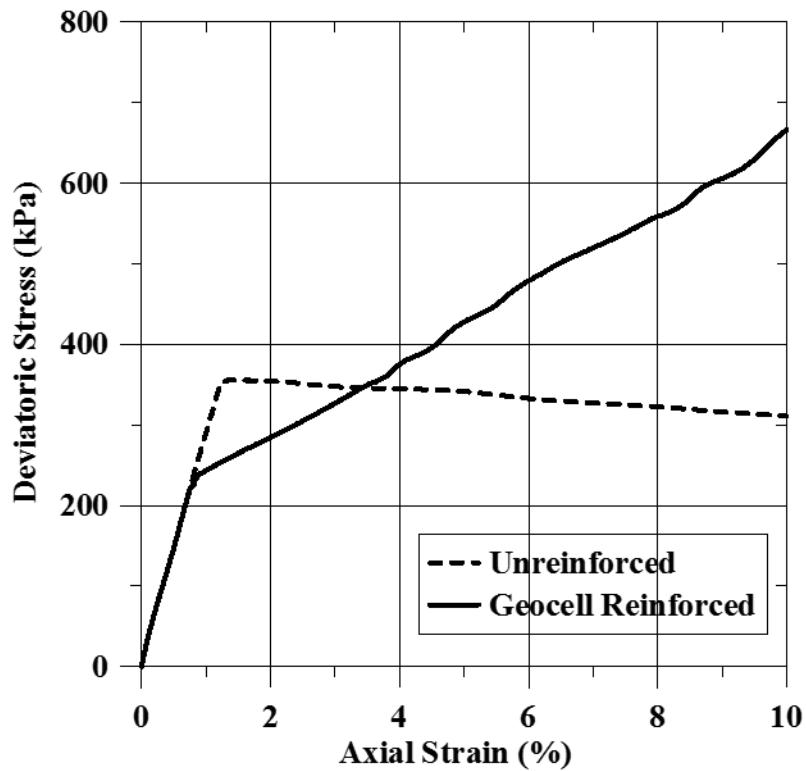
Figure 3.12: Deviatoric stress vs. axial strain – Bearing pressure comparison plot

3.6 Summary

This chapter discusses the modeling of natural honeycombed shape of geocell and validation of the geocell model using large triaxial test. The major conclusions from this chapter are:

(1) The three dimensional honeycomb structure of geocell was modeled by maintaining the actual curvature of the geocell.

(2) The model well simulated the initial modulus of the aggregate and the ultimate stress developed in the model by adopting Mohr-Coulomb as the material model instead of actual parabolic nature of the aggregates.

(3) Three different shapes of geocell such as diamond, primitive honeycomb and honeycomb shape were modeled and the honeycomb shaped geocell is found to simulate the actual behavior of geocell to a greater extend.

Chapter 4

Numerical Modeling of Geocell Reinforced Homogeneous Sand Beds

4.1 Overview

The modeling of honeycomb shaped geocell was discussed in section 3.4.2.3 of Chapter 3. In this Chapter the confining mechanism of geocell reinforced homogeneous sand bed is studied by carrying out numerical analysis using finite difference software FLAC 3D under static loads. The results obtained from the simulations were validated using the independent experimental results obtained from a large scale laboratory testing conducted at geotechnical laboratories of IIT Hyderabad. The definition sketch of the geocell reinforced sand bed model used for the experimental study is shown in the Figure 4.1. Numerical simulations were performed to model the test setup along with the geocell reinforcement in FLAC 3D. The material properties used for the simulations are obtained from the experimental data.

In the Definition sketch, D is the diameter of the loading plate which is 0.15m, H is the total height of the sand bed which is 0.9m, h is the height of the geocell reinforcement which is 0.2m and B is the width of the sand bed which is 1m as shown in the Figure 4.1.
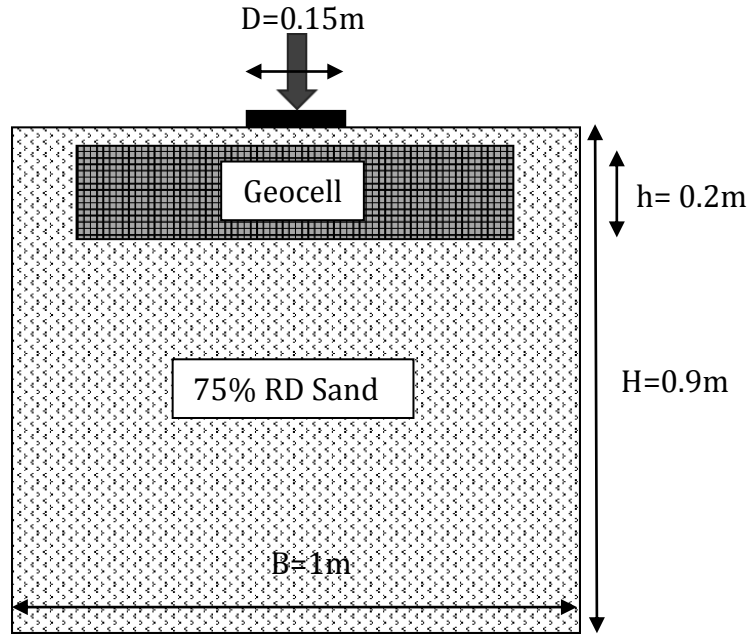
Figure 4.1: Geocell reinforced sand model

4.2 Material Models and Parameters

4.2.1 Sand

Based on the extensive literature review, the elastic-perfectly plastic Mohr-Coulomb model was used to model the behaviour of 75% relative density sand in the homogeneous beds. The model parameters used for the study is listed in Table 4.1. Shear strength properties (c and ϕ) of the sand were determined from the consolidated undrained triaxial compression tests. The tests were carried out at three different confining pressures of 50 kPa, 100 kPa and 150 kPa. The modulus of elasticity of the homogeneous sand was obtained from the large scale tank tests (from load-settlement data). The modulus of elasticity of the sand was found using Burmister elasctic layer theory as the confining stresses maintained in triaxial tests are much higher then the prevailed confining pressures in the large model test tank. The modulus of sand layer, E is given by

$$E = \frac{\pi \sigma_0}{2\Delta}(1 - v^2)$$

(4.1)

Where, σ_0 is the pressure applied on the surface of the plate, *r* is the radius of the plate, Δ is the deflection of the plate and v is the poisons ratio of the soil. From the elastic modulus, the

shear modulus and the bulk modulus values were determined by assuming the Poisson's ratio of 0.25.

Table 4.1: Material properties of sand and plate used in FLAC 3D

Properties	Sand	Plate
Bulk modulus (Pa)	5.0e6	1.4e11
Shear modulus (Pa)	3.0e6	8.04e10
Friction angle (degree)	40	-
Cohesion (kPa)	2.2	-
Dilation (degree)	8	-
Density (kg/m3)	1740	7.8e3

4.2.2   Geocell

Geogrid structural element is used to model geocell which are three-noded, flat, finite elements that are assigned a finite element type that resists membrane but does not resist bending loading. These elements will behave as an isotropic, linearly elastic material without failure limit. The elastic modulus of the geocell was determined from tensile stress-strain response. The secant modulus was determined corresponding to 2% axial strain. The interface shear strength properties (c_i and ϕ_i) for geocell were calculated as two third of the cohesion and friction angle of the infill material. The geocell used in the present study was having the rough texture on its surface.

The geocell model is shown in the Figure 4.2. The dimensions of the geocell used and the parameters used for modelling are given in the Tables 4.2 and 4.3 respectively. The procedure adopted for modelling geocell is explained in Chapter 3.

Figure 4.2: Honeycomb shaped geocell model in FLAC 3D

Table 4.2: Geocell material properties

Properties of Geocell	
Young's Modulus (MPa)	365
Poisson's Ratio	0.45
Interface shear Modulus (MPa/m)	2.36
Interface cohesion (kPa)	9.6
Interface friction angle (degrees)	27.28
Thickness (mm)	1.5

Table 4.3: Geocell dimensions used for modelling in FLAC 3D

Dimensions of Geocell	
Width (mm)	200
Length (mm)	300
Height (mm)	200

4.3   Modeling of Static Load Tests using FLAC 3D

Numerical models with and without geocell reinforcement were created in FLAC 3D and the model is validated by comparing the results from numerical simulation with the experimental results. The constitutive models and the parameters used in modeling have been discussed in the previous sections.

4.3.1   Numerical mesh and Boundary Conditions

The complete test box of the laboratory test with dimensions 1 m breadth, 1 m width and 0.9 m depth was modelled. The primitive mesh shape radial cylinder which is radially graded mesh around cylindrical-shaped footing was used to simulate the experimental test box setup. The use of radial cylinder mesh type was for ensuring the compatibility between footing and the soil. Vertical movement was fixed at the bottom boundary of the model, and horizontal movement was fixed at the four side boundaries. A velocity boundary (v=2.5*10-6 m/step) was applied at the top of the sand at a circular area having a diameter of 0.15 m. The model was solved for 12000 iteration steps until the settlement ratio at the top of the soil reached 10 percent. The numerical model of the unreinforced case used for the analysis is shown in the Figure 4.3.
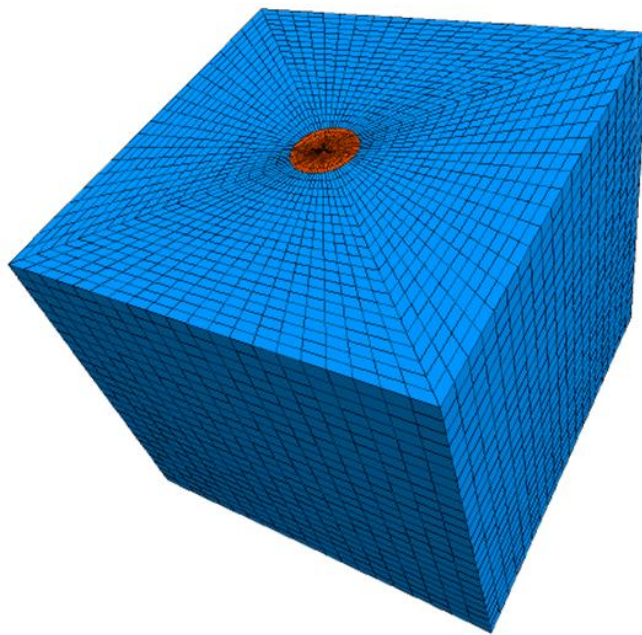
Figure 4.3: Soil model generated in FLAC 3D

In geocell reinforced bed case, geocell is placed by providing a clearance of 0.02m from the surface. The numerical model of geocell reinforced sand is shown in the Figure 4.4.
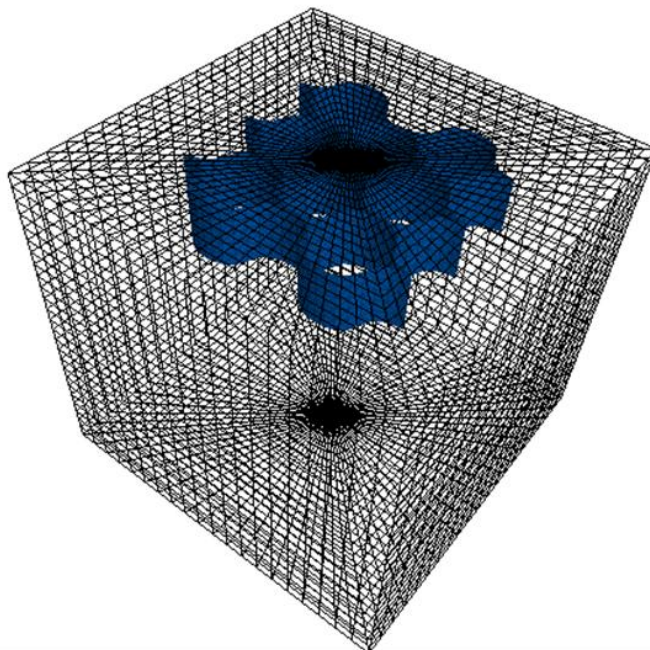
Figure 4.4: Geocell reinforced soil model in FLAC 3D

4.3.2 Experimental Validation

The variation of bearing pressure with settlement ratio was plotted and was compared with the experimental result for validation of the model. Overall, the numerical model well simulated the bearing capacities of the unreinforced and geocell reinforced sand. The comparison of the experimental and numerical results for the unreinforced and geocell reinforced cases are plotted and shown in Figure 4.5 and Figure 4.6 respectively. The comparison of the numerical simulation results of unreinforced and geocell reinforced case is plotted in the Figure 4.7. It can be observed that the geocell reinforcement improves the performance of the sand bed by 93%, 69%, 74% and 81% at settlement ratios of 1%, 3%, 5% and 9% respectively.
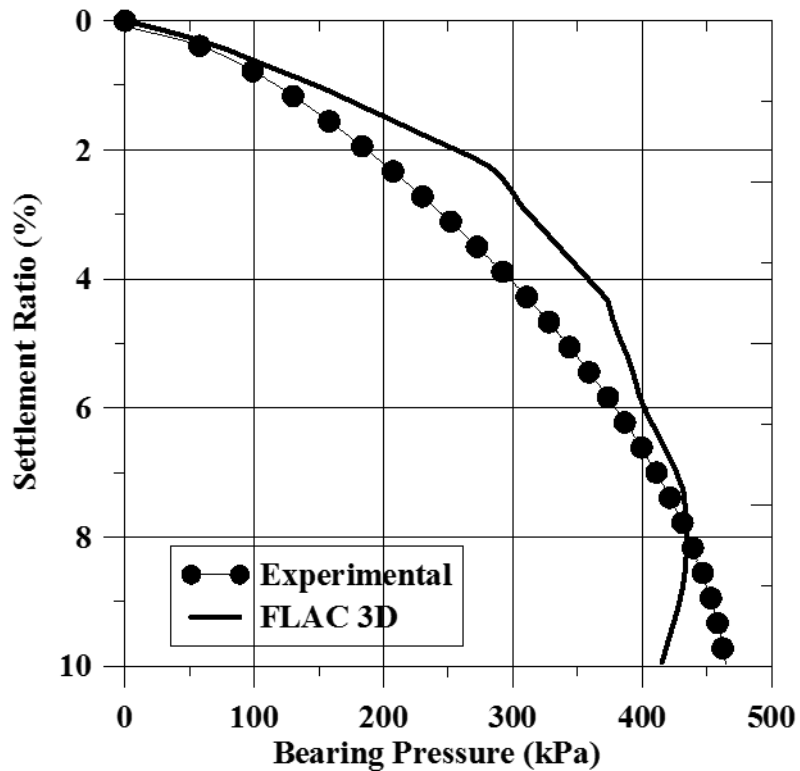
Figure 4.5: Bearing pressure vs. Settlement ratio curve for unreinforced case
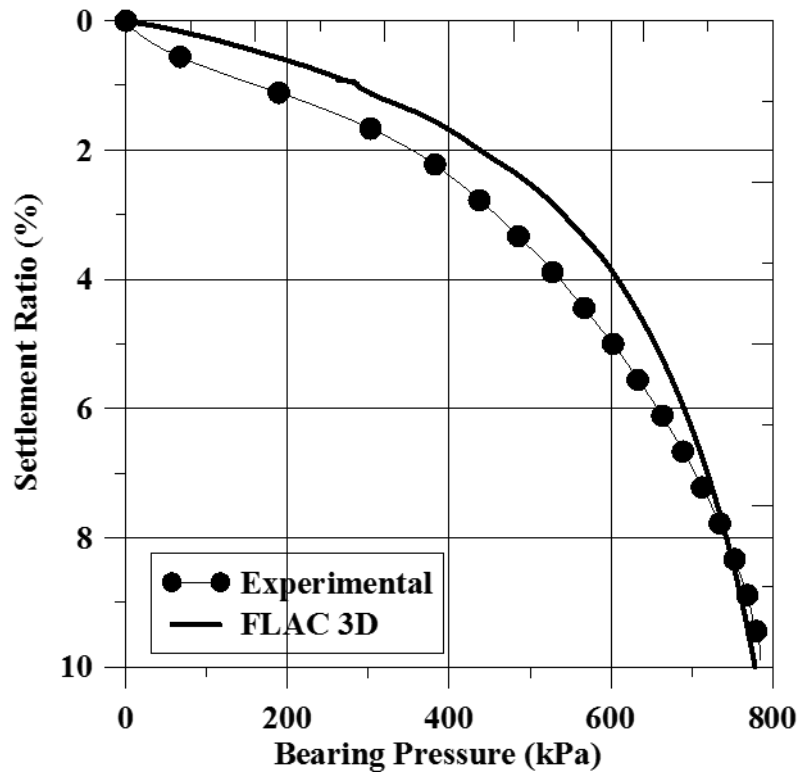
Figure 4.6: Bearing pressure vs. Settlement ratio curve for geocell reinforced case
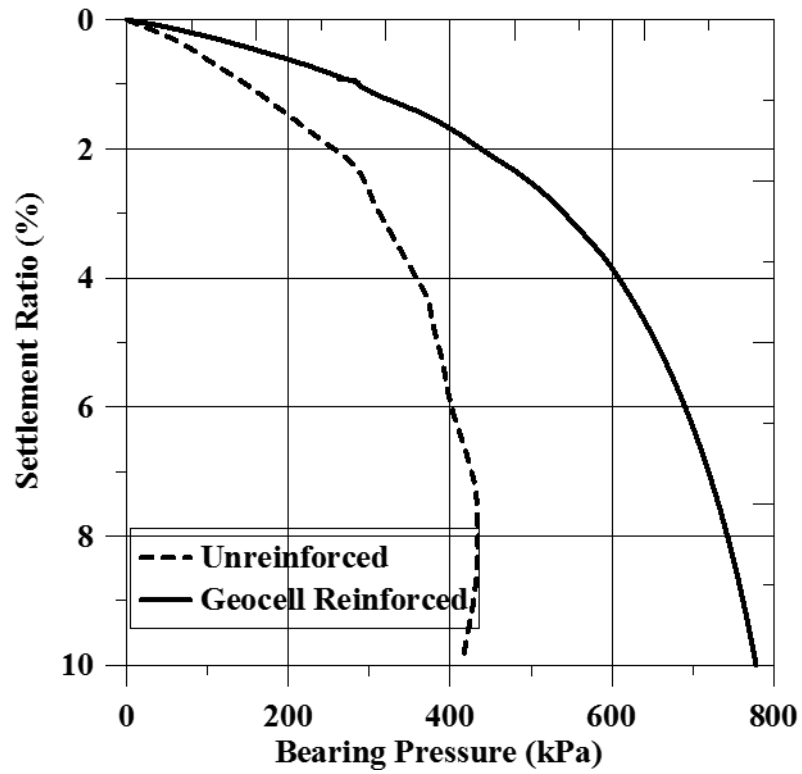
Figure 4.7: Comparison plot- Bearing pressure vs. Settlement ratio curve

4.3.3 Results and Discussions

The variation of horizontal stresses in both x-direction and y-directions at the mid height of the geocell were analysed as shown in the Figure 4.8 and Figure 4.9. The negative sign indicates compressive stresses and positive sign indicates tensile stresses. It can be observed that the stresses developed were maximum near the loading centre and it gradually reduces towards the boundaries of the model. The maximum stresses were observed in geocell 1 and 2 as shown in the Figure 4.8 and Figure 4.9 as the loading area is more in these two geocells as compared to others. The maximum horizontal stress developed in x-direction is 56.86 kPa and in y-direction is 56.48 kPa respectively.
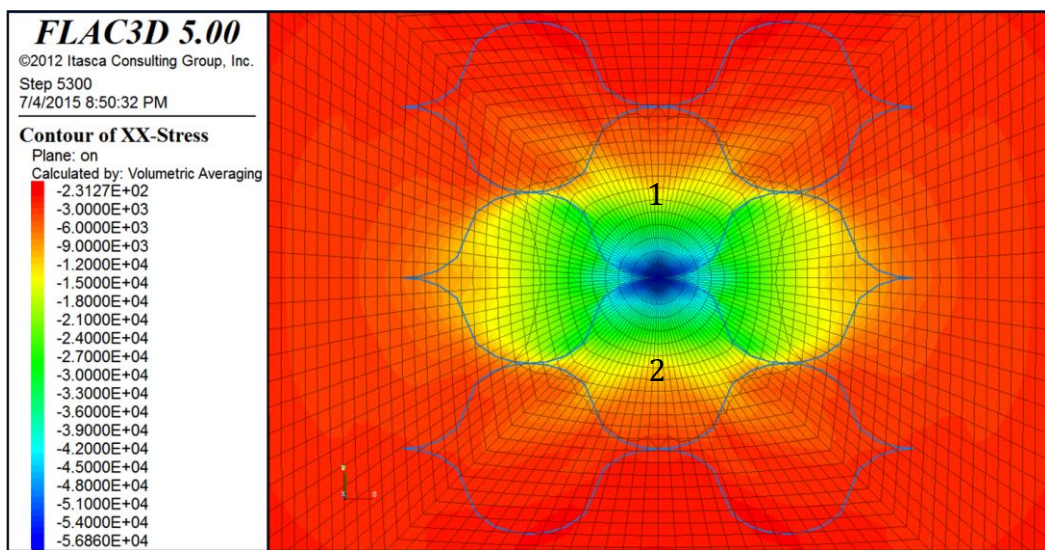
Figure 4.8: Horizontal stress in x-direction at mid height of geocell
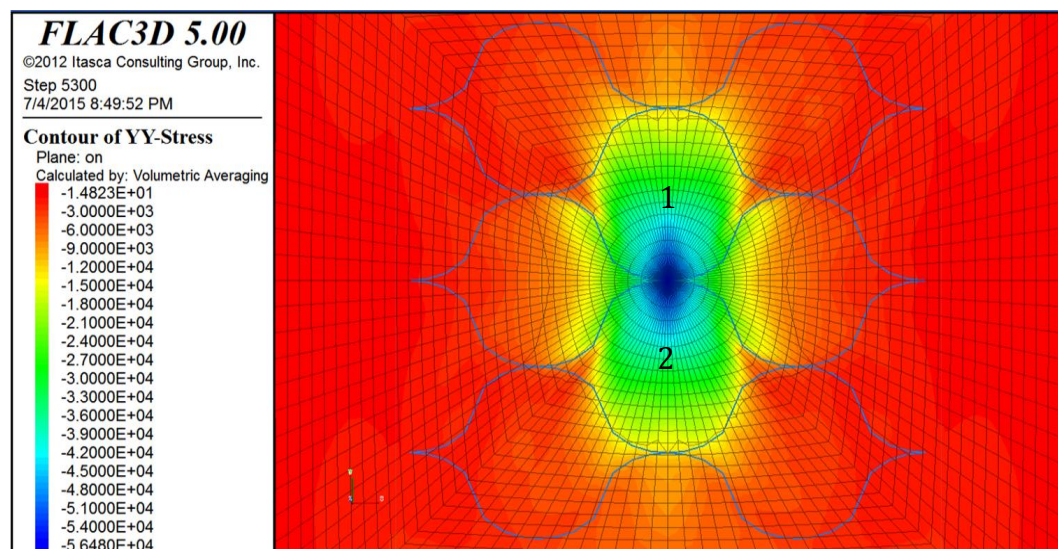
Figure 4.9: Horizontal stress in y-direction at mid height of geocell

40

For studying the confining mechanism in the geocell reinforcement, two sections such as section A-A and section C-C were considered and the variation of confining stresses developed in the infill soil across these two sections were studied. Confining stress variation is also plotted at four different h/D ratios, where h is the height of geocell and D is the diameter of the loading plate, to see the variation of confining stress with depth.

In Figure 4.10, the variation of confining stress along section A-A is shown. It can be observed that the confining stress is maximum near the centre of the loading and it gradually reduces towards the edges. The maximum confining stress of magnitude 90 kPa is developed at h/D ratio zero which is at the surface of the geocell reinforcement. The negative sign indicates the developed stresses are compressive in nature.
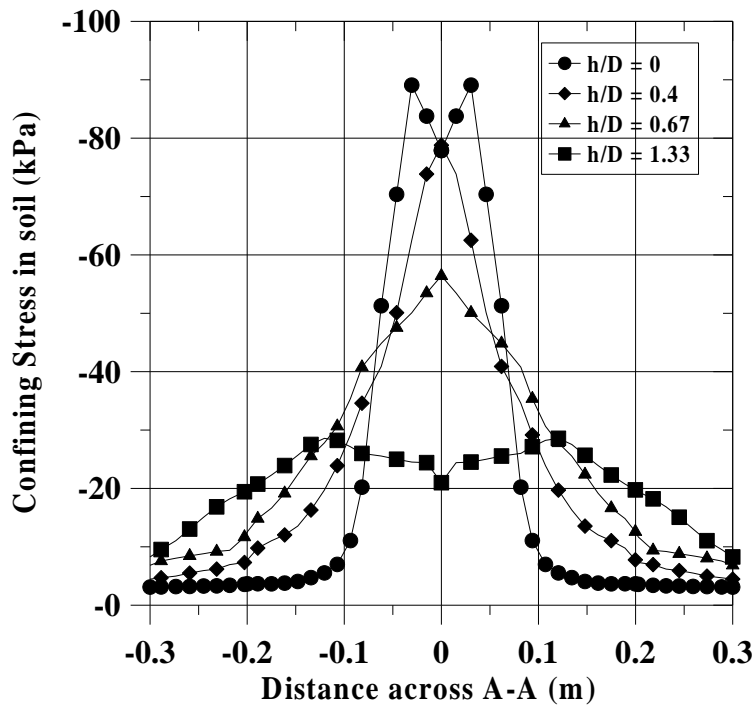
Figure 4.10: Variation of confining stress in the infill soil along section A-A at different h/D ratios

The confining stress variation in infill soil along section C-C is plotted in the Figure 4.11. The same trend along section A-A can be observed in this section. The maximum confining stress developed is 100 kPa and is nearer to the centre of the loading where h/B ratio is zero.
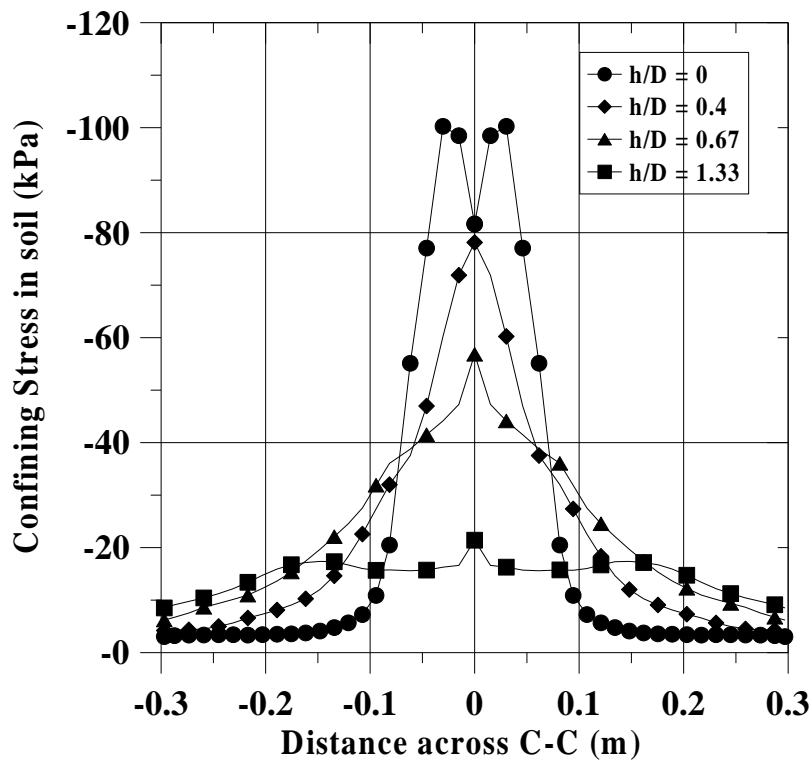
Figure 4.11: Variation of confining stress in the infill soil along section C-C at different h/D ratios

The displacement of the sand for unreinforced case is shown in Figure 4.12. It can be observed that the soil is moving radially outward under static loading and is represented using black arrows.
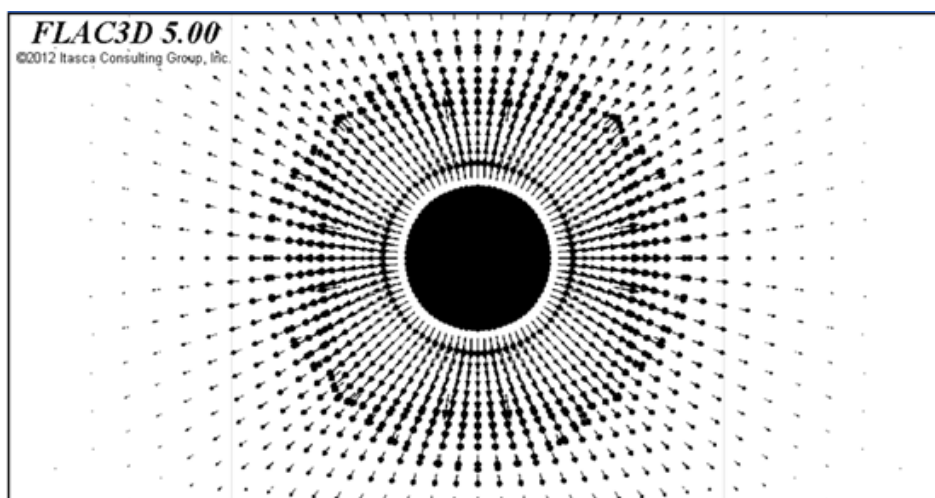
Figure 4.12: Displacement vector plot for unreinforced case

The displacement of the sand and geocell is shown in Figure 4.13. The red arrows represents the direction of movement of geocell reinforcement and the green arrows represents the direction of movement of soil under loading. It can be observed that under monotonic loading, the soil is moving radially outwards and this movement is restrained by the geocell walls. This will result in the development of confining stresses in geocell wall as well as in the infill soil. This will improve the performance of the geocell reinforced sand bed there by increasing the ultimate bearing pressure. It can also be observed that the confinement developed is more near the loading area and it goes on reducing towards the boundaries.
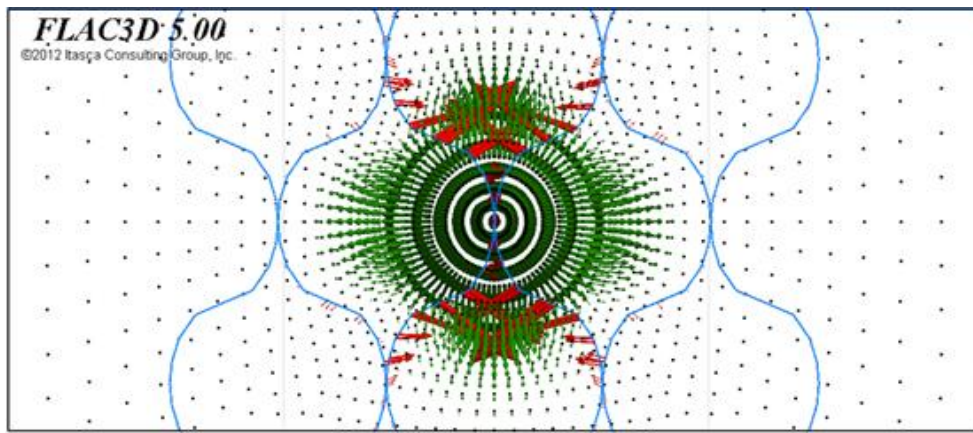
Figure 4.13: Displacement vector plot for reinforced case at mid height of geocell

Figure 4.14 shows the vertical displacement contour in the unreinforced and geocell reinforced models. It can be observed that the vertical movement is more in unreinforced case than in geocell reinforced case. In the reinforced case the vertical displacement was restrained by geocell and so the vertical displacement magnitude got reduced.
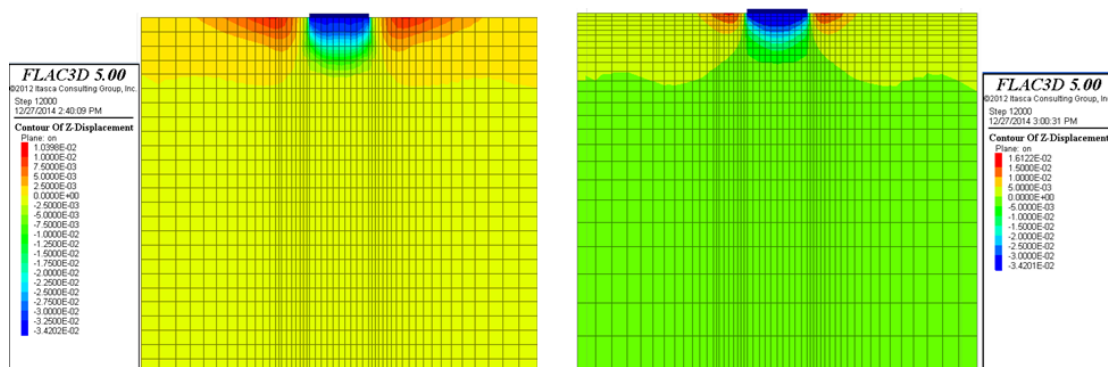
Figure 4.14: Comparison of vertical displacement (a) Unreinforced and (b) geocell reinforced

43

The vertical stress contour in the unreinforced and geocell reinforced case is shown in the Figure 4.15. It can be seen that the vertical stress magnitude has increased because of the geocell confinement under the same plate settlement of 30 mm. The maximum vertical stress developed in the unreinforced sand was 164.67 kPa. Whereas the maximum vertical stress developed at the geocell reinforced case was 387.1 kPa thereby improving the performance of the geocell reinforced sand bed.
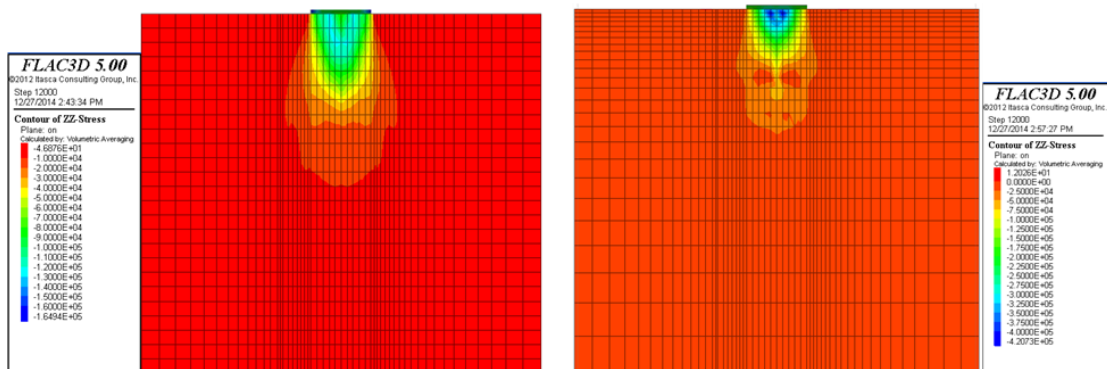
Figure 4.15: Comparison of vertical stress (a) Unreinforced and (b) geocell reinforced

4.4 Numerical Modeling of Single Geocell Reinforced Sand Bed

Numerical analysis were carried out by placing a single geocell in the homogeneous sand bed of 75% relative density to study the displacement mechanism of geocell reinforcement using finite difference software FLAC 3D.

4.4.1 Loading Patterns

Monotonic loading is applied on the surface of the sand bed using two loading plates of different diameters to study the behavior of geocell reinforcement. In the first case, the loading is applied through a plate diameter of 0.15m which is 20% less than the diameter of the geocell. In the second case, the loading is applied through a plate diameter of 0.4m which is 33.33% greater than the geocell diameter and the displacement mechanism is studied.

4.4.1.1 Loading Plate Diameter less than the Width of Geocell

The FLAC 3D model for the single geocell reinforced case with loading plate diameter of 0.15m is shown in the Figure 4.16. The geocell is placed at the center of the model and a velocity boundary of 2.85*10-6 m/step is applied through the loading plate and the displacement vectors at a settlement ratio of 10 percent is analyzed. Figure 4.16 shows the location of geocell reinforcement.
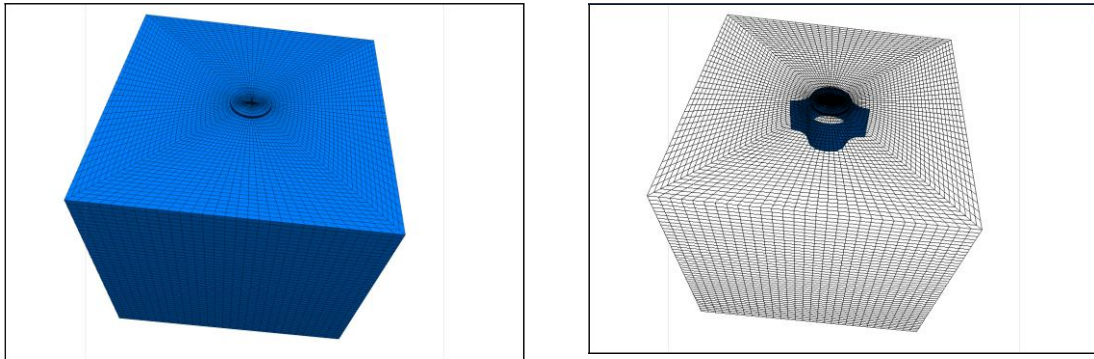
Figure 4.16: FLAC 3D model with single geocell reinforcement with 0.15m plate diameter

For studying the displacement behavior of geocell reinforcement under a loading area less than the diameter of geocell, two vertical sections A-A and C-C and one horizontal cross-section at the mid height of the geocell were considered as shown in the Figure 4.17, Figure 4.18 and Figure 4.19 respectively. It can be observed that the loading area is completely inside the geocell. The green arrows in the figure represents the direction of movement of soil and the red arrows represent the direction of movement of geocell wall.

Along section A-A, the movement of soil is taking place both in downward direction and radial direction. The radial movement of the soil is restrained by the presence of geocell walls which in turn results in the formation of confining stresses in the walls. It can also be observed that the geocell wall is moving radially inwards which further increases the confinement in the infill soil. Along section C-C, the same pattern of soil movement can be observed. But the movement of geocell is radially outward because of the outward movement of the soil. This can be clearly noticed in the Figure 4.19.
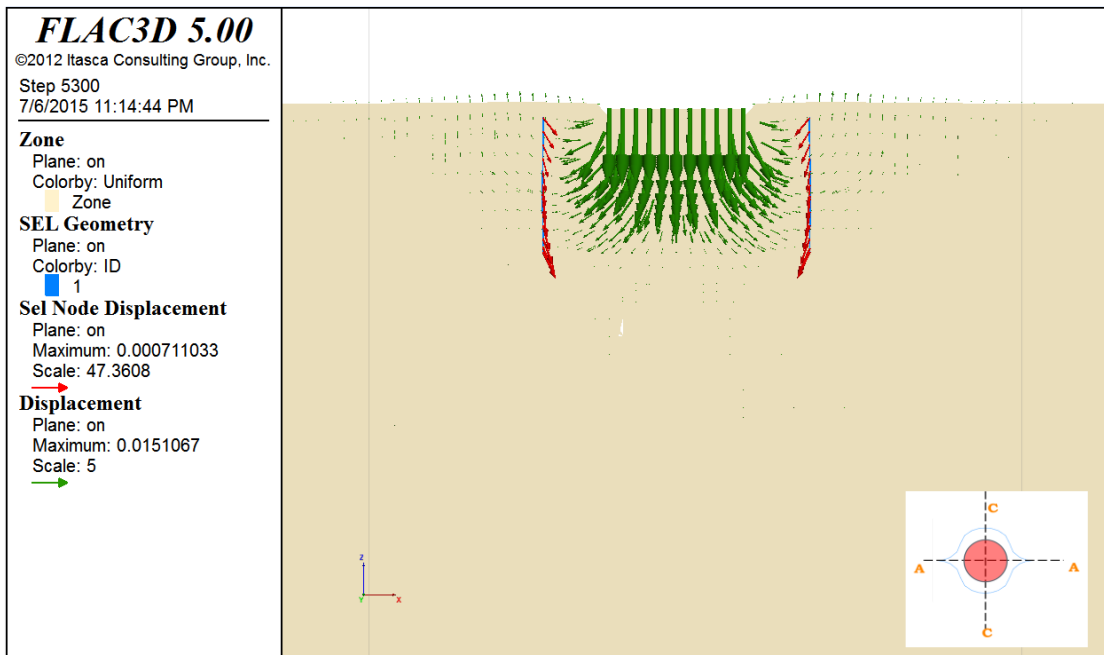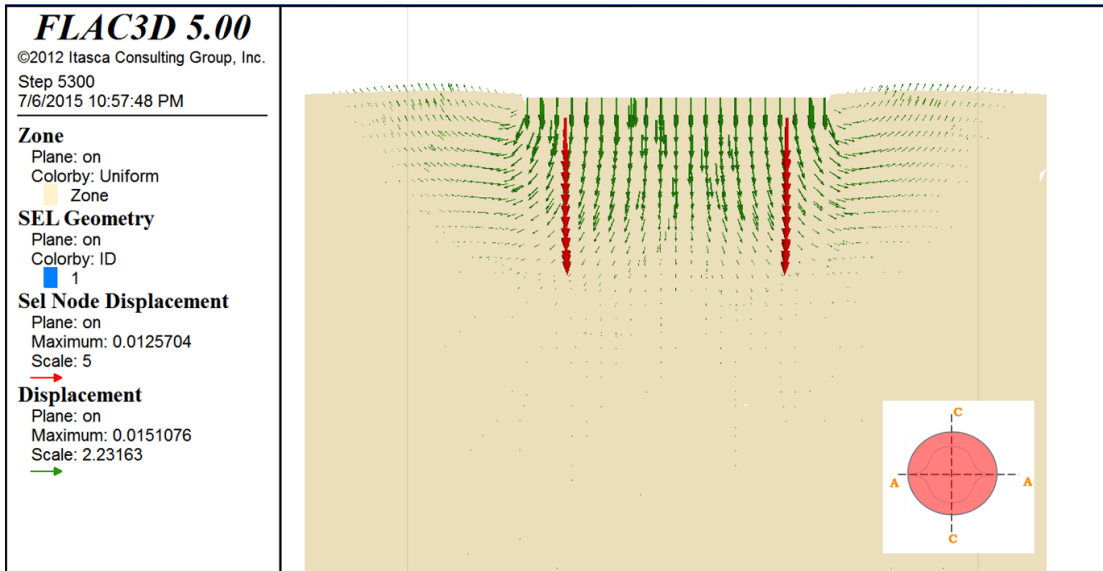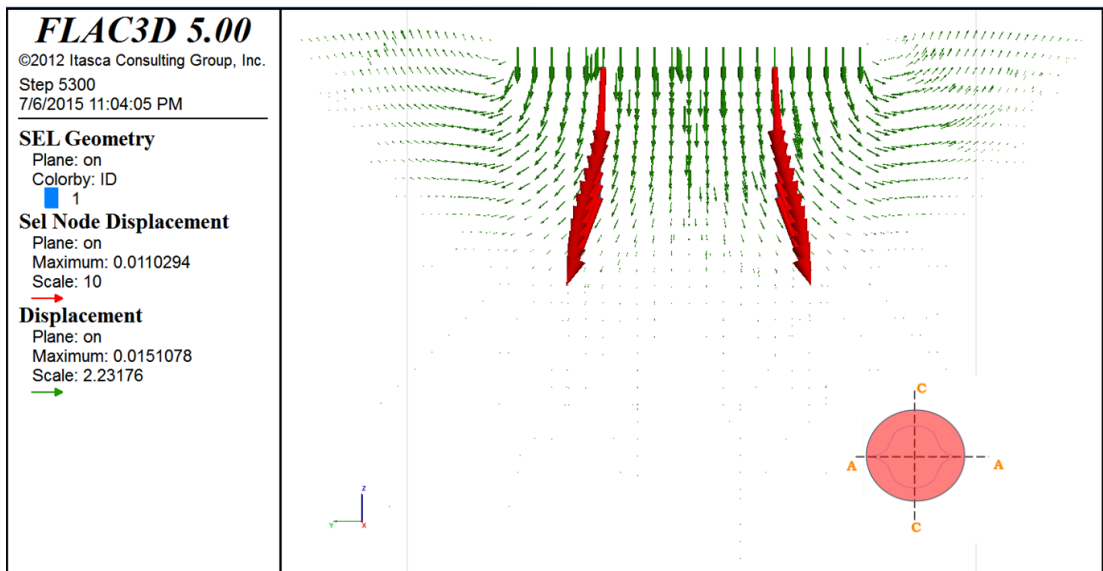
Figure 4.17: Vertical displacement vector plot along section A-A
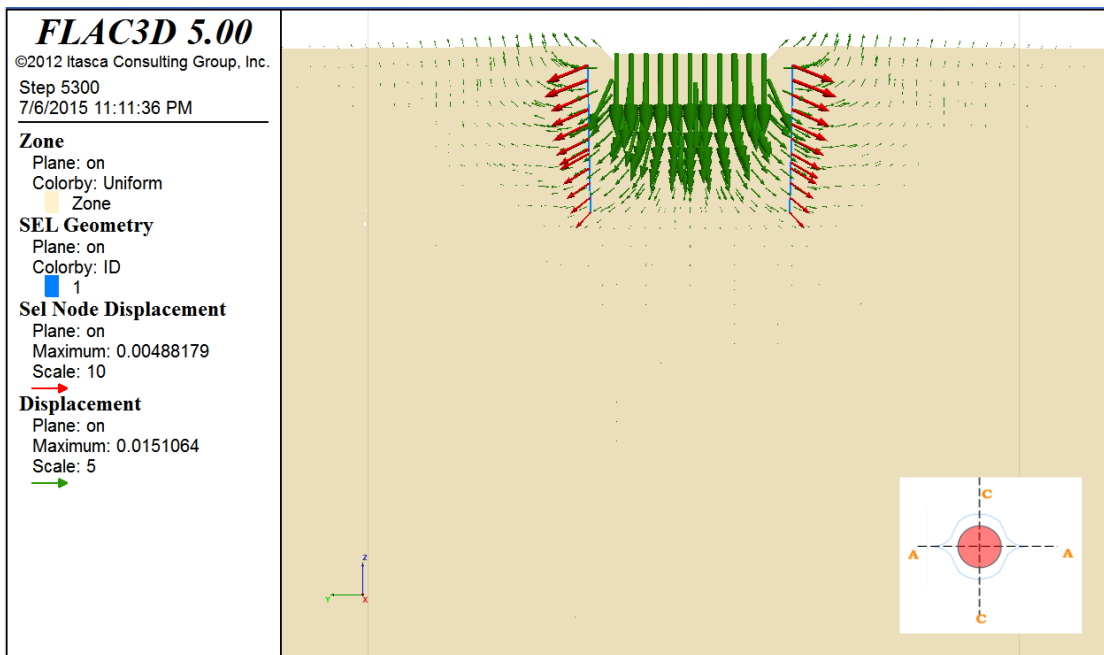
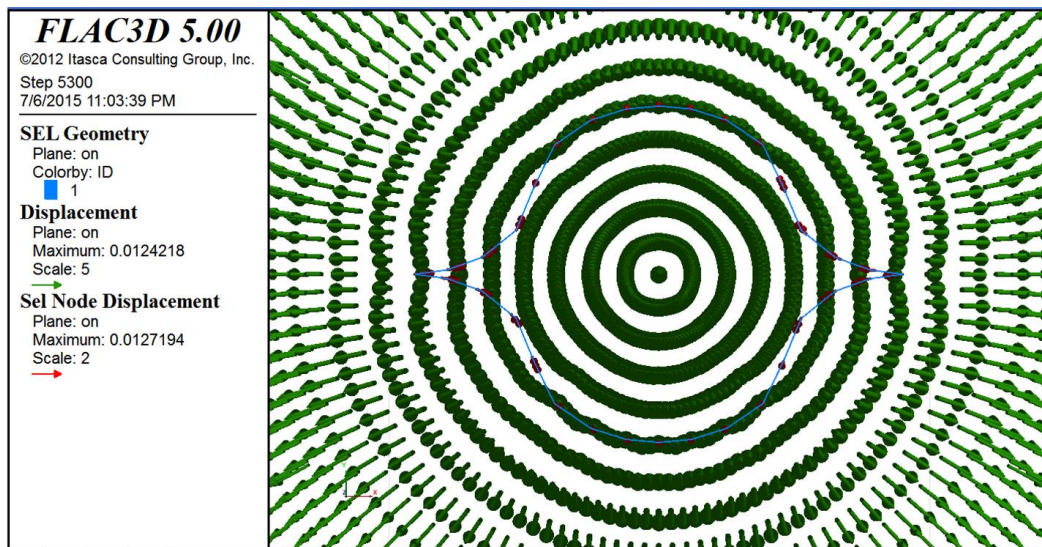**Figure 4.18: Vertical displacement vector plot along section C-C**
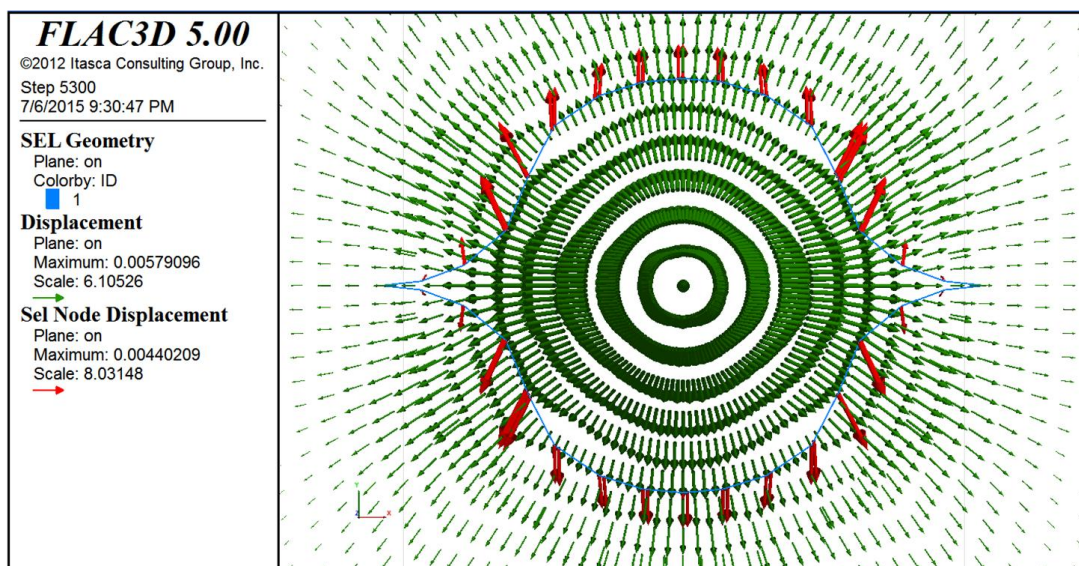
Figure 4.19: Displacement vector plot at mid-section of geocell

4.4.1.2 Loading Plate Diameter more than the Width of Geocell

Numerical simulations were performed in the previous model by increasing the diameter of the loading plate to 0.4m which is less than the diameter of the geocell reinforcement. A velocity boundary of $2.85*10-6$ was applied on the loading plate to simulate the monotonic loading condition. The model geometry and the location of geocell is shown in the Figure 4.20.
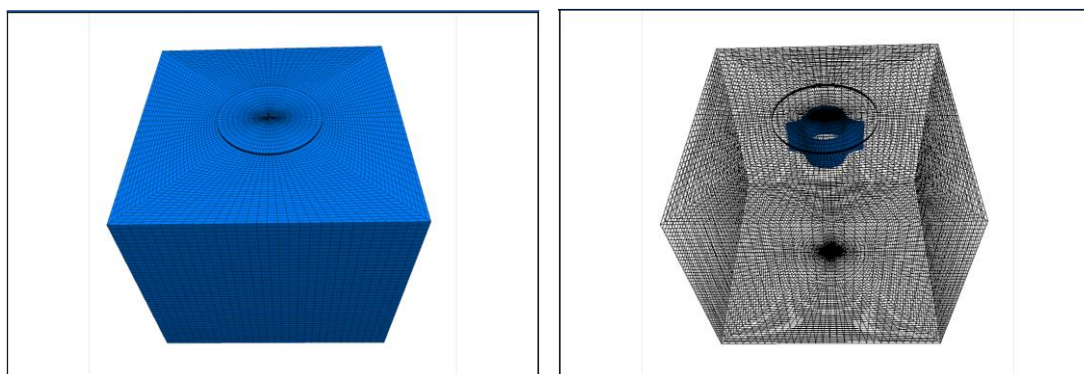
Figure 4.20: FLAC 3D model with single geocell reinforcement with a plate diameter of 0.4m

The displacement vectors are plotted by considering two vertical sections across the geocell and one horizontal cross-section at the mid height of the geocell. As the loading area is more than the diameter of geocell the displacement pattern observed is entirely different from the previous case. In section A-A, It can be noticed that the geocell reinforcement is moving downward along with the soil and in section C-C the geocell is slightly expanding along

47

normal direction to the plane of cut and simultaneously moving into the soil. This can be clearly visualized in the Figure 4.21, Figure 4.22 and Figure 4.23. The maximum displacement in geocell and soil are 1.27mm and 1.25mm respectively at the mid height of geocell.

Figure 4.21: Vertical displacement vector plot along section A-A

Figure 4.22: Vertical displacement vector plot along section C-C

Figure 4.23: Displacement vector plot at mid-section of geocell

4.5 Summary

This chapter describes the development of numerical model for geocell-reinforced granular soil under static load. In this model, the infill soil was modeled using Mohr-Coulomb model, and the geocell was modeled using linear elastic Geogrid structural element. The numerical model was validated using the laboratory load test conducted on geocell reinforced sand. The conclusions drawn from this part of the study are:

(1) Geocell reinforced soil bed showed an improvement in bearing capacity by 81% at a settlement ratio of 9%.

(2) The confining stresses developed in soil is studied by analyzing the horizontal stresses and displacement of geocell reinforcement and infill sand separately.

(3) The effect of loading diameter on geocell reinforcement mechanism is studied by placing a single geocell in the homogeneous 75% relative density sand.

(4) Smaller size geocells are more effective as compared to larger size geocells.

Chapter 5

Numerical Modeling of Geocell Reinforced Dense Sand Bed over Weak Sand Subgrade

5.1 Overview

The confining mechanism in geocell reinforced homogeneous sand bed was discussed in the Section 4.3.3 of Chapter 4. In this Chapter, numerical analysis were carried out using finite difference software FLAC 3D to study the confining mechanism of geocell reinforcement for geocell reinforced dense sand bed over weak sand subgrade of 30% relative density under monotonic loading. The results obtained from the simulation were validated using the experimental results from the large scale laboratory testing. Additionally, simulations were carried out with clay as the weak subgrade to observe the improvement in the performance of geocell reinforced sand bed. The layered soil model used for the experimental study is shown in Figure 5.1.

In the Figure 5.1, D is the diameter of the loading plate which is 0.15m, H is the total height of the sand bed which is 0.9m, H_1 is the top dense sand layer of 75% relative density with 0.25m depth, H_2 is the bottom weak soil layer with 0.65m depth, h is the height of the geocell reinforcement which is 0.2m and B is the width of the sand bed which is 1m.
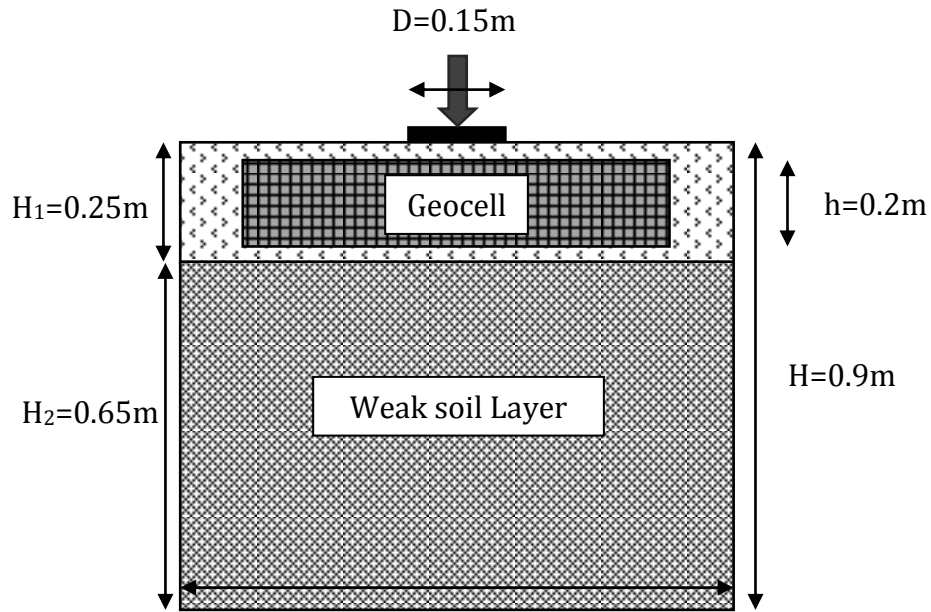
Figure 5.1: Geocell reinforced sand model

5.2 Material Models and Parameters

5.2.1 Sand

Two sand layers were considered with 30% relative density sand overlaid by 75% relative density sand. The elastic-perfectly plastic Mohr-Coulomb model was used to model both the sand types based on extensive literature review. Shear strength properties (c and ϕ) of the sand was determined from the consolidated undrained triaxial compression test. The test was carried out at three different confining pressures of 50 kPa, 100 kPa and 150 kPa. The modulus of elasticity of the 75 % relative density sand was found using Burmister's elastic layer theory. The modulus of 30% relative density sand layer, E_2 (of layer 2) is given by

$$E = \frac{\pi \sigma_0}{2\Delta}(1 - \nu^2)$$

(5.1)

Where, σ_0 is the pressure applied on the surface of the plate, r is the radius of the plate, Δ is the deflection of the plate and ν is the poisons ratio of the soil.

From the calculated E_2, deflection factor F_2 at 1.25mm is obtained using,

$$F_2 = \frac{W_0 E_2}{1.5qa}$$

(5.2)

Where W0=1.25 mm, q is the applied load and *a* is the radius of the plate.

Using F_2 and h_1/a (h_1 is the first layer thickness), the modulus of elasticity, E_1 of the top layer is found from the Figure 5.2.
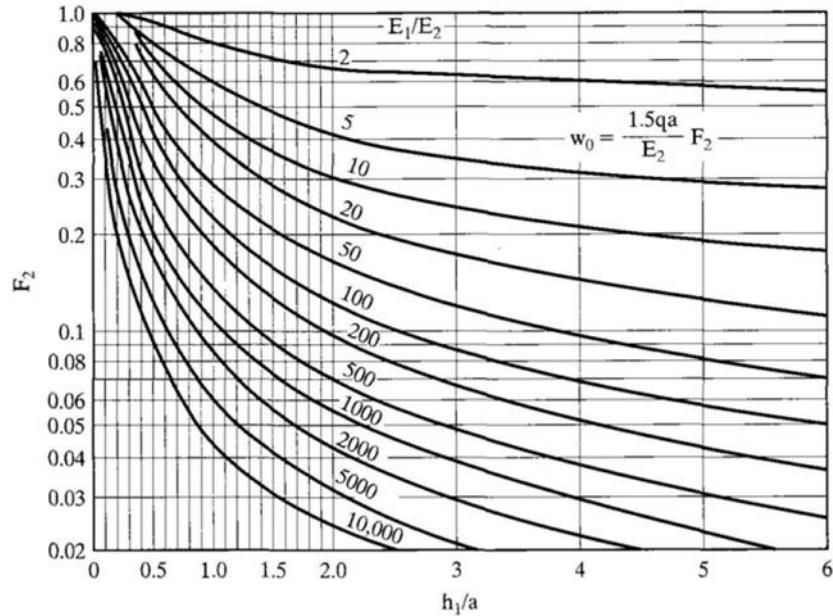
Figure 5.2: Burmister's Chart for F_2 for various h_1/a and E_1/E_2

From the elastic modulus, the shear modulus and the bulk modulus values were determined by assuming the Poisson's ratio of 0.25. The parameters used for modelling 75% relative density sand and 30% relative density sand are shown in the Table 4.1.

Table 4.1: Material properties of sand and plate used in FLAC 3D

Properties	75 % R_D Sand	30 % R_D Sand	Plate
Bulk modulus (Pa)	5.0e6	1.8e6	1.4e11
Shear modulus (Pa)	3.0e6	0.8e6	8.04e10
Friction angle (degree)	40	30	-
Cohesion (kPa)	2.2	0.7	-
Dilation (degree)	8	0.1	-
Density (kg/m3)	1740	1630	7.8e3

5.2.2 Clay

The elastic-perfectly plastic Mohr-Coulomb model was used to model clay layer. The properties of clay was obtained by performing the same procedure used for sand explained in section 5.2.1. The properties used in the analysis is given in the Table 4.2.

Table 4.2: Material properties of clay used in FLAC 3D

Properties	Clay
Bulk modulus (Pa)	9.1e6
Shear modulus (Pa)	0.184e6
Friction angle (degree)	3
Cohesion (kPa)	25
Dilation (degree)	0.1
Density (kg/m3)	2100

5.2.3   Geocell

Geogrid structural element was used to model geocell which are three-noded, flat, finite elements that are assigned a finite element type that resists membrane but does not resist bending loading. These elements will behave as an isotropic, linearly elastic material without failure limit. The elastic modulus of the geocell was determined from tensile stress-strain response. The secant modulus was determined corresponding to 2% axial strain. The interface properties of the geocell and the soil is incorporated in this model by providing interface shear modulus and interface friction angle as two third of the cohesion and friction angle of the infill material.

The parameters and the dimensions of geocell used for the analysis is given in the discussed in chapter 3. The procedure adopted for modelling geocell is also explained in Chapter 3.

5.3   Modeling of Static Load Test using FLAC 3D

Numerical models were created in FLAC 3D and the model is validated by comparing the simulation results with the experimental results. The constitutive models and the parameters used for modeling have been discussed in the previous sections.

5.3.1   Numerical mesh and Boundary Conditions

The complete test box of the laboratory test with dimensions 1 m breadth, 1 m width and 0.9 m depth was modelled. The primitive mesh shape radial cylinder which is radially graded mesh around cylindrical-shaped footing was used to simulate the experimental test box setup. The use of radial cylinder mesh type was for ensuring the compatibility between footing and the soil. Vertical movement was fixed at the bottom boundary of the model, and horizontal movement was fixed at the four side boundaries. A velocity boundary (v=2.5*10-6 m/step) was applied at the top of the sand at a circular area having a diameter of 0.15 m. The model was solved for 12000 iteration steps until the settlement ratio at the top of the

soil reached 10%. The numerical model of the unreinforced case used for the analysis is shown in the Figure 5.3.
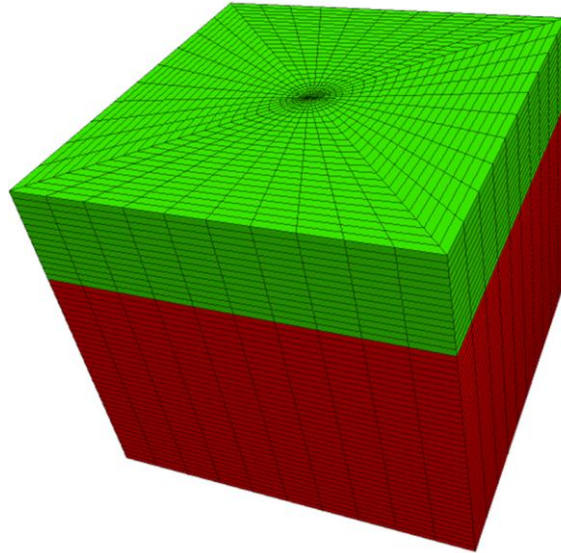
Figure 5.3: Soil model in FLAC 3D

In geocell reinforced case, geocell is placed by providing a clearance of 0.02m from the surface. The numerical model of geocell reinforced sand is shown in the Figure 5.4.
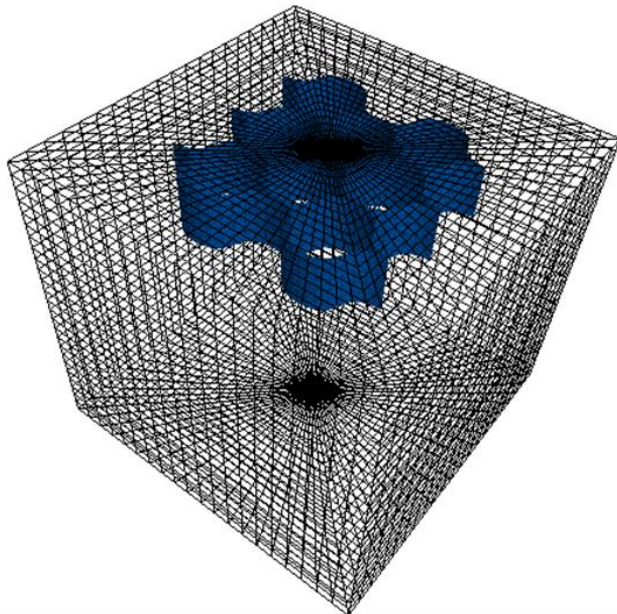

Figure 5.4: Soil model with geocell reinforcement in FLAC 3D

5.3.2 Experimental Validation

The variation of bearing pressure with settlement ratio was plotted and was compared with the experimental result for validation of the model. Overall, the numerical model well simulated the bearing capacities of the unreinforced and geocell reinforced sand. The comparison of the experimental and numerical results for the unreinforced and geocell reinforced cases are plotted and shown in Figure 5.5 and Figure 5.6 respectively. The comparison of the numerical simulation results of unreinforced and geocell reinforced case is plotted in the Figure 5.7. The geocell reinforced model improved the ultimate bearing pressure by 25%, 40% and 55% at 3%, 5% and 10% settlement ratio respectively.
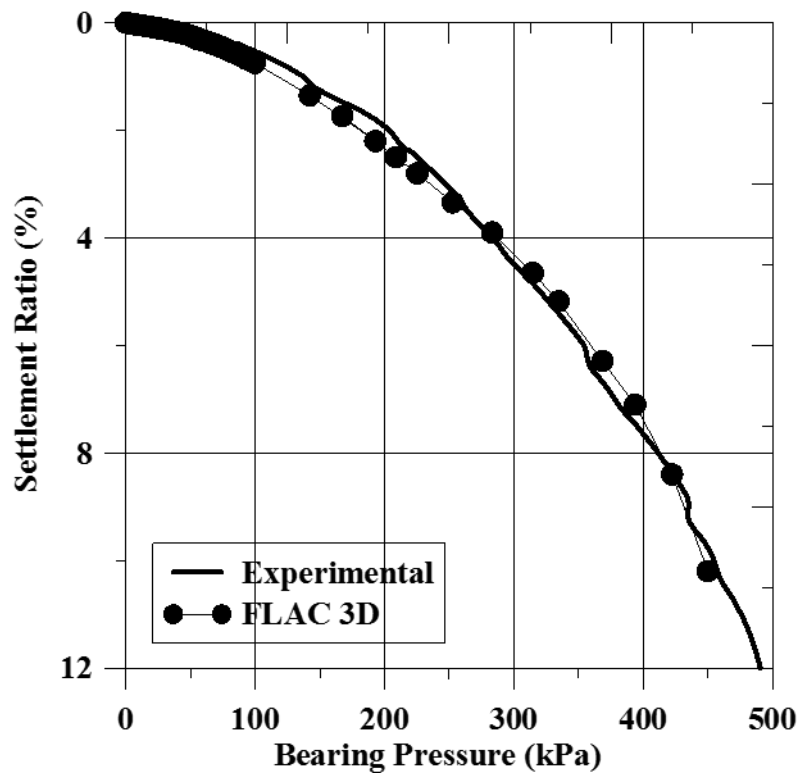
Figure 5.5: Bearing pressure vs. Settlement ratio curve for unreinforced case
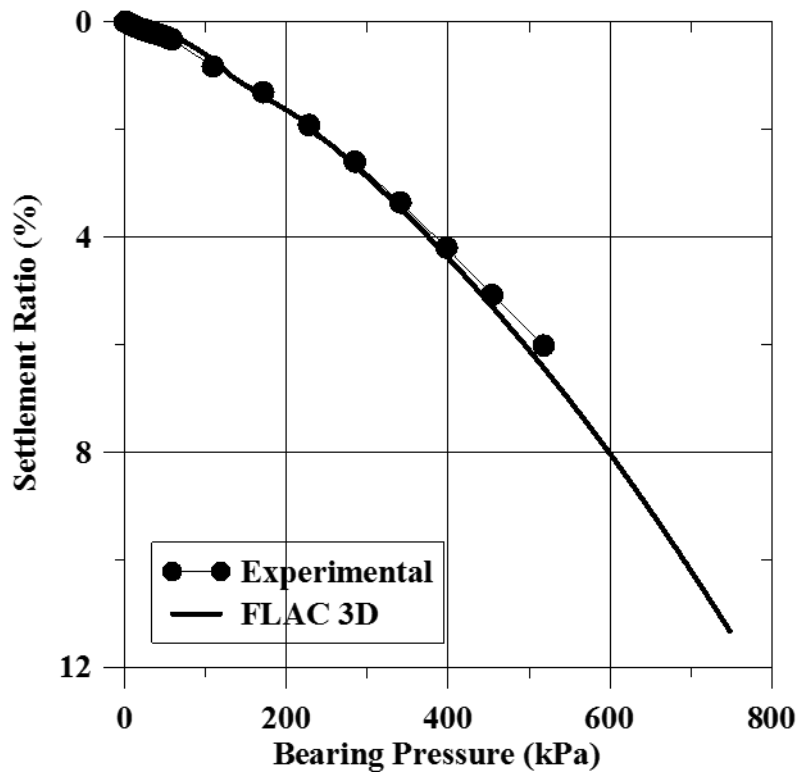
Figure 5.6: Bearing pressure vs. Settlement ratio curve for geocell reinforced case
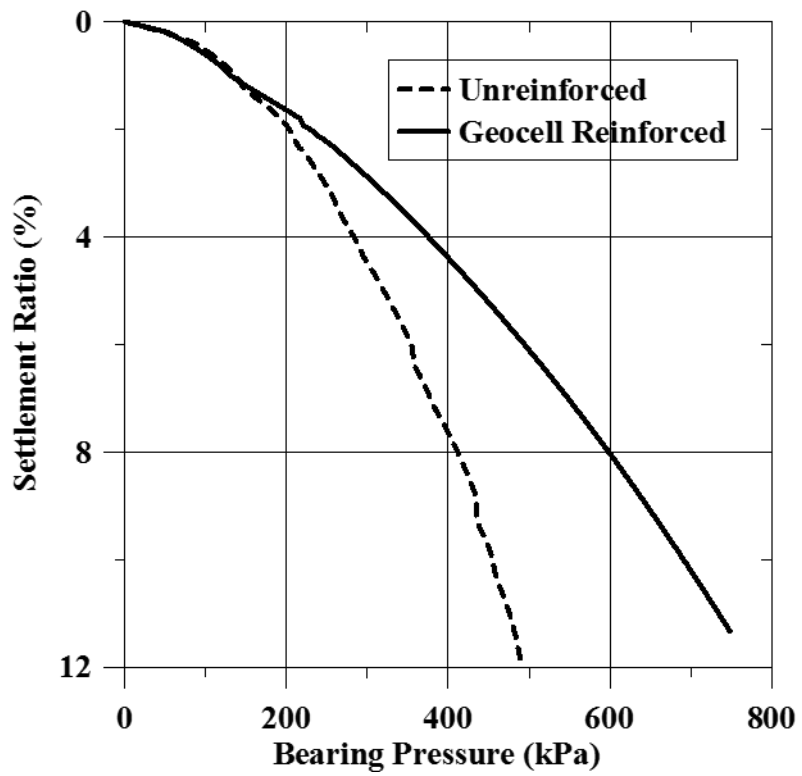
Figure 5.7: Bearing pressure vs. Settlement ratio curve- Comparison plot

5.3.3   Results and Discussions

For studying the confining mechanism of geocell reinforced sand bed, the stresses developed in the geocell walls and in the infill sand are analysed. The confining stresses developed in the geocell wall under monotonic loading is showed in the Figure 5.8. It can be observed that, the stress developed is maximum at the centre of the loading and it gradually reduces towards the other sides. But in numerical analysis, the confining stress developed in the geocell is assumed to be constant throughout the geocell. From this study, it is clear that the confining stress developed in the geocell varies with distance from loading and so the minimum value of the confining stress must be considered for the design applications.

The stress developed in the geocell under monotonic loading is plotted by selecting four locations (1, 2, 3 and 4) as shown in the Figure 5.9 and Figure 5.10. It can be observed that the stress developed in the geocell increases with increase in applied stress and the increase in developed stress is higher at the location 1 which is directly below the centre of the loading and the rate of increase in developed stress is less as the distance of location from the loading centre increases.
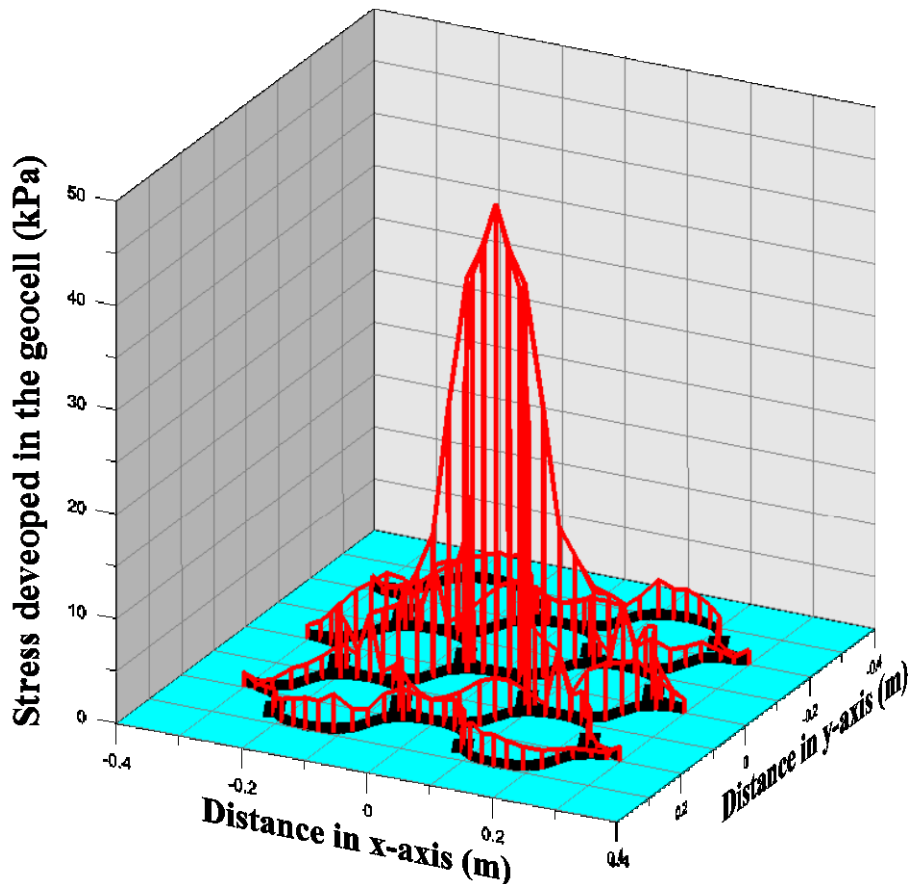
Figure 5.8: Confining stress developed in the geocell wall

57
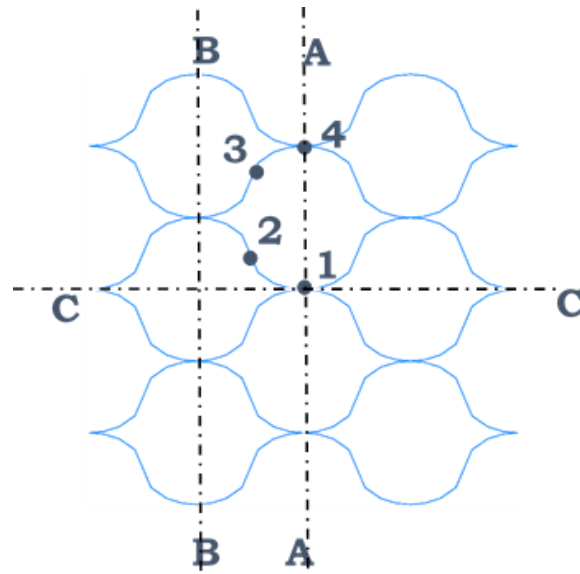
Figure 5.9: Locations in the geocell reinforcement
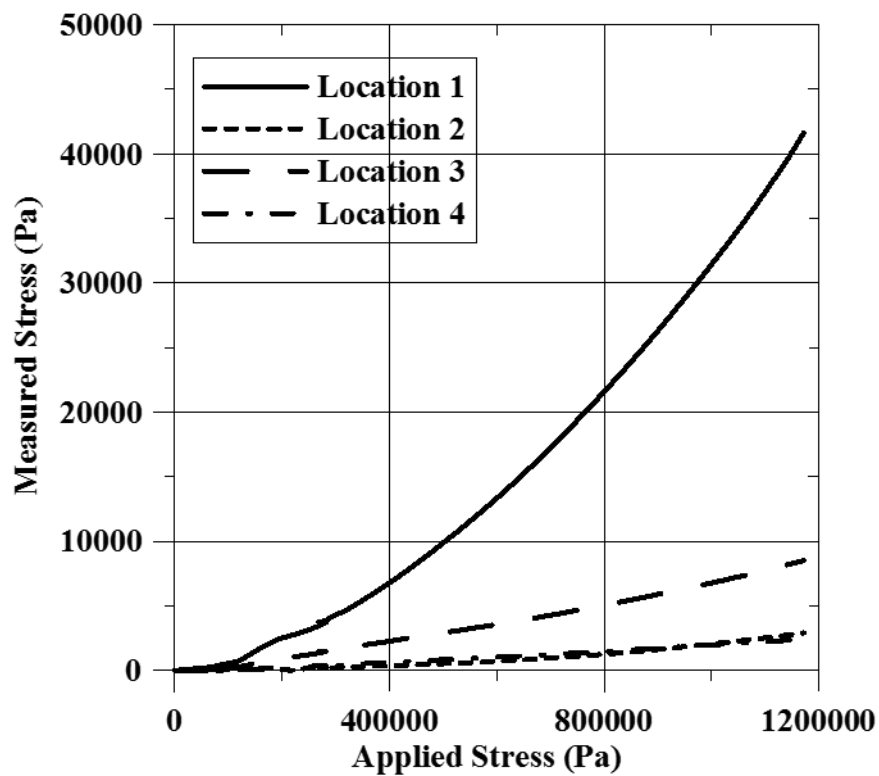
Figure 5.10: Stress developed in the geocell wall under monotonic loading

The Figure 5.11 and Figure 5.12 shows the variation of horizontal stresses in both x-direction and y-directions at a section at the mid height of the geocell. As similar to the

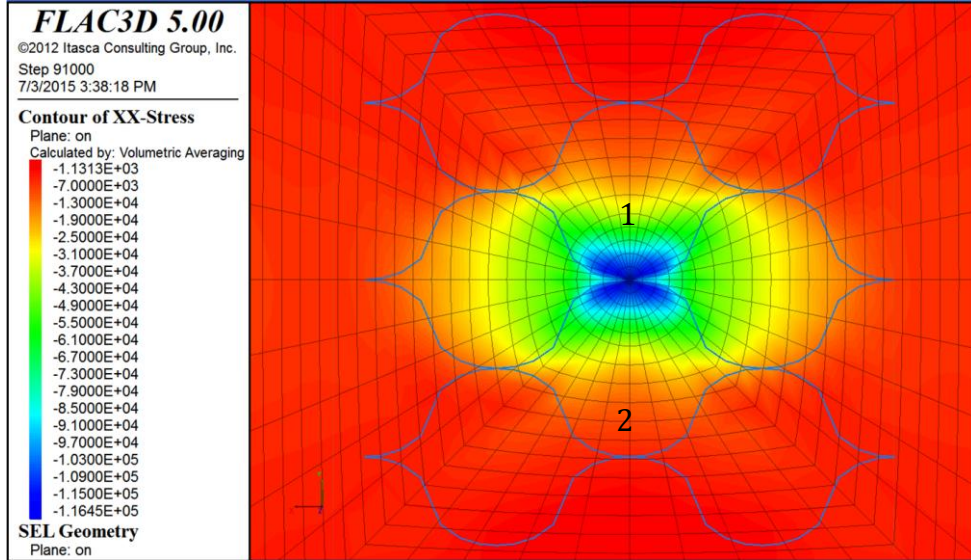homogeneous sand case, the maximum stress is developed in the cells 1 and 2, which are directly below the loading plate and with the loading area more than that of the other cells.

Figure 5.11: Horizontal stress in x-direction at the mid height of geocell
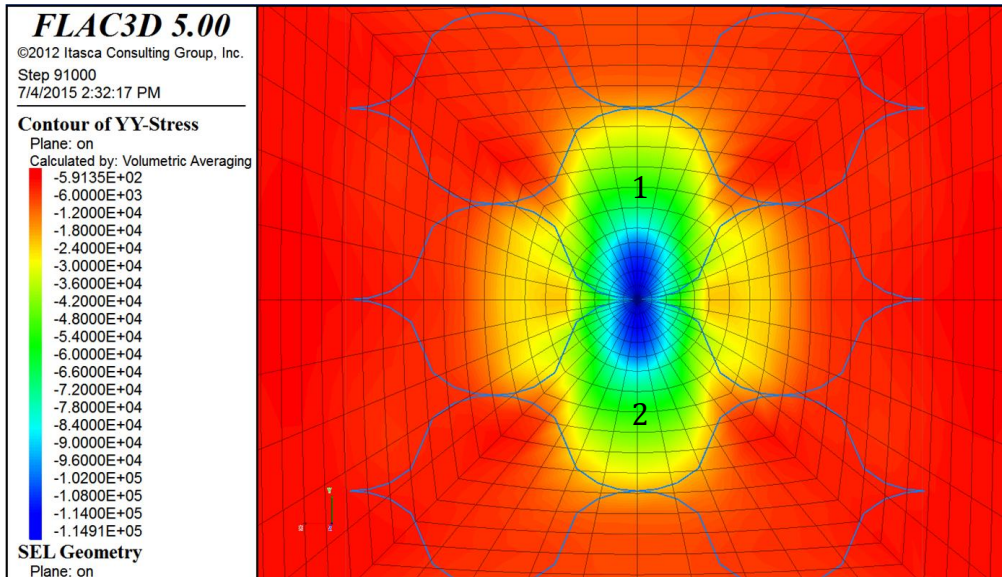
Figure 5.12: Horizontal stress in y-direction at the mid height of geocell

Figure 5.13 and Figure 5.14 shows the variation of horizontal stresses along section A-A and section C-C. It can be observed that the stress developed is maximum at an h/D ratio of 0.4 with a magnitude of 193.89 kPa.
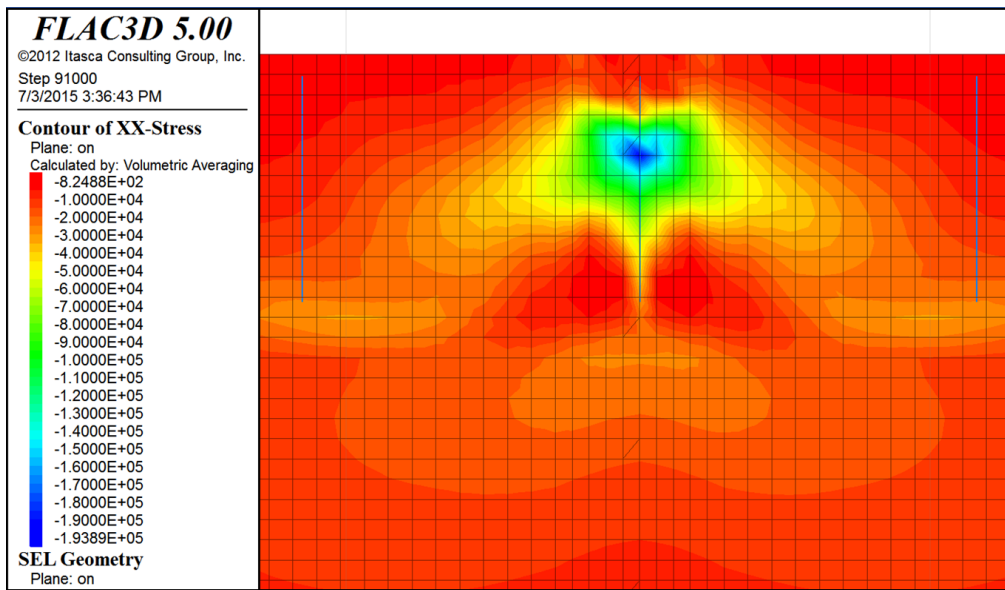
Figure 5.13: Horizontal stress in x-direction at vertical cross-section
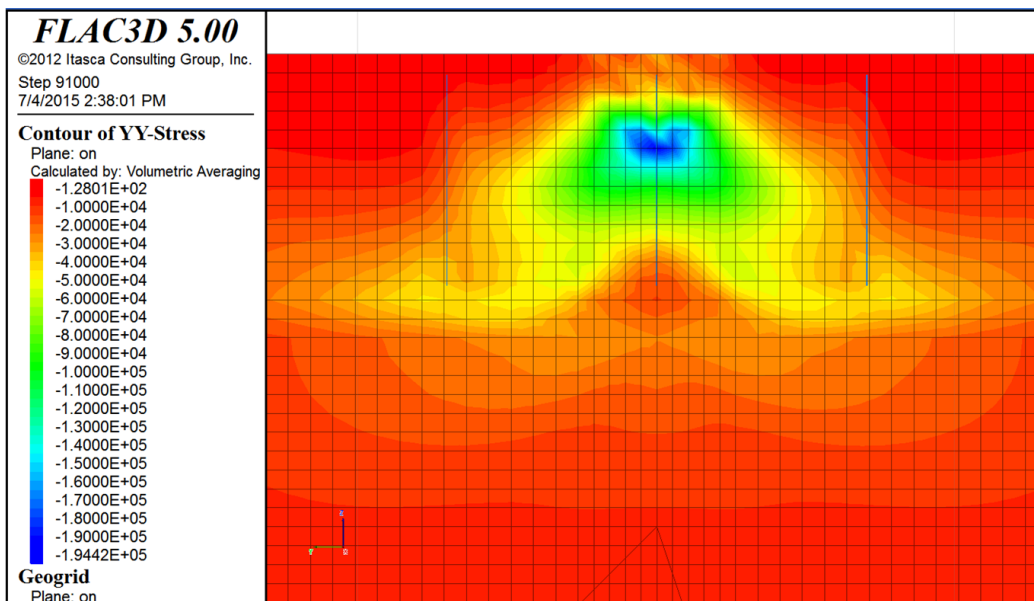
Figure 5.14: Horizontal stress in y-direction at vertical cross-section

The variation of confining stresses developed in the infill soil across these two sections A-A and C-C were studied in the Figure 5.16 and Figure 5.17. Confining stress variation is also plotted at four different h/D ratios as shown in Figure 5.15, where h is the height of geocell and D is the diameter of the loading plate, to see the variation of confining stress with depth.

In Figure 5.16, the variation of confining stress along section A-A is shown. It can be observed that the confining stress is maximum near the centre of the loading and it gradually reduces towards the edges. The maximum confining stress of magnitude 170 kPa is developed at h/D ratio of 0.4 which is at the surface of the geocell reinforcement. The negative sign indicates the developed stress is compressive in nature.

The confining stress variation in infill soil along section C-C is plotted in the Figure 5.17. The same trend along section A-A can be observed along section C-C. The maximum confining stress developed is 158 kPa and is nearer to the centre of the loading where h/B ratio of 0.4.
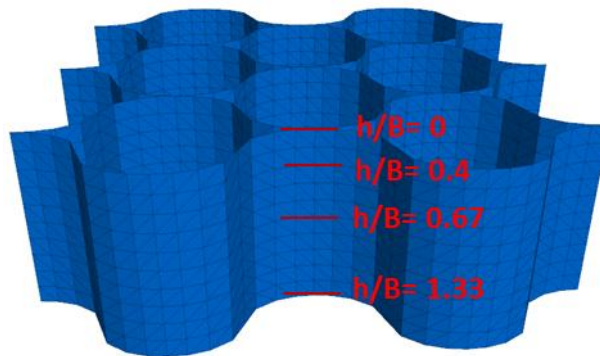
Figure 5.15: Locations along the depth of geocell reinforcement
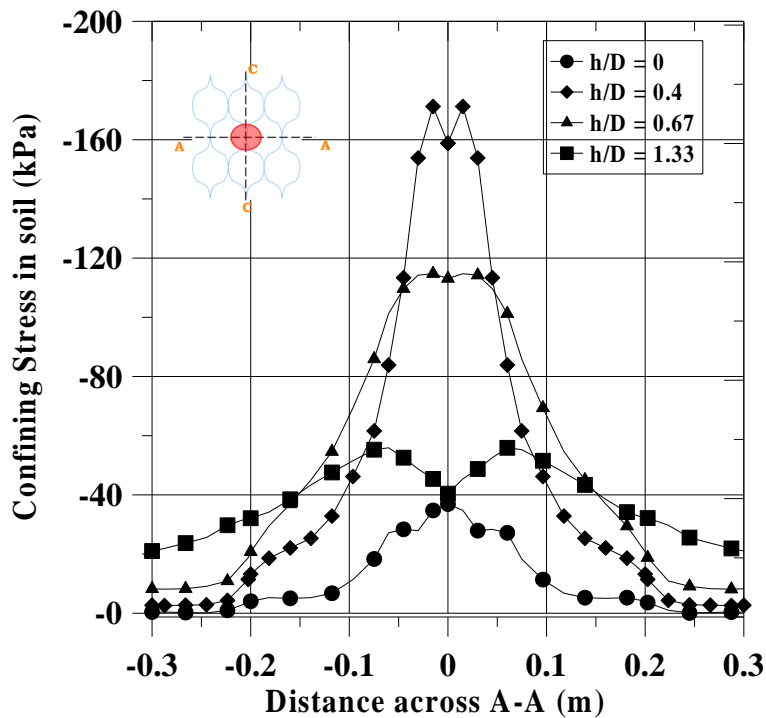
Figure 5.16: Variation of confining stress in the infill soil across A-A at various h/D ratios

61
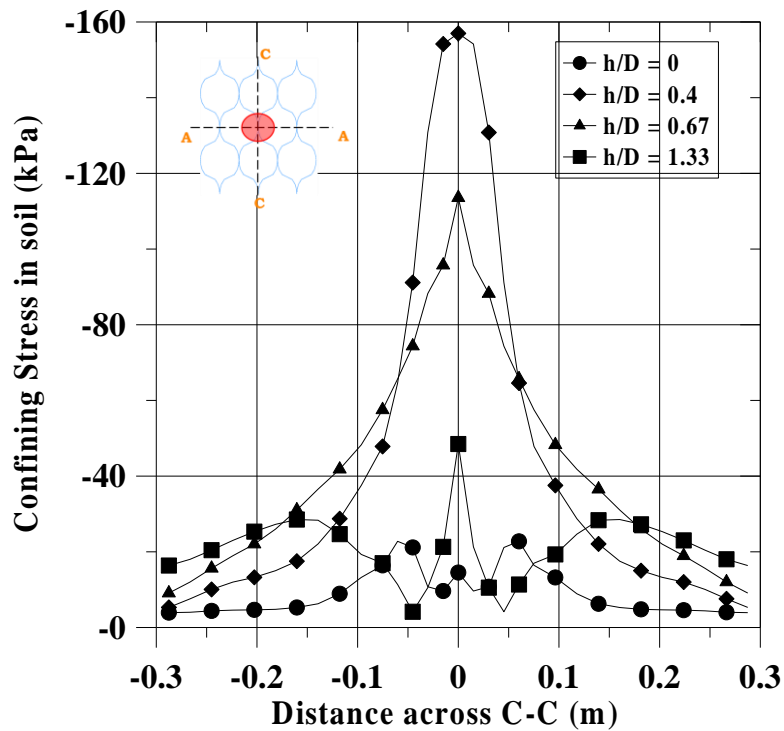
Figure 5.17: Variation of confining stress in the infill soil across C-C at various h/D ratios

The displacement of sand in unreinforced case is shown in the Figure 5.18. As there is no restriction for movement, the direction of sand movement will be both downwards and radially outwards. In geocell reinforced case the geocell walls restrains the movement of sand thereby developing confining effect on the infill material. This is shown in the Figure 5.20. The displacement vectors of soil is represented in green and geocell displacement vectors are represented in red.

For better understanding of the geocell mechanism, three sections across geocell reinforced sand bed is considered such as A-A, B-B and C-C as shown in the Figure 5.19 and the displacement vectors of sand and geocell are plotted. From the Figure 5.20, it can be observed that the top portion of geocell is bending inward and the bottom portion of the geocell is moving outward. This same trend can be observed in Figure 5.21 and Figure 5.22. Thus it can be concluded that the geocell bed is undergoing bending under monotonic static when it is placed over a weak subgrade.
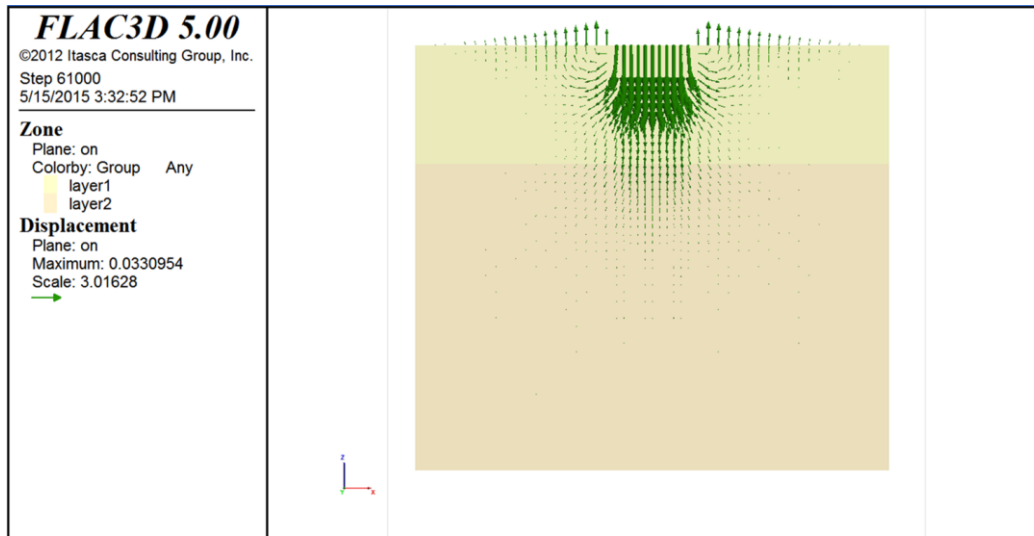
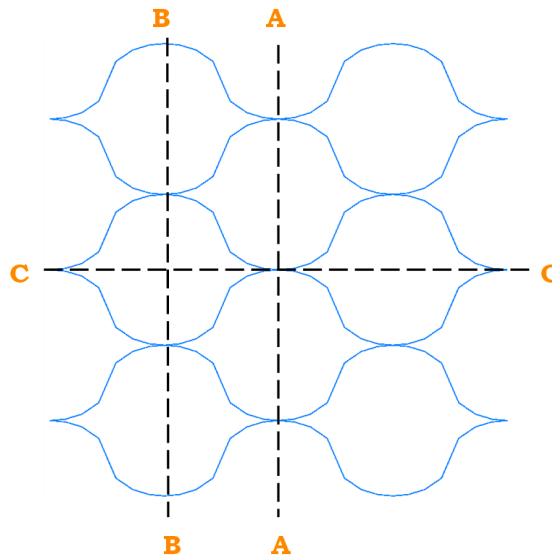**Figure 5.18: Displacement vector plot of unreinforced case**

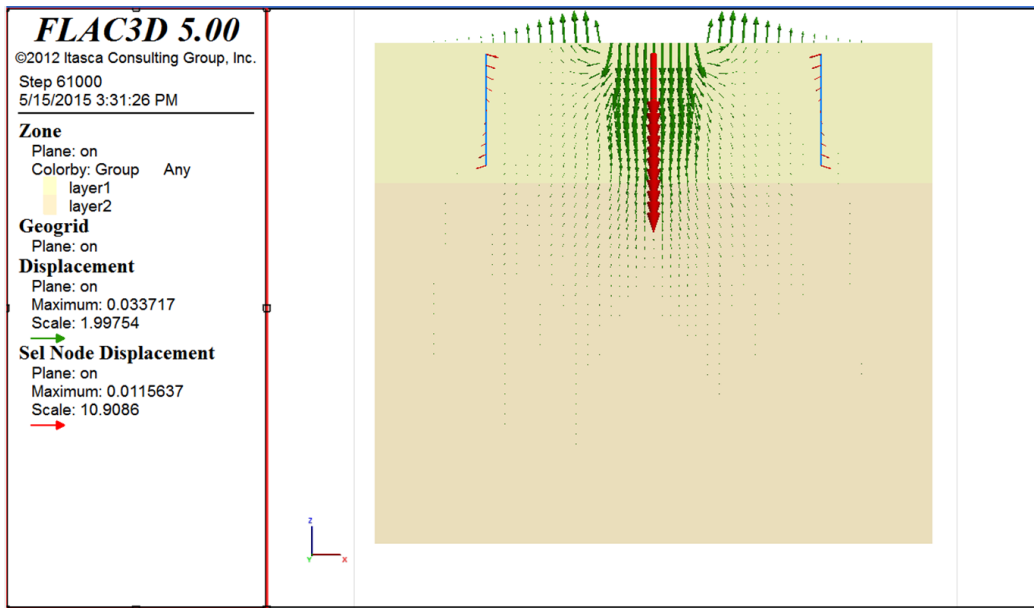**Figure 5.19: Sections considered for studying the displacement mechanism of geocell**

Figure 5.20: Displacement vector plot at section A-A
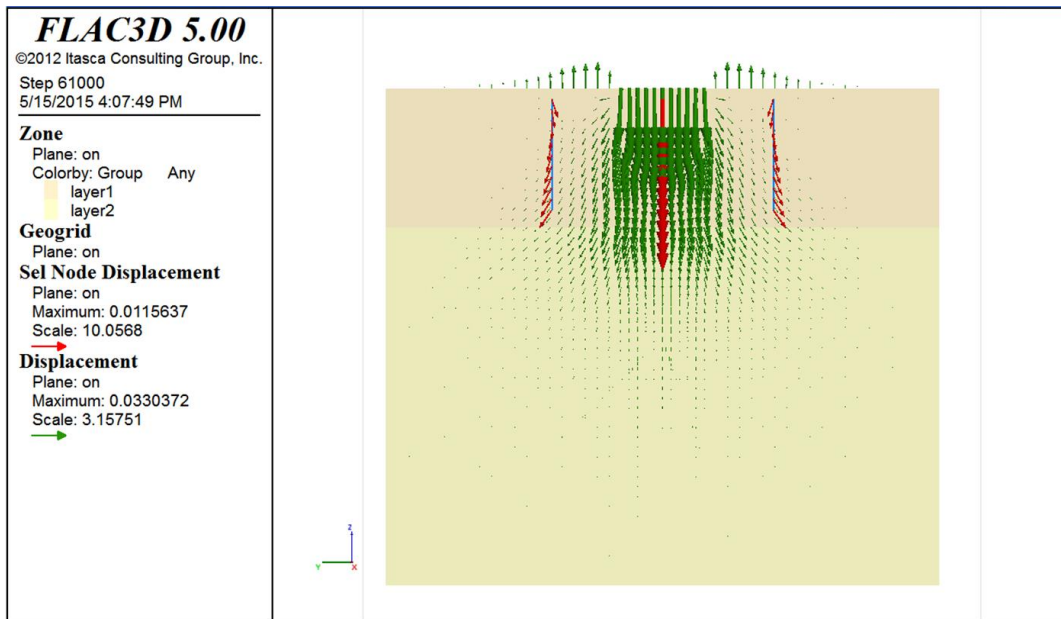

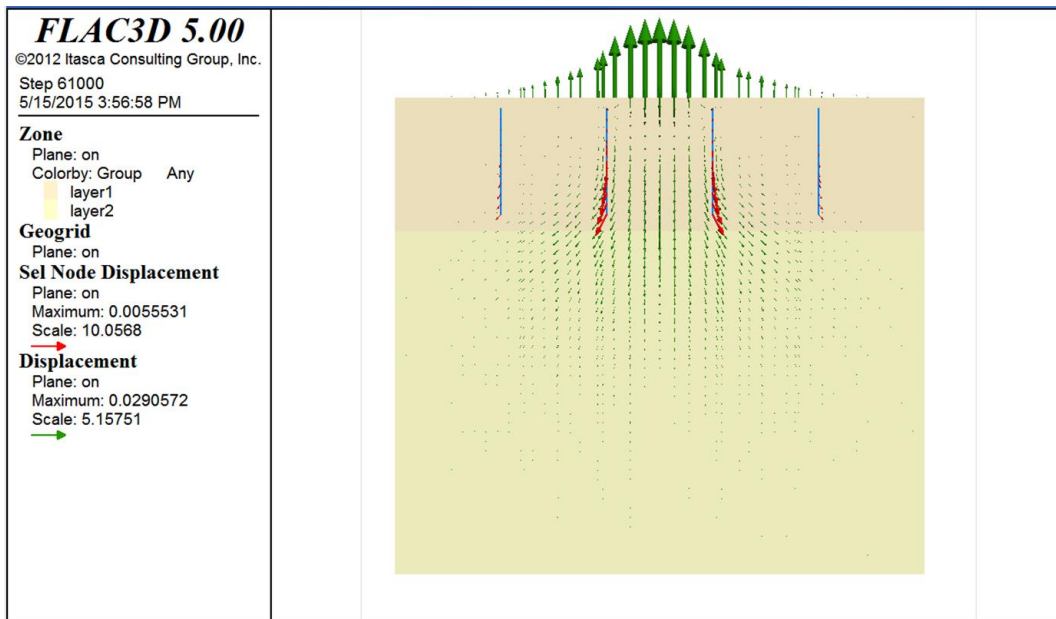**Figure 5.21: Displacement vector plot at section C-C**

Figure 5.22: Displacement vector plot at section B-B

The vertical displacement contour in the unreinforced and geocell reinforced models are shown in the Figure 5.23. It can be observed that the vertical movement is more in unreinforced case than in geocell reinforced case. In the reinforced case the vertical displacement was restrained by geocell and so the vertical displacement magnitude got reduced.
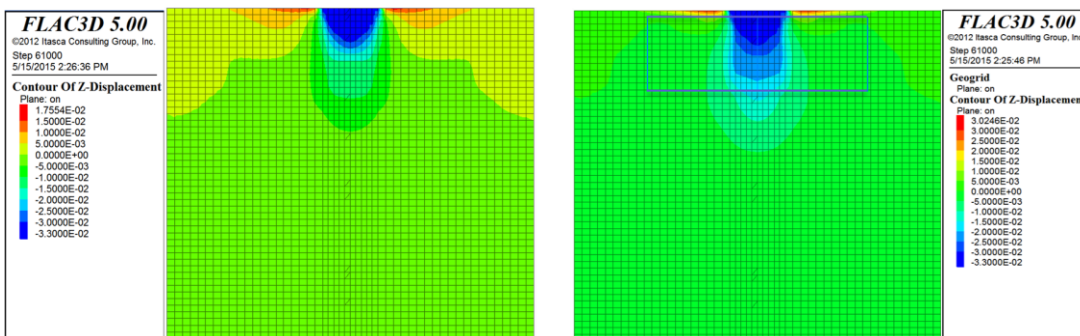

Figure 5.23: Variation of vertical displacement

Figure 5.24 shows the horizontal stress contour in the unreinforced and geocell reinforced layered models. It can be observed that the magnitude of horizontal stress is more in geocell reinforced case than in unreinforced case because of the lateral confinement offered by the geocell walls on the infill sand. The maximum horizontal stress developed in the unreinforced sand was 61.44 kPa. Whereas the maximum horizontal stress developed at the

65

geocell reinforced case was 149.5 kPa. A sudden change of horizontal stress was observed at the location of the geocell in the reinforced model, which means that the horizontal stress inside the geocell was taken mostly by the geocell rather than the same outside the geocell.
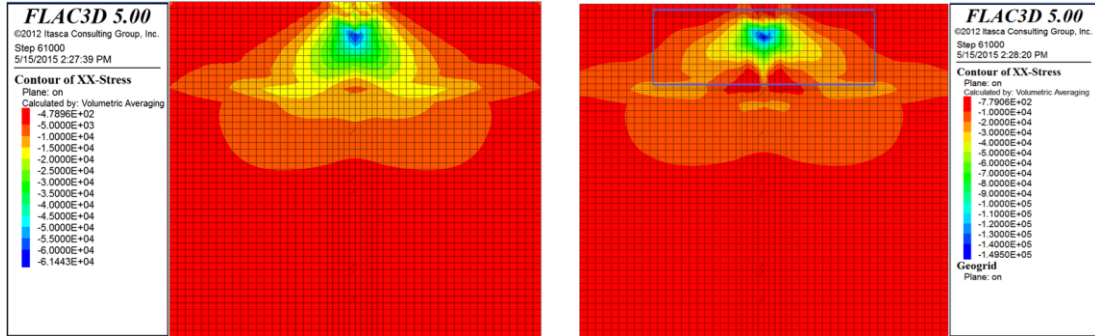

Figure 5.24: Variation of horizontal stress

The displacement in the geocell is plotted in the Figure 5.25. The maximum displacement can be observed at the region directly under the loading and has a magnitude of $1.4*10^{-2}$. The Figure 5.26 shows the coupling stress developed in the geocell under loading. The maximum stress is 50.15 kPa and is observed at an h/D ratio of 0.4.
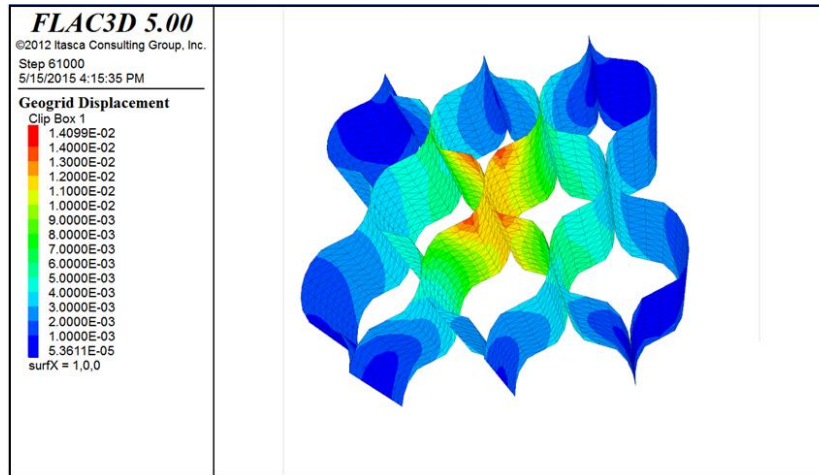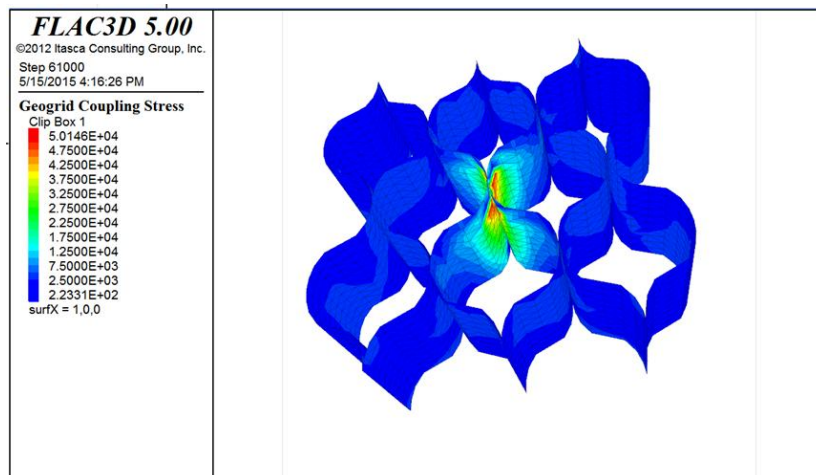

Figure 5.25: Geocell displacement

Figure 5.26: Geocell coupling stress

5.4 Parametric Studies

Parametric studies were performed on the geocell reinforced sand bed over weak sand subgrade under monotonic loading to find the behavior of the geocell with change in modulus of elasticity of geocell and interface shear stress.

5.4.1 Effect of modulus of geocell

Based on the actual modulus of geocell used in the study, the modulus of geocell was changed to 1/5th of its original modulus (i.e. 75 MPa) and 5 times the original modulus (i.e. 1825 MPa). The pressure settlement behaviour of three different cases is compared in the Figure 5.27. The bearing capacity of the reinforced bed increased with the increase in modulus of the geocell. As the geocell modulus increases, the higher confining pressure will be exerted on the infill material under same lateral deformation. The additional confining pressure leads to the increase in the bearing capacity of the foundation bed.
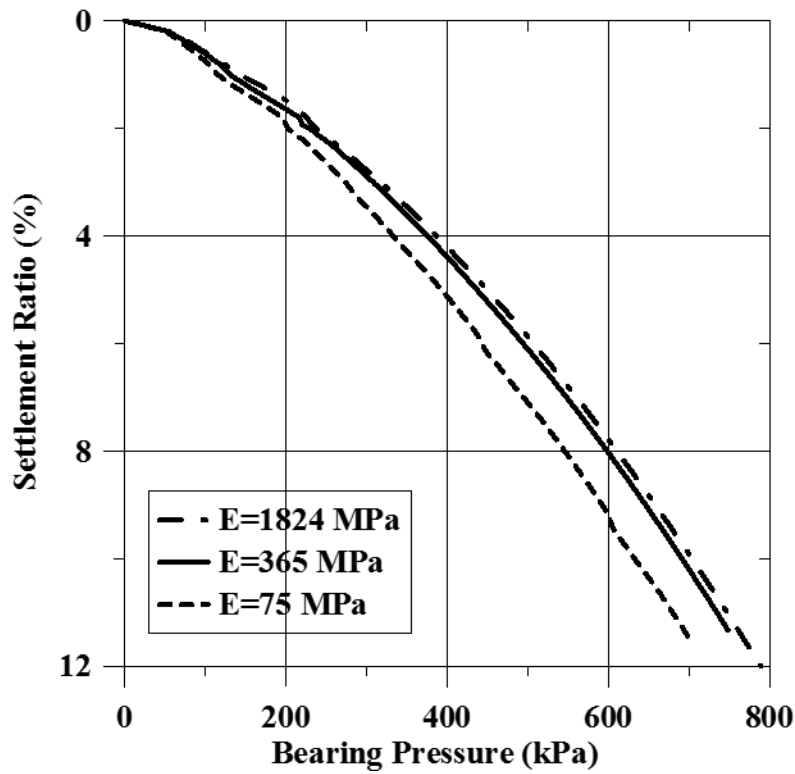
Figure 5.27: Comparison of geocell modulus

5.4.2   Effect of geocell-soil interface shear modulus

Based on the baseline case used in the analysis, the geocell-soil interface shear modulus of the geocell was changed to 1 MPa/m and 19.7 MPa/m. The pressure-displacement curves from the numerical analysis are plotted together in the Figure 5.28. It can be observed that the geocell soil interface shear modulus have considerable influence on the bearing capacity of the foundation bed. The bearing capacity of the reinforced bed increased with the increase in soil geocell interface shear modulus. As the interface shear modulus increases, the friction between soil and geocell increases which in turn increases the load carrying capacity of the geocell reinforced foundation bed.
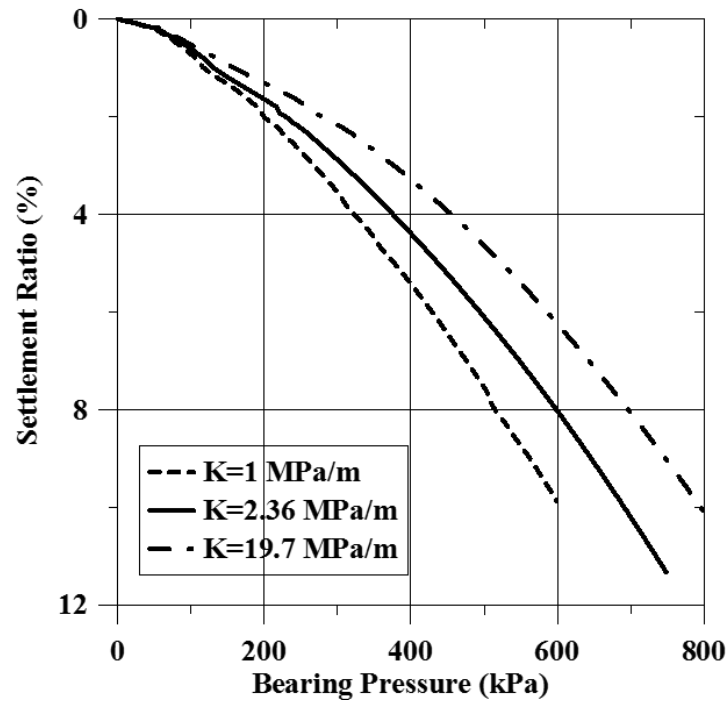
Figure 5.28: Comparison of modulus of subgrade of geocell

5.4.3   Effect of aperture on geocell walls

To study the effect of aperture on geocell walls, geocell was modelled with aperture with an area of 5% of the total geocell area as shown in the Figure 5.29. Numerical simulations were carried out by using geocell with aperture as the reinforcement and the bearing pressure vs. settlement ratio were compared with actual geocell reinforced case as shown in the Figure 5.30. It can be observed that the presence of aperture reduces the ultimate bearing pressure of the sand bed. This is because of the reduction in geocell stiffness due to the reduction in area of geocell.
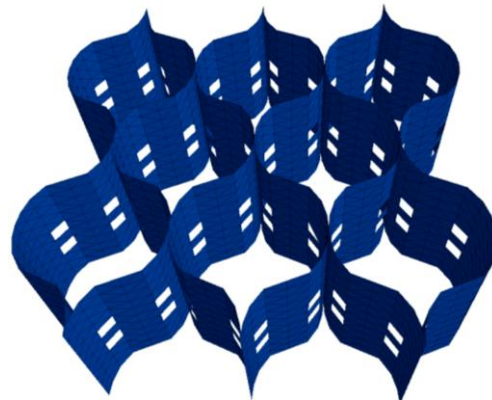

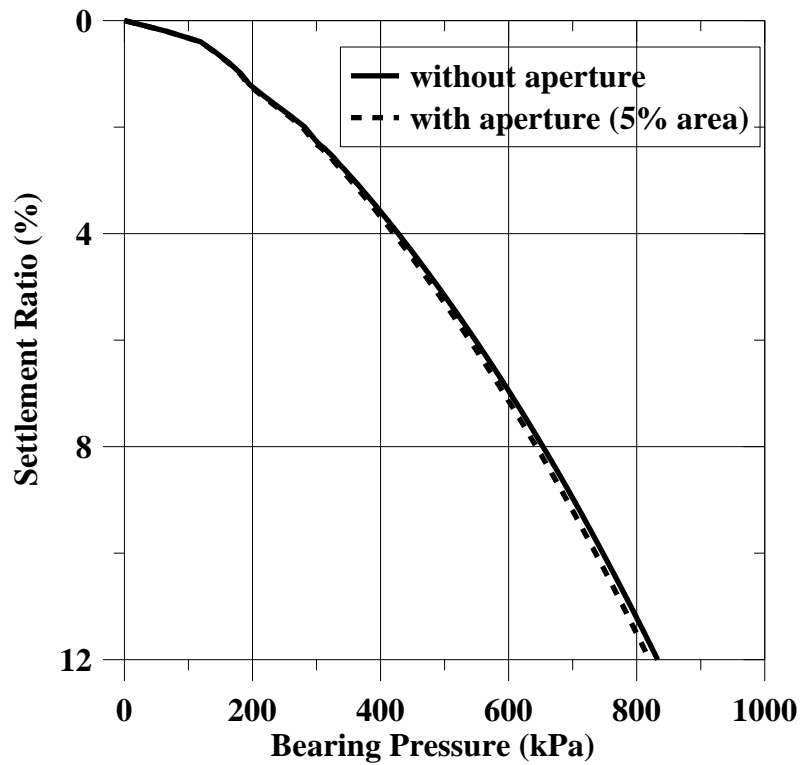**Figure 5.29: Geocell with aperture**

Figure 5.30: Comparison of behaviour of geocell with and without aperture

5.4.4 Geocell with Geogrid at the base

A layer of Geogrid is placed at the interface of the two sand layers to study the improvement in the performance of the sand bed with geocell and Geogrid reinforcement. The model used for the study is shown in the Figure 5.31. It can be observed that the geogrid is improving the performance of geocell reinforced sand bed by 7% at 3%, 5% and 10% settlement ratios which can be clearly observed in the Figure 5.32. The displacement vector plot is also shown in the Figure 5.33. It can be seen that under monotonic loading, the Geogrid is also undergoing bending there by providing additional tension membrane support to the sand bed.
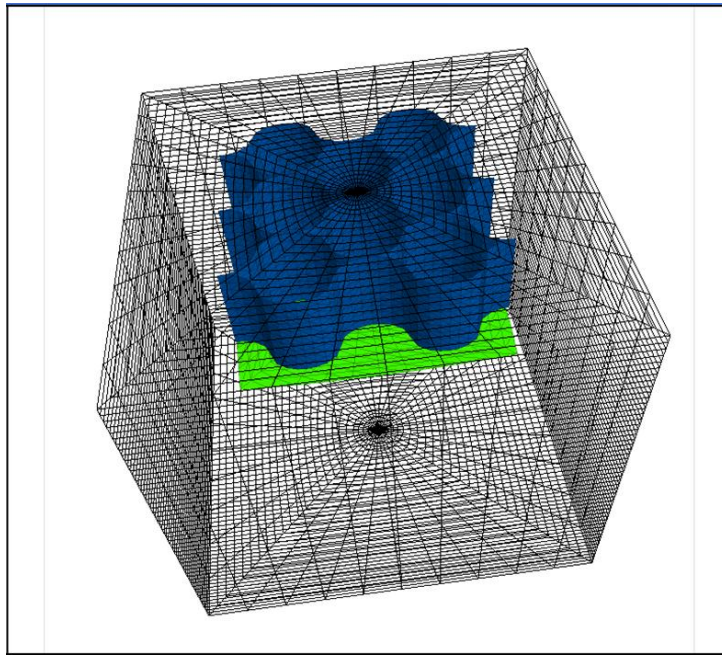
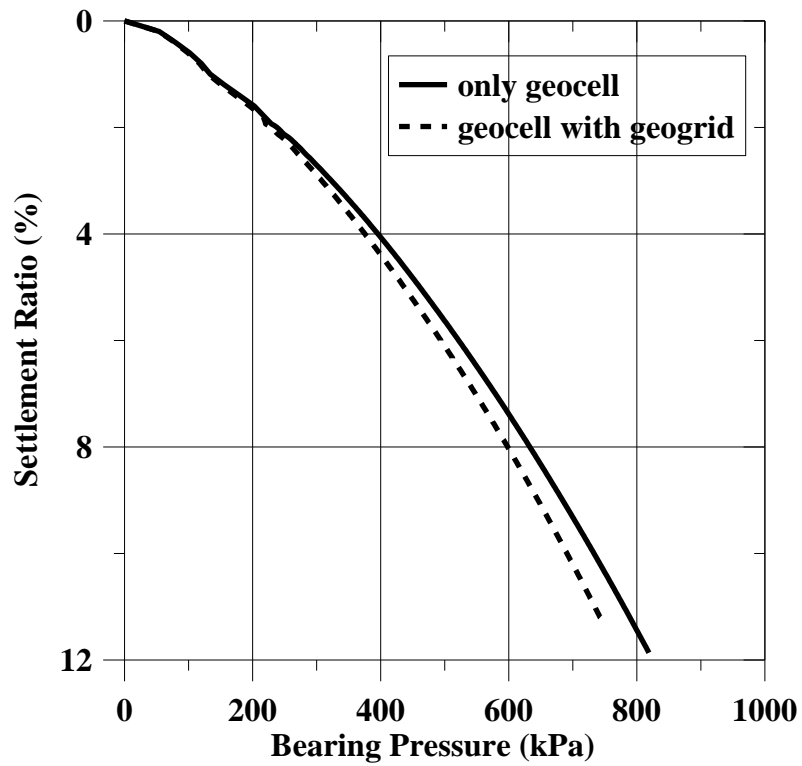**Figure 5.31: Geocell with Geogrid reinforcement at the base**

Figure 5.32: Comparison of behaviour of geocell and geocell with Geogrid
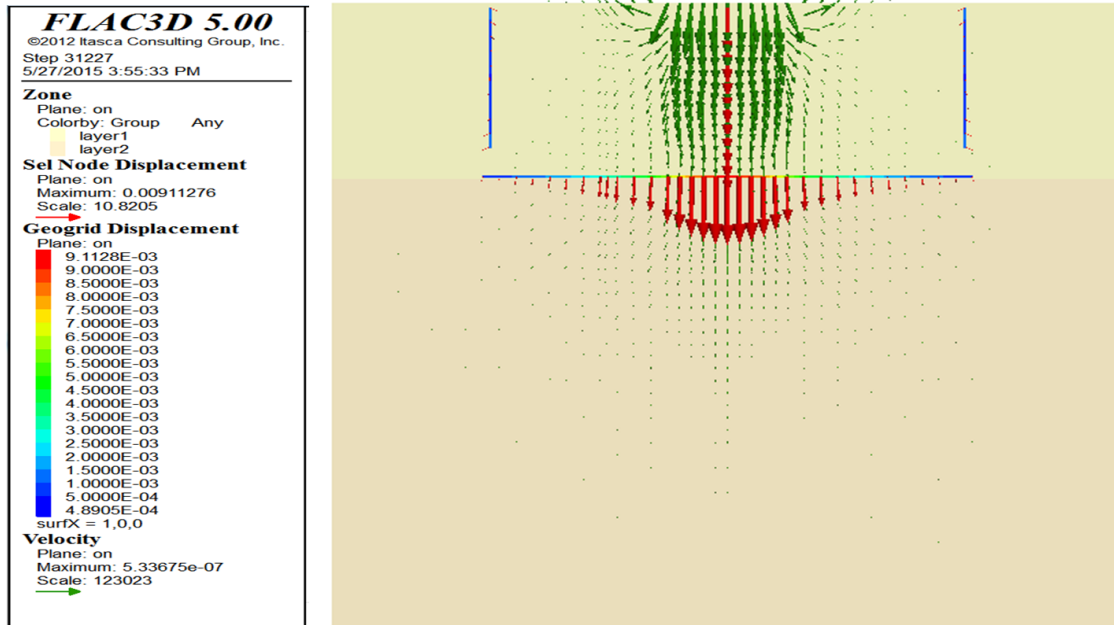
Figure 5.33: Displacement vector plot

5.5 Geocell Reinforced sand bed over clay subgrade under monotonic loading

In the same test tank model, 30% relative density sand is replaced by clay to study the performance of geocell over clay subgrade. The bearing pressure vs. settlement plot obtained from the numerical simulation is compared with the experimental results for both unreinforced and geocell reinforced cases and is plotted in the Figure 5.34 and Figure 5.35 respectively. Additionally, the improvement in the performance of geocell reinforced case is compared with the unreinforced case as shown in the Figure 5.36. Geocell reinforced clay subgrade 55%, 18%, 45% and 86% improvement in the bearing pressure at 1%, 3%, 5% and 10% settlement ratios respectively.
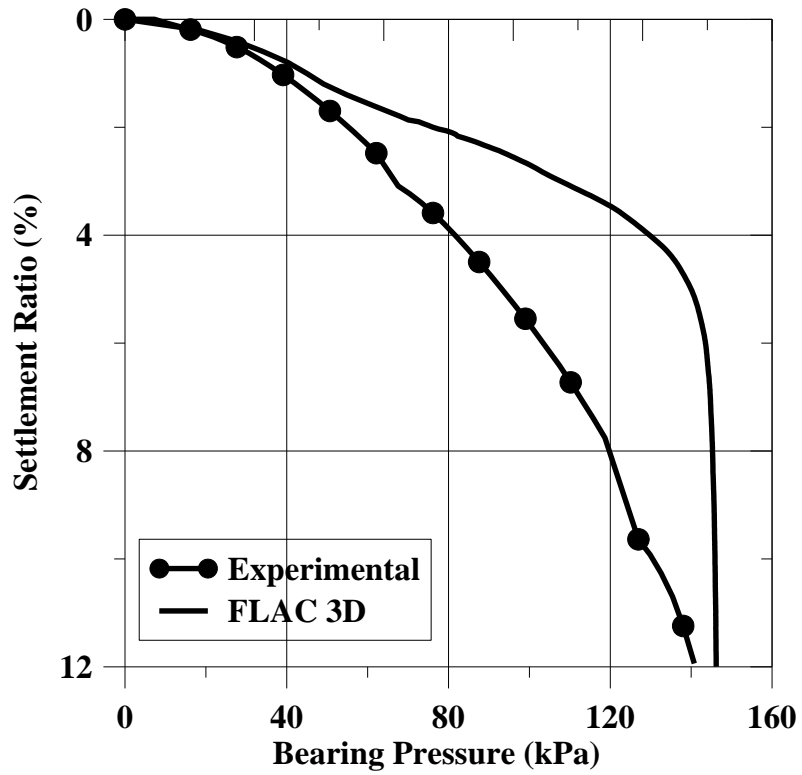
Figure 5.34: Bearing pressure vs. settlement ratio cure for unreinforced case
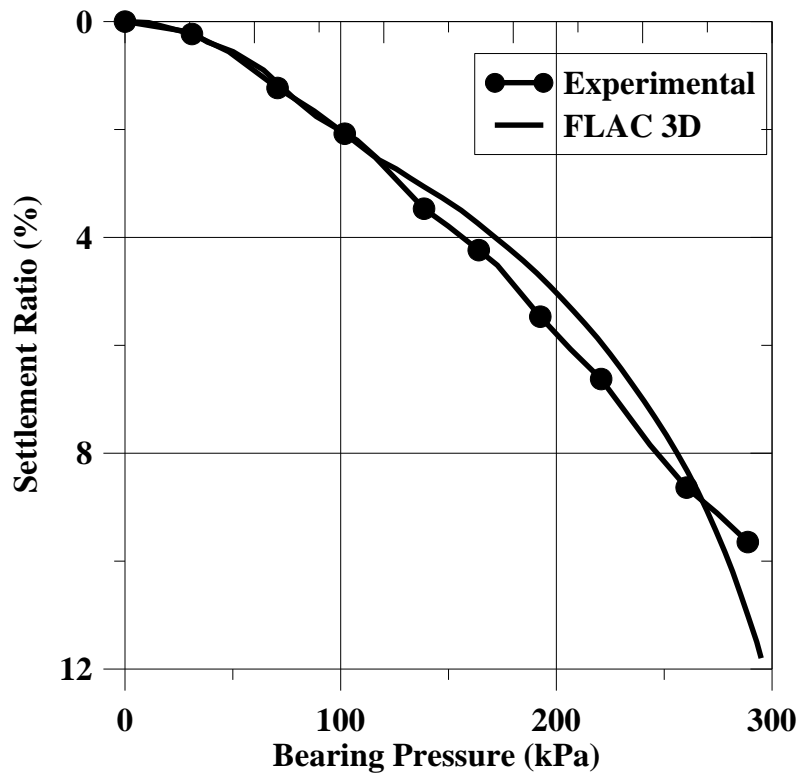

Figure 5.35: Bearing pressure vs. settlement ratio cure for geocell reinforced case
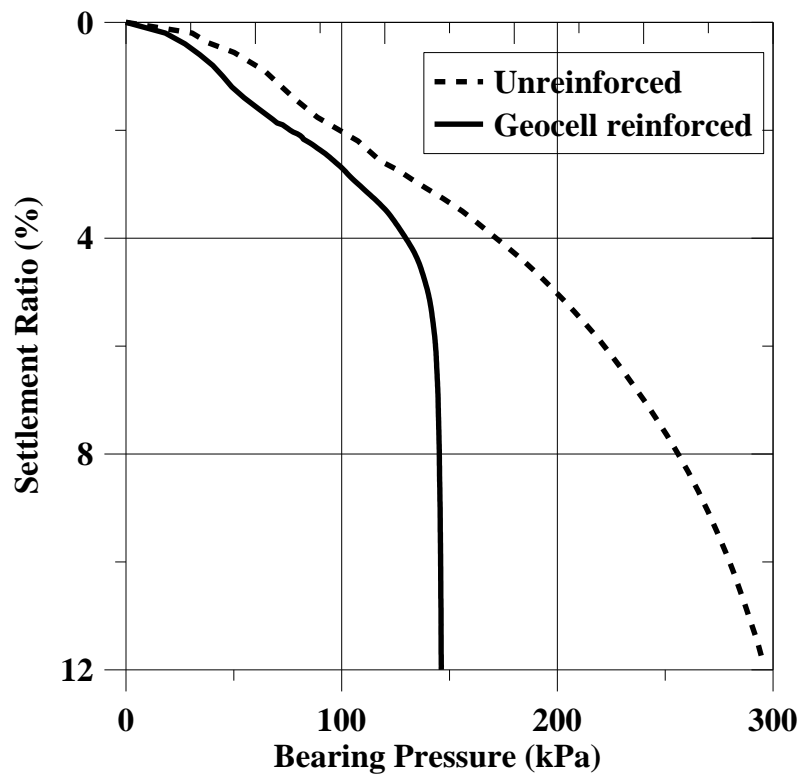
Figure 5.36: Comparison of bearing pressure vs. settlement ratio curve for unreinforced and geocell reinforced case

5.6 Summary

This chapter describes the development of numerical model for geocell-reinforced sand bed overlying weak layer under static loading. In this model, both the top and bottom soil layers are modeled using Mohr-Coulomb model, and the geocell was modeled using linear elastic Geogrid model. This numerical model was validated using the laboratory tank test conducted on geocell reinforced sand. The conclusions drawn from this part of the study are:

(1) Geocell reinforced soil bed over weak sand subgrade showed an improvement in bearing capacity by 54% at a settlement ratio of 10%.

(2) The confining mechanism of geocell reinforced sand bed overlying weak subgrade is brought out.

(3) Parametric studies were performed by varying the modulus of geocell and interface shear modulus.

(4) Geocell reinforced soil bed over weak clay subgrade showed an improvement in bearing capacity by 86% at a settlement ratio of 10%.

Chapter 6

Numerical Modeling of Stacked Geocell Reinforced Sand Bed over Weak Sand Layer under Monotonic Loading

6.1 Overview

Numerical modeling and validation of geocell reinforced sand bed over weak subgrade layer is done in the previous chapter. In certain situations in field the height of geocell reinforcement will not be sufficient so that it becomes necessary to used stacked geocell. Experimental studies in the stacked geocell case is very difficult in the laboratory because of the restrictions in the dimensions of the test tank. In this chapter, numerical analysis were performed to study the effect of stacked geocell reinforcement on the ultimate bearing pressure of the soil using FLAC 3D finite difference software. The same model used in the previous studies were adopted for this case and was reinforced with stacked geocell. Analysis were performed in four cases.

    (1) Weld of top layer reinforcement over the weld of bottom layer reinforcement

    (2) Weld of top layer reinforcement over the cell of bottom layer reinforcement

    (3) Weld of top layer reinforcement over the weld of bottom layer reinforcement with geogrid between two layers

    (4) Weld of top layer reinforcement over the cell of bottom layer reinforcement with geogrid between two layers.

The model used for the study is shown in the Figure 6.1. In the model, D is the diameter of the loading plate which is 0.15m, H is the total height of the sand bed which is 0.9m, H_1 is the top dense sand layer of 75% relative density with 0.25m depth, H_2 is the bottom weak soil layer with 0.65m depth, h is the total height of the two geocells which is 0.2m and B is the width of the sand bed which is 1m.
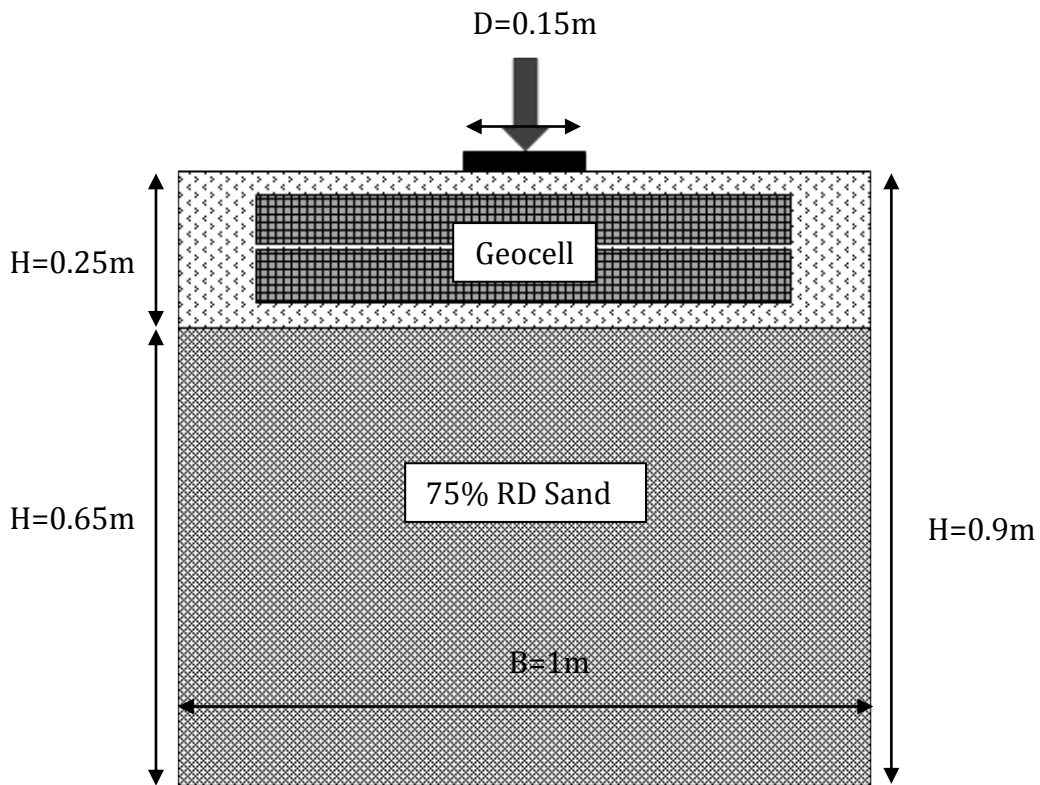
Figure 6.1: Sand model reinforced with stacked Geocell

6.2 Material Models and Parameters

The material models and parameters used for modeling are discussed in section 5.2 in Chapter 5.

6.3 Patterns of Geocell Reinforcement

In the previous chapters, a 200 mm height geocell mat was used as the reinforcement. In this study, the 200mm geocell is made into two 100mm height geocell mats in different patterns to see the behavior of stacked geocell under monotonic loading. Mainly two cases were studied by performing numerical simulations– Type 1 with the central weld of the top geocell layer over the central weld of bottom geocell layer and Type 2 with the central weld of the top geocell layer over the cell of bottom geocell layer. Studies were also performed on the above two cases by placing geogrid in between the two geocell layers.

6.3.1 Type 1- Weld over weld

The central weld of the top geocell layer was placed over the central weld of bottom geocell layer as shown in the Figure 6.2. The top geocell layer with 100mm height was modeled initially using the procedure discussed in the chapter 3 and then the second layer of geocell was modelled using the same procedure.
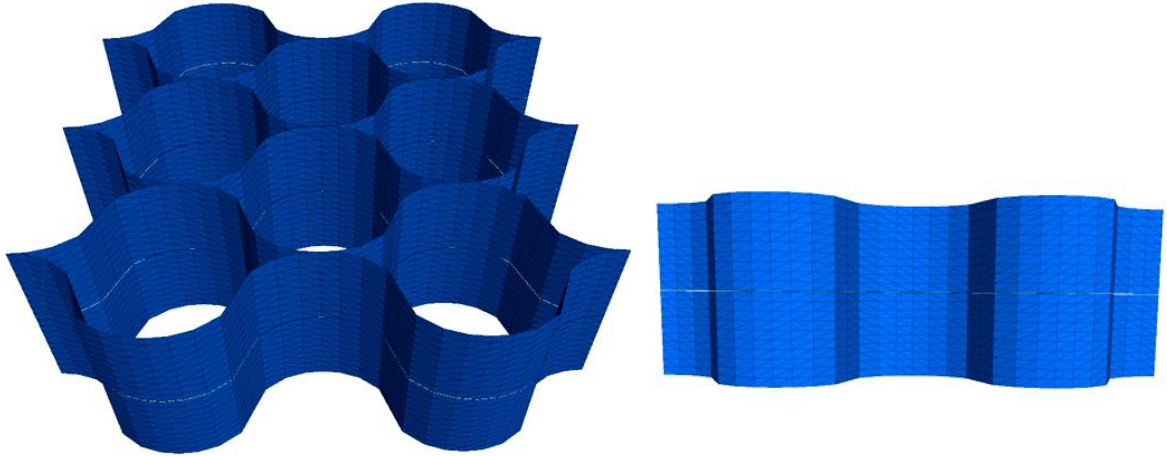

Figure 6.2: Type 1- weld over weld

6.3.2 Type 2- Weld over cell

In this case, the central weld of the top geocell layer was placed over the cell of bottom geocell layer as shown in the Figure 6.3. The top 0.1m height geocell was modeled and placed over the cell portion of bottom 0.1 height geocell.
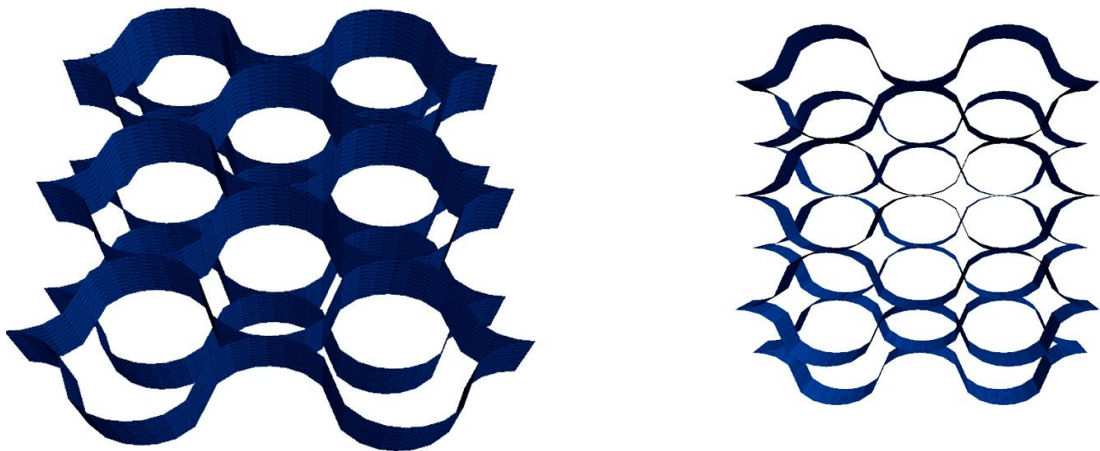

Figure 6.3: Type 2- weld over cell

6.3.3   Type 1 with Geogrid

A geogrid layer was placed in between the two layers of geocell in the first case as shown in Figure 6.4 and the behavior of sand bed is studied.
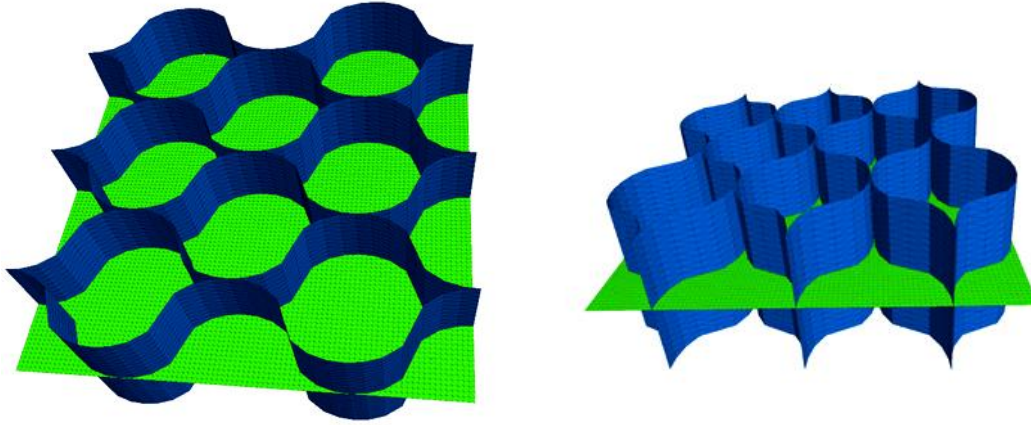

Figure 6.4: Type 1- with geogrid

6.3.4   Type 2 with Geogrid

A layer of Geogrid was placed in between the two layers of geocell in the second case as shown in Figure 6.5 and the behavior of sand bed is studied.
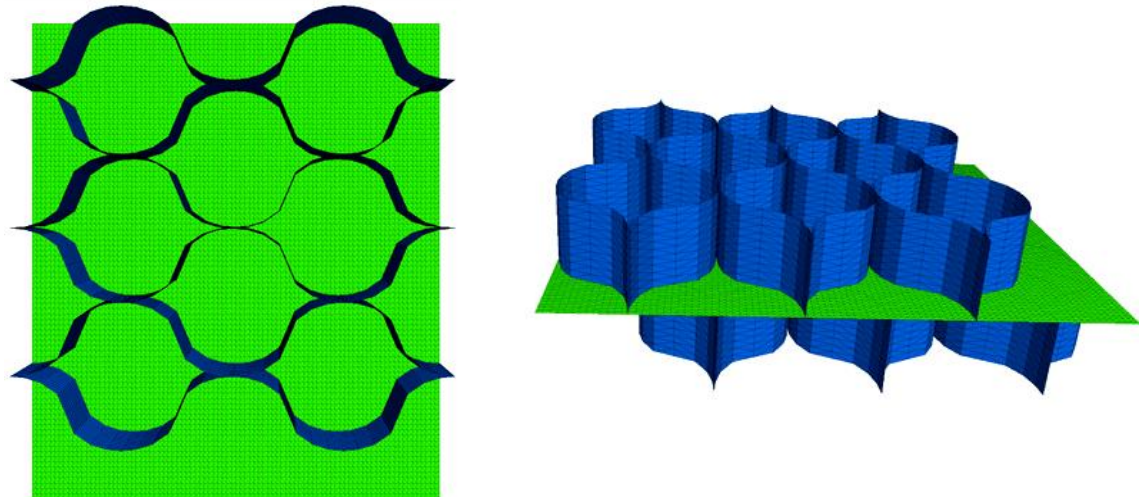

Figure 6.5: Type 2- with geogrid

6.4 Modeling of Static Load Test using FLAC 3D

6.4.1 Numerical mesh and Boundary Conditions

Numerical models were created in FLAC 3D software and the results obtained were compared. The constitutive models and the parameters used in modeling have been discussed in the chapter 5.

6.4.2 Results and Discussions

Numerical simulations were performed using FLAC 3D software and the bearing pressure vs. settlement ratio curves were plotted for all the case to study the behavior of sand bed when reinforced with stacked geocell in different patterns as shown in the Figure 6.6. It can be observed that, initially up to 4% settlement ratio there is no significant difference in the bearing pressure. But after 4% settlement ratio there is slight reduction in the bearing pressure developed and it goes on increasing with the increase in settlement ratio. This is because of the slippage occurring between the two layers of geocell under static loading. The bearing pressure reduction at various settlement ratios when the actual geocell is replaced by stacked geocell of different pattern is shown in the Table 6.1.
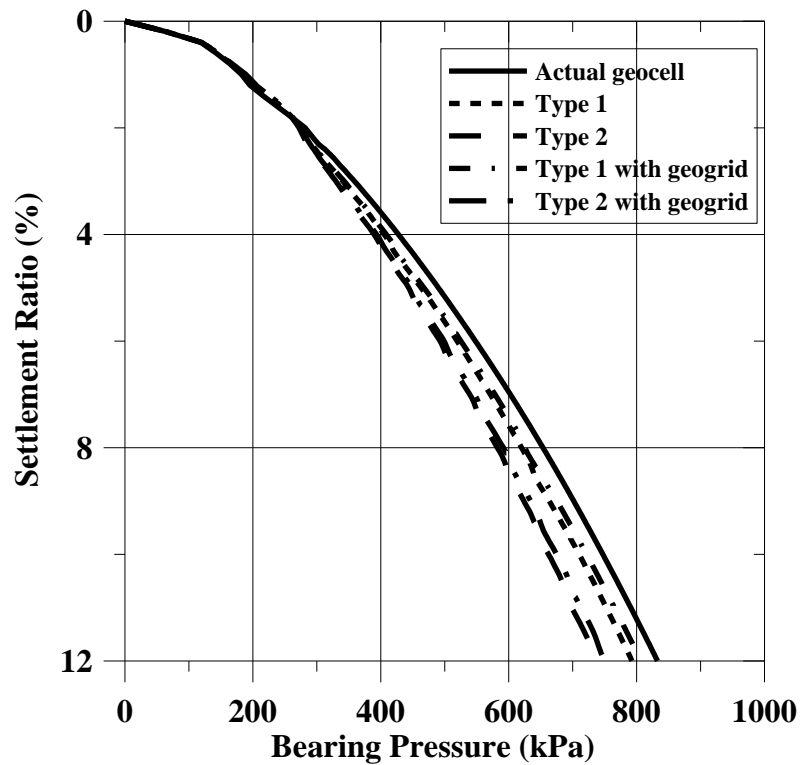

**Figure 6.6: Comparison of bearing pressure vs. settlement ratio curve**

Table 6.1: Bearing Pressure reduction in stacked geocell

Settlement Ratio (%)	Type 1	Type 2	Type 1 with geogrid	Type 2 with geogrid
1	No significant variation			
3	4.3%	9%	2.9%	9%
5	6.5%	10.1%	4.25%	10.1%
10	4.9%	14.5%	3.4%	12.9%

The variation of horizontal stresses in x-direction at the mid height of the two geocells for four cases are shown in the Figure 6.7, Figure 6.8, Figure 6.9 and Figure 6.10. It can be observed that the stresses developed were maximum near the loading centre and it gradually reduces towards the boundaries of the model. The maximum stresses were observed in geocell 1 and 2 in all cases expect the bottom geocell of the two cases of Type 2. This is because of more loading area in these two cells. In the case of bottom geocell of Type 2 case, the loading comes directly above the cell 1 as shown in Figure 6.8 (b) and Figure 6.10 (b). So the maximum stresses developed inside that particular cell.
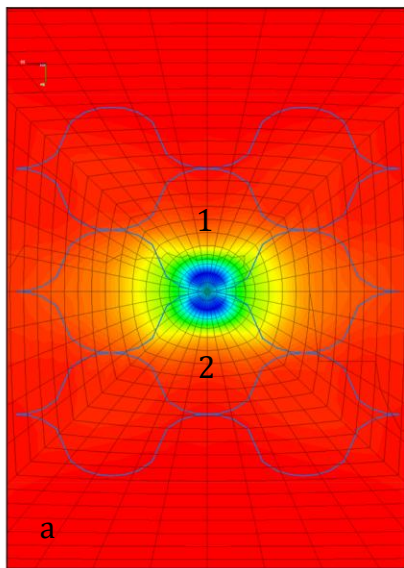
Type1 at d=0.0722 m
Max Sxx: -83.4 kPa
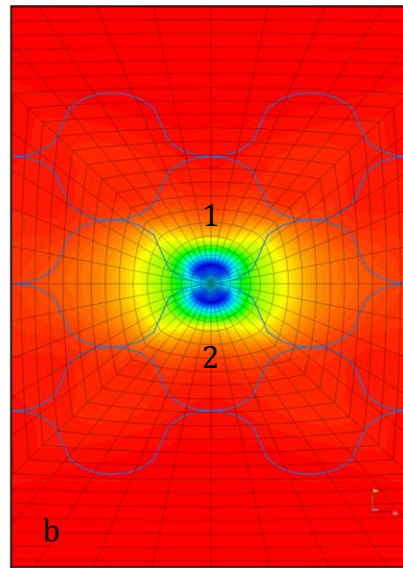
Type2 at d=0.0722 m
Max Sxx: -81.42 kPa

Figure 6.7: Horizontal stress in x-direction at mid height of the top geocell
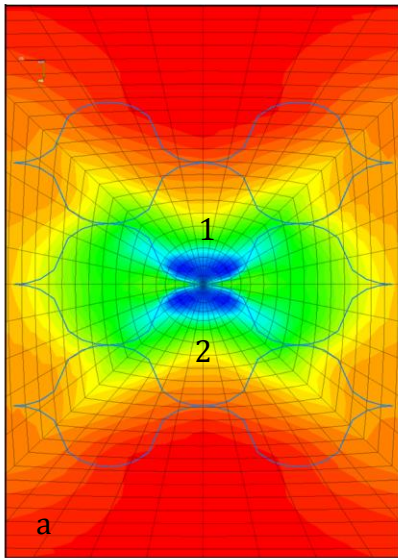
Type1 at d=0.1723 m
Max Sxx: -33.4 kPa

Type2 at d=0.1723 m
Max Sxx: -31.8 kPa

Figure 6.8: Horizontal stress in x-direction at mid height of the bottom geocell

Type1 with Geogrid
at d=0.0722 m
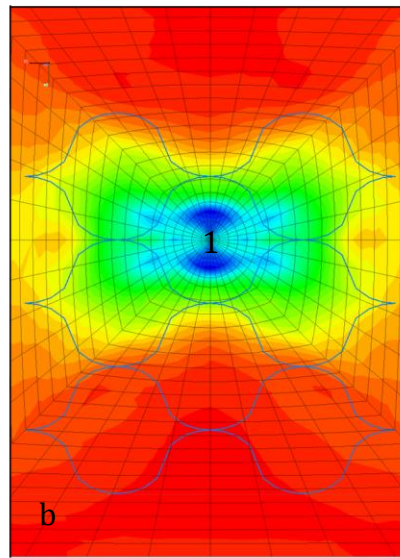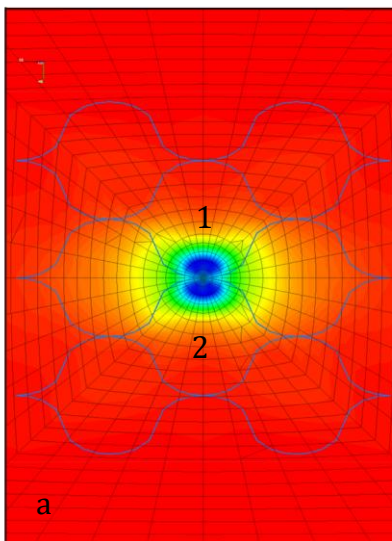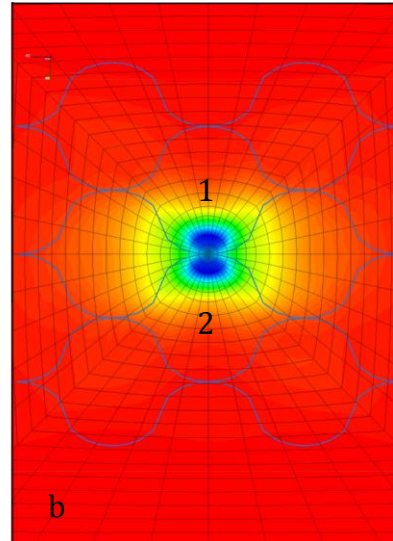Max Sxx: -84.78 kPa

Type2 with Geogrid
at d=0.0722 m
Max Sxx: -81.78 kPa

Figure 6.9: Horizontal stress in x-direction at mid height of the top geocell
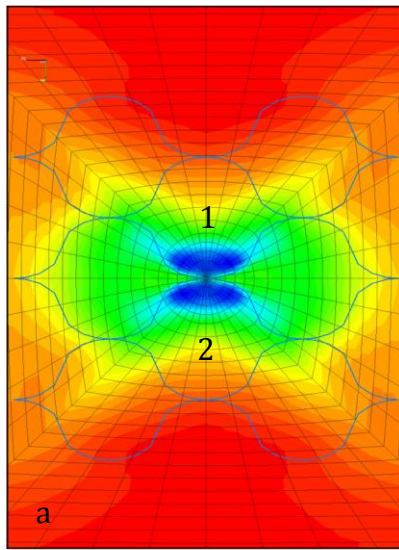
Type1 with Geogrid
at d=0.1723 m
Max Sxx: -34.52 kPa
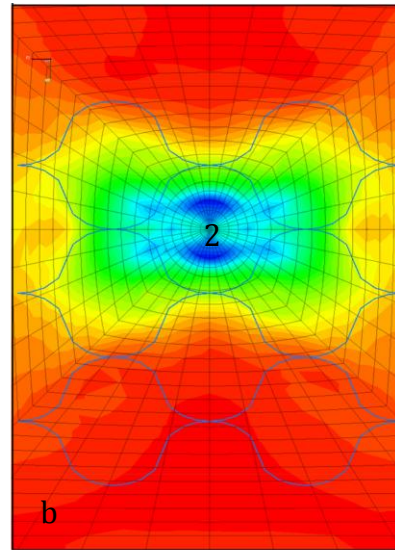
Type2 with Geogrid
at d=0.1723 m
Max Sxx: -32.12 kPa

Figure 6.10: Horizontal stress in x-direction at mid height of the bottom geocell

For studying the displacement mechanism in the geocell reinforcement, a vertical cross-section was considered and the displacement in the geocell reinforcement as well as in the soil were analysed separately as shown in the Figure 6.11 and Figure 6.12. The red arrows represents the direction of movement of geocell and Geogrid and the green arrows represents the direction and movement of soil. It can be clearly observed from the figure that, in stacked geocell case, the two geocell layers are performing separately as each geocell top surface is moving inward and the bottom surface is moving outward under monotonic loading. When a geogrid is placed in between the two geocell layers, the geogrid is providing an additional tension membrane support there by improving the performance of the reinforced sand bed.
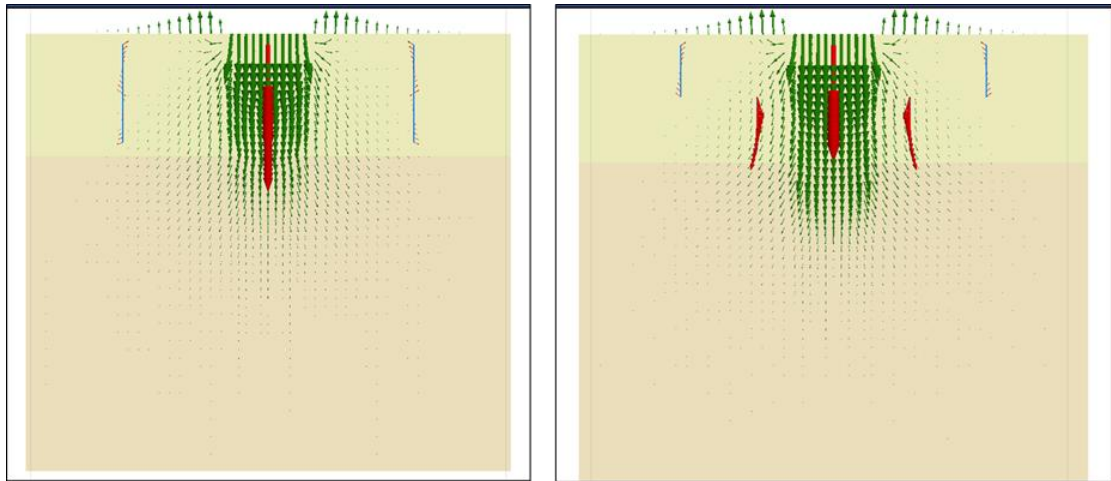
Figure 6.11: Displacement vector at the cross-section (a) Type 1 and (b) Type 2
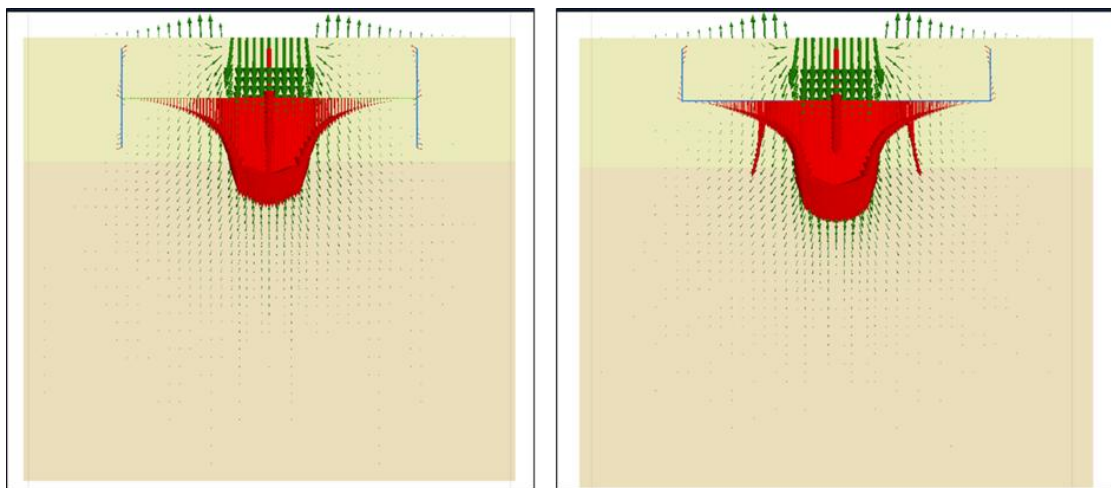
Figure 6.12: Displacement vector at the cross-section (a) Type 1 with Geogrid (b) Type 2 with geogrid

6.5 Summary

This chapter describes the performance of sand bed over weak soil layer reinforced with stacked geocell in different patterns. Two 100mm height geocells were modeled for this study and the analysis is performed for four different cases. The conclusions drawn from this part of the study are:

(1) Even though there is a slight reduction in the ultimate bearing capacity of the reinforced sand bed with stacked geocell, stacked geocell can be adopted in the field where there is a requirement of more geocell height which is not available in the market.

(2) Type 1, where the weld of top cell is placed above the weld of bottom geocell, performs better as compared to Type 2.

(3) When geogrid is placed in between two geocells, an improvement in the bearing pressure can be observed at higher settlement ratios.

(4) The displacement vector plots are made to figure out displacement mechanism of stacked geocell reinforcement.

Chapter 7

Conclusion

7.1 General

In the present study, a realistic approach for modeling the actual three dimensional honeycomb shape of geocell reinforcement. Numerical simulations were performed in FLAC 3D finite difference software by placing the geocell reinforcement in the sand bed for homogeneous and layered cases separately and the confinement mechanism was studies by analyzing the stresses and displacements developed under monotonic loading. Mohr coulomb material model was used to simulate soil behavior and linear elastic material model was used for geocell element. The numerical model of geocell was validated using the large triaxial test and found that the results were in good agreement with each other. The parametric studies performed on geocell revealed that the tensile strength of the geocell is majorly responsible for imparting strength to the sand bed. The provision of the additional Geogrid below the geocell, further improves the performance of reinforced sand bed by virtue of the membrane mechanism.

7.2 Conclusions

7.2.1 Numerical Modeling of Geocell Reinforced Sand Bed under Monotonic Loading

Numerical simulations were carried out on geocell reinforced homogeneous sand of 75% relative density to study the confining mechanism of geocell reinforcement under monotonic loading. The following are the conclusion drawn from the study:

(1) The unreinforced and geocell reinforced numerical model for homogeneous sand case were able to simulate the load- settlement behavior of the actual sand bed.

(2) The geocell reinforced soil bed showed an improvement in bearing capacity by 93%, 69%, 74% and 81% at settlement ratios of 1%, 3%, 5% and 9% respectively.

(3) The confining stress developed in the infill sand at the mid height of the geocell reinforcement is plotted by considering different sections and the variation is studied.

(4) The displacement vector diagram is plotted for both unreinforced and geocell reinforced cases and the reinforcement mechanism of geocell is studied.

(5) The vertical displacement and vertical stresses developed in the model for both unreinforced and geocell reinforced case is compared.

(6) The behavior of single geocell under different loading areas are studies.

7.2.2 Numerical Modeling of Geocell Reinforced Sand Bed over Weak Subgrade under Monotonic Loading

Layered soil model with 75% relative density sand as top layer and weak soil as subgrade is modeled to study the mechanism of geocell reinforcement when it is placed over a weak subgrade. Two weak subgrades were used for the study- 30% relative density sand and clay. The following conclusions are drawn from the study:

(1) Geocell reinforced soil bed over weak sand subgrade showed an improvement in bearing capacity by 54% at a settlement ratio of 10%.

(2) The confining mechanism of geocell reinforced sand bed overlying weak subgrade is brought out by analyzing the stresses and displacement developed in the geocell and soil model under monotonic loading.

(3) Parametric studies were performed by varying the modulus of geocell and interface shear modulus. Additionally, the studies were also performed by placing geocell with aperture and geocell with geogrid layer at the base for studying the behavior of the sand bed under static loading.

(4) The vertical stress and vertical displacement were analyzed by comparing the unreinforced and geocell reinforced cases and it was observed that the geocell reinforcement reduced the vertical stresses and displacements due to confining mechanism.

(5) Geocell reinforced soil bed over weak clay subgrade showed an improvement in bearing capacity by 86% at a settlement ratio of 10%.

7.2.3 Numerical Modeling of Stacked Geocell Reinforced Sand Bed over Weak Subgrade under Monotonic Loading

In the validated model of layered soil with weak sand subgrade, numerical simulations were performed by placing two geocells of 100 mm height in two different patterns to study the behavior of stacked and staggered geocell under monotonic loading over weak sand subgrade. The simulations were again performed by placing geogrid layer in between two geocell layers and the performance of the sand bed is studied. The conclusions obtained from this study are:

(1) Stacked geocells can be adopted in the field case where the height required for the geocell reinforcement is not sufficient by slightly sacrificing the ultimate bearing capacity of the reinforced sand bed.

(2) Type 1, where the weld of top cell is placed above the weld of bottom geocell, performs better as compared to Type 2 where the weld of the top geocell layer is kept above the cell of bottom geocell layer.

(3) When geogrid is placed in between two geocells, an improvement in the bearing pressure can be observed at higher settlement ratios.

7.3 Scope of Future work

The present study has attempted to model the actual honeycomb shape of geocell and to perform numerical simulations on the geocell reinforced soil bed to study the improvement in the performance of the soil bed. This study mainly focuses on the confining mechanism of the geocell reinforced sand bed over weak sand layer under monotonic loading. This study can be further extended to cyclic loading where the loading is applied incrementally or repeatedly in cycles. The current study is only based on Mohr-Coulomb model as the soil material model. As the actual soil behavior is hyperbolic in nature, the work can be extended by adopting Duncan-Chang model as the soil material model.

References

[1] Asha M. N and Madhavi Latha, G. Large Diameter Triaxial Tests on Geosynthetic-Reinforced Granular Subbases. Journal of Materials in Civil Engineering, (2014) 899-1561

[2] Bathurst, R. J., and Karpurapu, R. Large-Scale triaxial compression testing of geocell-reinforced granular soils. Geotechnical Testing Journal, 16(3), (1993) 296-303.

[3] Bathurst, R. J., and Knight, M. A. Analysis of Geocell Reinforced-Soil Covers over Large Span Conduits. Computers and Geotechnics, 22(3/4), (1998) 205-219.

[4] Dash, S.K., Krishnaswamy, N. R. and Rajagopal, K. Bearing capacity of strip footings supported on geocell-reinforced sand. Geotextiles and Geomembranes, 19, (2001a) 235-256.

[5] Dash, S.K., Sireesh, S., and Sitharam, T.G. Model studies on circular footing supported on geocell reinforced sand underlain by soft clay. Geotextiles and Geomembranes, 21, (2003).197-219.

[6] Dash, S. K., Rajagopal, K., and Krishnaswamy, N. R. Performance of different geosynthetic reinforcement materials in sand foundations. Geosynthetics International, 11(1), (2004) 35-42.

[7] Dash, S.K., Rajagopal, K., and Krishnaswamy, N.R. Behavior of geocell-reinforced sand beds under strip loading. Canadian Geotechnical Journal, 44, (2007) 905-916

[8] Dash, S. K., and Bora, M. C. Improved performance of soft clay foundations using stone coloumns and geocell-sand mattress. Geotextiles and Geomembranes, 41, (2013) 26-35.

[9] Han, J., Yang, X., Leshchinsky, D., and Parsons, R. L. Behavior of geocell reinforced sand under a vertical load. Journal of Transportation Research Board, n 2045, (2008) 95-101.

[10] Hegde, A., and Sitharam, T. G. Experimental and numerical studies on footings supported on geocell reinforced sand and clay beds. International Journal of Geotechnical Engineering, 7(4), (2013) 347-354.

[11] Hegde, A., and Sitharam, T. G. 3-Dimensional Numerical Analysis of Geocell Reinforced Soft Clay Beds by considering the actual geometry of Geocell Pockets. Canadian Geotechnical Journal. (2015).

[12] Hegde, A., and Sitharam, T. G. 3-Dimensional numerical modelling of geocell reinforced sand beds. Geotextiles and Geomembranes. (2014d)

[13] Itaska. Fast Lagrangian Analysis of Continua (FLAC3D 4.00). Itasca Consultin Group Inc, Minneapolis, USA, 2008.

[14] Krishnaswamy, N. R., Rajagopal, K. and Madhavi Latha, G. Model studies on geocell supported embankments constructed over soft clay foundation. Geotechnical Testing Journal, ASTM, 23, (2000) 45-54.

[15] Madhavi Latha, G. Investigations on the behaviour of geocell supported embankments, Ph.D. Thesis, Indian Institute of Technology Madras, Chennai, India, 2000.

[16] Madhavi Latha, G., Dash, S. K., and Rajagopal, K. Equivalent Continuum Simulations of Geocell Reinforced Sand Beds Supporting Strip Footings. Geotechnical and Geological Engineering. (2008).

[17] Madhavi Latha, G., Dash, S. K., and Rajagopal, K. Numerical simulation of the behavior of geocell reinforced sand in foundations. International Journal of Geomechanics, 9(4), (2009) 143-152.

[18] Madhavi Latha, G., and Rajagopal, K. Parametric Finite Element Analyses of Geocell-Supported Embankment. Canadian Geotechnical Journal, 44(8), (2007) 917-927.

[19] Madhavi Latha, G., Rajagopal, K., and Krishnaswamy, N. R. Experimental and Theoretical Investigations on Geocell-Supported Embankments. International Journal of Geomechanics, 6(1), (2006) 30-35.

[20] Moghaddas and Dawson , Laboratory model tests for a strip footing supported on geocell reinforced sand beds Geotechnical special publications No: 207, 2010.

[21] Moghaddas Tafreshi, S.N., and Dawson, A.R. Behavior of footings on reinforced sand subjected to repeated loading comparing use of 3D and planar geotextile. Geotextiles and Geomembranes, 28, (2010) 434-447.

[22] Moghaddas Tafreshi, S. N., Khalaj, O., and Dawson, A. R. Pilot-scale load tests of a combined multi layered geocell and rubber-reinforced foundation. Geosynthetics International, 20 (3), (2013) 143-161.

[23] Pokharel, S. K. Experimental Study on Geocell-Reinforced Bases under Static and Dynamic Loading, Ph.D. Dissertation, University of Kansas, Kansas, USA, 2010.

[24] Pokharel, S. K., Han, J., Leshchinsky, D., Parsons, R. L., and Halahmi, I. Experimental evaluation of influence factors for single geocell-reinforced sand. Oral presentation and CD publication at the TRB 88th Annual Meeting, Washington, DC, 2009b.

[25] Rajagopal, K., Krishnaswamy, N. R., and Latha, G. M. Behaviour of Sand Confined with Single and Multiple Geocells. Geotextiles and Geomembranes, 17, (1999) 171-184.

[26] Rea, C., and Mitchell, J. K. Sand reinforcement using paper grid cells. Symposium on Earth Reinforcement, ASCE, Pittsburgh, (1978) 644-663.

[27] Sireesh, S., Gowrisetti, S., Sitharam,T.G., and Puppala, A.J. Numerical simulations of sand and clay. Ground Improvement, 162 (GI4), (2009) 185-198.

[28] Sireesh, S., Sitharam, T.G., and Dash, S.K. Bearing capacity of circular footing on geocell sand mattress overlying clay bed with void. Geotextiles and Geomembranes, 27 (2), (2009) 89-98.

[29] Sitharam, T.G., Sireesh,S., and Dash, S.K. Model studies of a circular footing supported on geocell-reinforced clay. Canadian Geotechnical Journal, 42, (2005)693–703.

[30] Sitharam, T.G., and Hegde, A. Design and construction of geocell foundation to support embankment on soft settled red mud. Geotextiles and Geomembranes, 41, (2013) 55-63.

[31] Sitharam, T. G. and Sireesh, S. Behaviour of embedded footings supported on geogrid-cell reinforced foundation beds. Geotechnical testing Journal, ASTM, 28, (2005a) 452 – 463.

[32] Thallak, S. G., Saride, S., and Dash, S. K. Performance of surface footing on geocell-reinforced soft clay beds. Geotechnical and Geological Engineering, 25, (2007) 509-524.

[33] Wesseloo, J. The Strength and Stiffness of Geocell Support Packs, Ph.D. Dissertation, University of Pretoria, Pretoria, South Africa, 2004.

[34] Yang X., Numerical Analyses of Geocell-Reinforced Granular Soils under Static and Repeated Loads, Ph.D. Dissertation, University of Kansas, Kansas, USA, 2010.

[35] Yang, X., Han, J., Parsons, R.L., and Leshchinsky, D. 2010. Three-dimensional numerical modelling of single geocell reinforced sand. Front. Archit. Civ. Eng. China, 4(2), 233-240.